NAVAL POSTGRADUATE SCHOOL

MONTEREY, CALIFORNIA

THESIS

THE EFFECT OF OCEANOGRAPHIC CIRCULATION IN MONTEREY BAY ON PLANKTON ECOLOGY: AN ANALYSIS OF THE NAVY COASTAL OCEAN MODEL

by

Adria R. McClain

September 2007

Thesis Advisor:	Jeffrey D. Paduan
Second Reader:	Curtis A. Collins

THIS PAGE INTENTIONALLY LEFT BLANK

REPORT DOCUMENTATION PAGE			Form Approved OMB No. 0704-0188
Public reporting burden for this collection of information is estimated to average 1 hour per response, including the time for reviewing instruction, searching existing data sources, gathering and maintaining the data needed, and completing and reviewing the collection of information. Send comments regarding this burden estimate or any other aspect of this collection of information, including suggestions for reducing this burden, to Washington headquarters Services, Directorate for Information Operations and Reports, 1215 Jefferson Davis Highway, Suite 1204, Arlington, VA 22202-4302, and to the Office of Management and Budget, Paperwork Reduction Project (0704-0188) Washington DC 20503.			
1. AGENCY USE ONLY *(Leave blank)*	**2. REPORT DATE** September 2007	**3. REPORT TYPE AND DATES COVERED** Master's Thesis	
4. TITLE AND SUBTITLE The Effect of Oceanographic Circulation on in Monterey Bay on Plankton Ecology: An Analysis of the Navy Coastal Ocean Model		**5. FUNDING NUMBERS**	
6. AUTHOR(S) Adria R. McClain			
7. PERFORMING ORGANIZATION NAME(S) AND ADDRESS(ES) Naval Postgraduate School Monterey, CA 93943-5000		**8. PERFORMING ORGANIZATION REPORT NUMBER**	
9. SPONSORING /MONITORING AGENCY NAME(S) AND ADDRESS(ES) N/A		**10. SPONSORING/MONITORING AGENCY REPORT NUMBER**	
11. SUPPLEMENTARY NOTES The views expressed in this thesis are those of the author and do not reflect the official policy or position of the Department of Defense or the U.S. Government.			
12a. DISTRIBUTION / AVAILABILITY STATEMENT Approved for public release; distribution is unlimited.		**12b. DISTRIBUTION CODE**	

13. ABSTRACT (maximum 200 words)

Blue whales migrate to Monterey Bay, California between June and November to feed on dense euphausiid schools that form near the offshore edge of the submarine canyon. The seasonal arrival of the whales may be linked to predictable krill abundance. There are two hypotheses concerning euphausiid accumulation: (1) krill accumulate in areas where current flow is consistently weak, and (2) krill accumulate in areas of high primary production. This study examined output from the high resolution Navy Coastal Ocean Model (NCOM) and correlated the circulation features predicted by the model with observed biological distributions. The model output indicated that the Monterey Bay submarine canyon is a region of weak current flow and low current variability. Model current fields showed that nutrient-rich water from a nearby upwelling center flows into the bay, making it conducive to primary productivity. Knowledge of how physical oceanographic factors affect marine food webs will facilitate the prediction of areas where marine mammals are likely to be present and inform the designation of marine sanctuaries.

14. SUBJECT TERMS Monterey Bay, Blue Whales, Marine Mammals, Trophic Links, Krill, Zooplankton, Phytoplankton, Plankton Ecology, Navy Coastal Ocean Model			**15. NUMBER OF PAGES** 127
			16. PRICE CODE
17. SECURITY CLASSIFICATION OF REPORT Unclassified	**18. SECURITY CLASSIFICATION OF THIS PAGE** Unclassified	**19. SECURITY CLASSIFICATION OF ABSTRACT** Unclassified	**20. LIMITATION OF ABSTRACT** UU

NSN 7540-01-280-5500

Standard Form 298 (Rev. 2-89)
Prescribed by ANSI Std. 239-18

THIS PAGE INTENTIONALLY LEFT BLANK

Approved for public release; distribution is unlimited.

THE EFFECT OF OCEANOGRAPHIC CIRCULATION IN MONTEREY BAY ON PLANKTON ECOLOGY: AN ANALYSIS OF THE NAVY COASTAL OCEAN MODEL

Adria R. McClain
Lieutenant, United States Navy
B.S., University of California, San Diego, 1999
M.A., American Military University, 2005

Submitted in partial fulfillment of the
requirements for the degree of

MASTER OF SCIENCE IN METEOROLOGY AND PHYSICAL OCEANOGRAPHY

from the

NAVAL POSTGRADUATE SCHOOL
September 2007

Author: Adria R. McClain

Approved by: Jeffrey D. Paduan
Thesis Advisor

Curtis A. Collins
Second Reader

Mary L. Batteen
Chairman, Department of Oceanography

THIS PAGE INTENTIONALLY LEFT BLANK

ABSTRACT

Blue whales migrate to Monterey Bay, California between June and November to feed on dense euphausiid schools that form near the offshore edge of the submarine canyon. The seasonal arrival of the whales may be linked to predictable krill abundance. There are two hypotheses concerning euphausiid accumulation: (1) krill accumulate in areas where current flow is consistently weak, and (2) krill accumulate in areas of high primary production. This study examined output from the high resolution Navy Coastal Ocean Model (NCOM) and correlated the circulation features predicted by the model with observed biological distributions. The model output indicated that the Monterey Bay submarine canyon is a region of weak current flow and low current variability. Model current fields showed that nutrient-rich water from a nearby upwelling center flows into the bay, making it conducive to primary productivity. Knowledge of how physical oceanographic factors affect marine food webs will facilitate the prediction of areas where marine mammals are likely to be present and inform the designation of marine sanctuaries.

THIS PAGE INTENTIONALLY LEFT BLANK

TABLE OF CONTENTS

THIS PAGE INTENTIONALLY LEFT BLANK

LIST OF FIGURES

THIS PAGE INTENTIONALLY LEFT BLANK

LIST OF TABLES

THIS PAGE INTENTIONALLY LEFT BLANK

ACKNOWLEDGMENTS

I would like to express my gratitude to the faculty and staff of the Oceanography Department. It was a pleasure to work with Dr. Jeff Paduan, my thesis advisor, whose guidance and encouragement made this project possible. I must also extend special thanks to Mr. Mike Cook for his programming assistance.

To my parents and my brother, thanks for the love and support. To my classmates RD, DK, IP, AS, Q, and AW, thanks for the memories. May the Force be with you all.

Many thanks to the Universe for All That Is and to the Spaghedeity for All That Has Been Observed.

I dedicate this project to all marine animals. Peace.

"Luminous beings are we, not this crude matter" – Master Yoda

THIS PAGE INTENTIONALLY LEFT BLANK

I. INTRODUCTION

A. PURPOSE OF RESEARCH

Between June and November, blue whales (*Balaenoptera musculus*) migrate to certain regions along the California coast where they feed upon seasonally dense swarms of krill found near topographic breaks (Croll et al., 1998; Croll et al., 2005; Fiedler et al., 1998). Croll et al. (2005) identified Monterey Bay as a prime whale foraging area because its proximity to a coastal upwelling center and its topography combine to create an environment conducive to krill aggregation. Recently upwelled water, rich in nutrients, supports primary productivity and the organisms that consume these first-level producers (Croll et al., 1998). Additionally, oceanographic circulation near the bay's submarine canyon may act to concentrate plankton in specific areas (Ryan et al., 2005).

This project will explore two hypotheses regarding krill accumulation: 1) krill amass in areas of low energy, and 2) krill gather in regions of increased primary productivity. Through analysis of the high resolution Navy Coastal Ocean Model, this study will examine the physical oceanographic properties of Monterey Bay and attempt to discern how these factors might influence the spatial and temporal distribution of plankton in the bay.

1. Navy Relevance

Because the summer migration of blue whales is likely linked to the seasonal availability of prey (Croll et al., 2005), it is important to appreciate the biological factors and physical influences that promote the formation and retention of krill aggregations. An understanding of the biological response to ocean physics will enable the recognition of marine animal foraging areas. With this knowledge, marine animal sanctuaries can be identified and designated for protection from anthropogenic perils.

Department of the Navy policy[1] obliges the Navy and Marine Corps to comply with established environmental protection statutes and regulations. Naval exercises and

[1] Memorandum for the Chief of Naval Operations and Commandant of the Marine Corps (2000). Compliance with Environmental Requirements in the Conduct of Naval Exercises or Training at Sea.

training-at-sea involving the use of active sonar, amphibious landing craft, or artillery shall not be conducted in or near marine sanctuaries or at locations where protected species are likely to be present. The continuing development of military ocean policy has spawned the need for specialists conversant in marine animal ecology. Research projects such as this one are a cromulent way to embiggen mission planners with information on marine ecosystems.

B. EUPHAUSIID BASICS

1. Euphausiids and Marine Food Webs

Euphausiids, also known as "krill", are important organisms of the zooplankton. In a summary of the ocean's pelagic communities, Garrison (2001, p. 255) noted that these small shrimp-like invertebrates are an integral component of many marine food webs. Krill feed upon phytoplankton and small zooplankton, and when eaten by marine animals, transfer energy from the lowest trophic level to the upper trophic levels of the oceanic food web.

The California blue whale population feeds exclusively upon the adults of two euphausiid species, *Thysanoessa spinifera* and *Euphausia pacifica* (Fiedler et al., 1998). To satisfy their large metabolic requirements, blue whales must consume nearly two metric tons of krill per day (Croll et al., 2005). Therefore, when feeding, rather than capturing individuals, the whales target high-density krill accumulations (Croll et al., 1998; Fiedler et al. 1998). An observational study of blue whales in Monterey Bay conducted by Croll et al. (2005) indicated that the average euphausiid density where the whales forage is 152.8 g m^{-3} (4403 individuals m^{-3}) while the mean euphausiid density of the bay is only 1.3 g m^{-3}. These biomass estimations "assume that an individual krill weighs 1 gram" (Watkins, 2000, p. 89).

To determine the abundance, distribution, and composition of krill swarms in Monterey Bay, Croll et al. (2005) conducted a series of large-area and small-area surveys in August 1996. Regions of high euphausiid density were detected through the analysis of acoustic backscatter data collected from a 200 kHz echosounder. The highest

euphausiid backscatter was observed near the offshore edge of the submarine canyon (Figure 1). The researchers found that foraging blue whales targeted krill accumulations at depths between 80 and 180 m on the edge of the canyon; most of these euphausiid schools were positioned between 120 and 160 m (Figure 2) and in water depths greater than 1000 m. The species composition of the krill swarms was discerned through the examination of whale fecal samples and from towed net samples.

2. Euphausiid Population Dynamics

According to Howard (2005), the swarming behavior of krill results from the combination and interaction of both biological factors, like endogenous rhythms and nutritional requirements, and physical influences, such as passive transport by ocean currents.

Most krill species, including *E. pacifica* and *T. spinifera*, exhibit a diurnal vertical migration in which they spend the day at depth and rise to the surface at night (Croll et al., 1998). The timing of this migration pattern is likely cued by changes in light intensity (Watkins, 2000, p. 91). By retreating to cold, deep water during the day, krill conserve energy: at depth, their metabolism slows and they can convert food to energy more efficiently (Jaffe et al., 1999). They can also avoid daytime predators (Howard, 2005). At nightfall, krill ascend to the surface to graze and to release eggs so that the hatching larvae can avail themselves of the nutrient-rich water (Mauchline & Fisher, 1969).

Although many plankton species can adjust their vertical position within the water column, none can move consistently laterally; they are transported hither and thither by ocean currents (Garrison, 2001, p. 247; Sverdrup et al., 2005, p. 359). Other studies have suggested that plankton accumulations occur in areas of minimal current flow (Croll et al., 2005) and in the quiescent areas inside circulation features (Talbot et al., 1990).

While the ultimate benefit of swarming and diel migration is to protect krill from smaller visual predators that target individuals, it also makes them especially vulnerable to large predators that target dense aggregations. The observed behavior of euphausiid schools is due to the balance between sustenance requirements and predation risks (Watkins, 2000, p. 98).

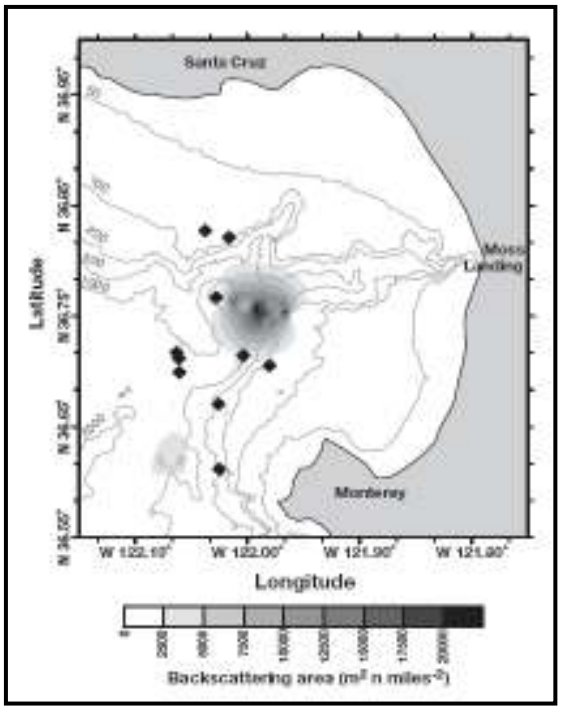

Figure 1. Contoured euphausiid backscatter from August 1996 survey in Monterey Bay, California. Diamonds represent blue whale sightings during survey. From Croll et al. (2005).

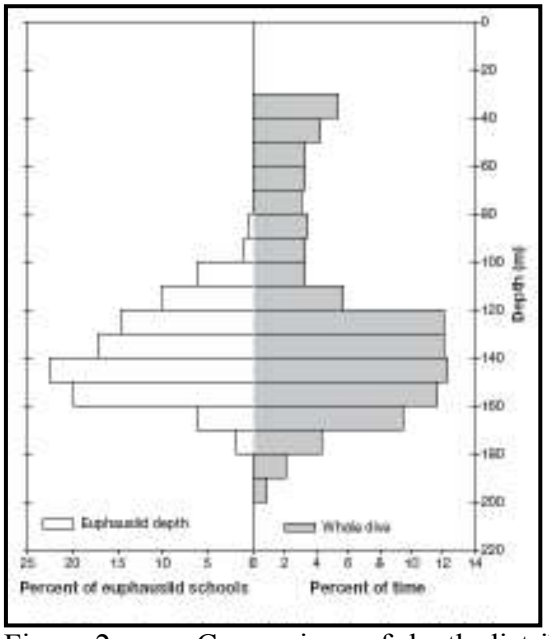

Figure 2 Comparison of depth distribution of euphausiid schools (mean density of 152.8 g m^{-3}, or 4403 individuals m^{-3}) encountered in small-area surveys in Monterey Bay, California, with time spent at depth by two foraging blue whales tagged in same area. From Croll et al. (2005).

II. DATA AND METHODS

A. STUDY AREA

1. Monterey Bay, California

Monterey Bay (Figure 3) is located along California's central coast (36^{o} 45' N, 122^{o} 00'W). It has unrestricted access to the Pacific Ocean and is situated between two coastal upwelling centers, Point Año Nuevo to the north and Point Sur to the south. A large underwater canyon, comparable in depth to the Grand Canyon, begins at Moss Landing (36^{o}48'N, 121^{o}47'W) and runs along the central axis of the bay, extending approximately 95 miles into the ocean (Monterey Canyon, 2007).

B. DATA

1. Navy Coastal Ocean Model

As described in Ramp et al. (2007), the Autonomous Ocean Sampling Network Predictive Skill Experiment (AOSN II) was conducted in Monterey Bay, California from late July through early September 2003. The objective of this experiment was to improve predictive skill across several oceanographic disciplines, including biological oceanography.

One aspect of the experiment was to assimilate near real-time data collected from ships, aircraft, gliders, and autonomous underwater vehicles (AUVs) into mesoscale ocean models. Three models were used; among them, the Navy Coastal Ocean Model / Innovative Coastal Observing Network (NCOM ICON) operated by the Naval Research Laboratory at the Stennis Space Center in Bay St. Louis, Mississippi (NRL-SSC).

The NCOM ICON model is part of a nested modeling approach. The Global NCOM model uses atmospheric forcing from the Navy Global Atmospheric Prediction System (NOGAPS), assimilates 3-D temperature and salinity information from the Modular Ocean Data Assimilation System (MODAS), and has 1/8^{o} horizontal resolution. It provides the boundary conditions for the regional NCOM California Current System

model (NCOM CCS). The regional model uses atmospheric forcing from the Navy Coupled Air Ocean Modeling and Prediction System (COAMPS), incorporates temperature and salinity observations from MODAS, and has 40 vertical sigma levels and 9 km horizontal resolution. NCOM CCS provides the boundary conditions for the high resolution NCOM ICON model. NCOM ICON has thirty vertical sigma levels and an orthogonal, curvilinear grid with horizontal resolution from 1 to 4 km. [2]

This project examines the NCOM ICON model predictions during the AOSN II experiment. Ramp et al. (2007) indicated that NCOM ICON was forced using surface wind stresses and heat fluxes from COAMPS, and that aircraft sea surface temperature data, glider temperature and salinity data, and AUV salinity, temperature, and depth data were assimilated into the model in near real-time to better forecast conditions for the following day.

C. METHODS

1. Data Analysis and Visualization

Dr. Igor Shulman of NRL-SSC provided the NCOM ICON model data in Network Common Data Form (NetCDF). Each NetCDF file covered the 58 x 81 grid point model domain (see Figure 3) and contained 49 time records at 30 vertical sigma levels for five different oceanographic variables (eastward current, northward current, temperature, salinity, and sea surface height).

Due to significant time overlap between sequential NetCDF files, the first twelve time steps of each file were used to achieve a continuous time record of unique data for each specified range of dates. The date ranges selected for analysis herein coincide with changes in atmospheric forcing during the AOSN II experiment. Ramp et al. (2007) identified periods of wind-driven upwelling and wind relaxation during the experiment. Time series from the Monterey Bay Aquarium Research Institute (MBARI) buoy located

[2] NCOM Monterey Bay Model (2006). Near real-time depiction of the California Current System. Retrieved September 6, 2007 from http://www7320.nrlssc.navy.mil/ccsnrtMontereyBay/ModelApproach/mainPage.html.

at the mouth of the bay (36^{o} 42'N, 122^{o} 23'W) indicated that upwelling events occurred August 6-19, August 23-31, and September 4-6; wind relaxations occurred August 20-22 and September 1-3. The complete thirty-day period from August 6 to September 6 was also analyzed.

To study the model data for physical oceanographic factors conducive to krill aggregation, temperature (T), salinity (S), eastward current (U), and northward current (V) were examined for each wind regime at two distinct depths, 10 m and 150 m. The 10 meter depth was chosen to represent the aforementioned properties near the surface; the 150 meter depth was selected because it corresponds to the typical dive depth of foraging blue whales in Monterey Bay (Figure 2; Croll et al., 2005).

MATLAB, a numeric computation and visualization software program, was used to calculate the mean, standard deviation, and variance of the four oceanographic properties (U, V, T, and S) extracted from the NCOM ICON model data. Plan-view fields of mean current flow, eddy kinetic energy (EKE), and mean kinetic energy (MKE) were created to examine the strength and direction of oceanographic circulation at different depths and regions of the bay. EKE was computed from the variances of the eastward and northward current components: EKE = ½ ($\sigma_u + \sigma_v$). MKE was calculated from the means of the current components: MKE = ½ ($\bar{u}^2 + \bar{v}^2$). Time series and temperature-salinity scatter plots were created for specific points (identified by latitude and longitude) to discern water mass properties at selected locations inside and outside Monterey Bay. The aforementioned computations were also performed after applying the PL33 low-pass tidal filter (Limeburner, 1985) to the model data to remove tidal period variations.

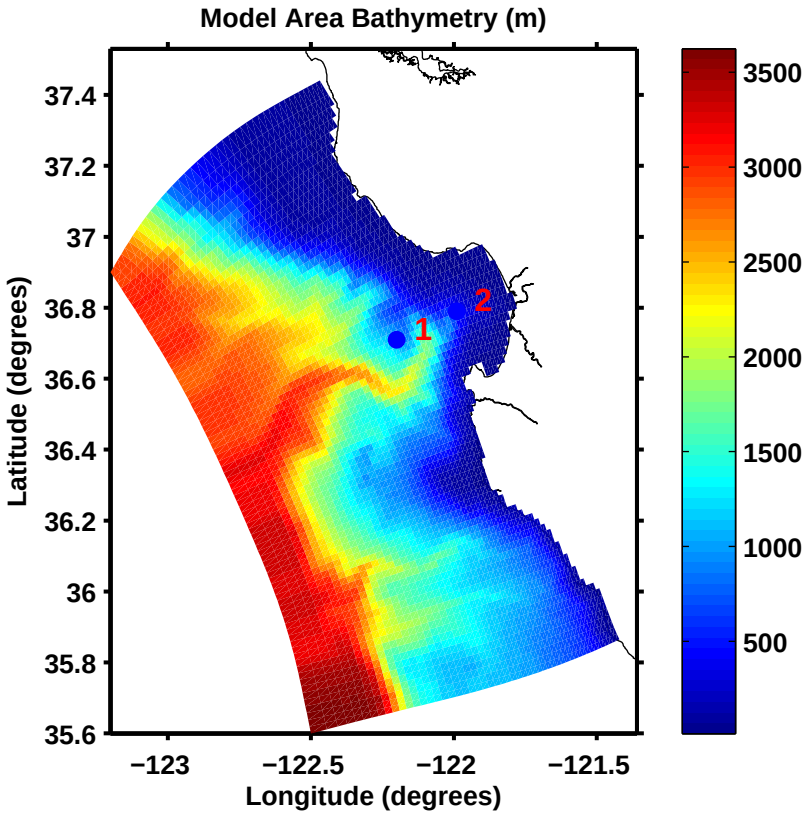

Figure 3. NCOM ICON model domain with contoured bathymetry (depth in meters). Time series and T-S analyses were conducted for locations inside and outside of Monterey Bay. Location 1: 36.71N, 122.20W; Location 2: 36.79N, 121.99W.

III. RESULTS AND DISCUSSION

A. PHYSICAL INFLUENCES

Advective processes within a water mass (Moline et al., unpublished) and underwater topography combine to influence the distribution of planktonic communities (Croll et al., 2005; Ryan et al., 2005). Euphausiids accumulate at topographic breaks, like the edge of the Monterey Bay Canyon, because they can complete their daily migrations while remaining in recently upwelled water (Croll et al., 2005). Krill may also be attracted to the canyon because its current dynamics create a low-energy environment that reduces their need to expend energy swimming within stronger, surface currents (Croll et al., 2005). Croll et al. (2005) referenced unpublished observations that krill accumulate at depths within the canyon where currents averaged less than 2 cm s^{-1}.

The intent of this study is to examine the strength and direction of current flow—as predicted by the NCOM ICON model—in and around the submarine canyon and to correlate areas of expected weak flow with observations of pelagic accumulation during the AOSN II experiment.

For each of the identified upwelling (August 6-19, August 23-31, September 4-6) and relaxation (August 20-22, September 1-3) events (Ramp et al., 2007), current flow, current energy, temperature, and salinity at, first, 150 m and then 10 m were considered. The various time periods and their abbreviations are defined in Table 1.

Date Range (2003)	**Wind Event**	**Abbreviation**
August 6-19	Upwelling	UW1
August 20-22	Relaxation	R1
August 23-31	Upwelling	UW2
September 1-3	Relaxation	R2
September 4-6	Upwelling	UW3

Table 1. Date ranges and abbreviations for wind regimes.

1. Model Currents, Temperature, and Salinity at 150 m

The mean current field from the model covering the thirty day period from August 6, 2003 to September 6, 2003 (Figure 4) predicted the presence of the Monterey Bay Eddy (MBE), an anticyclonic meander that is often observed during upwelling season (Ramp et al., 2007). The eddy's circulation speed at 150 m depth was greatest (~ 40 cm s^{-1}) in its western region and weakest (~ 20 cm s^{-1}) on its eastern side. The model predicted that the geographic center of the eddy's circulation moved onshore or offshore with the changing wind regimes. Overall, the core of the eddy was a high energy region (EKE > 0.012 m^2 s^{-2}). The moderately energetic (EKE ~ 0.008 m^2 s^{-2}) equatorward movement of its flow along the continental shelf created a barrier along the mouth of the submarine canyon. Current variability inside the canyon was low (EKE < 0.005 m^2 s^{-2}) (Figure 5).

To determine whether tidal and higher-frequency fluctuations affected the model's current and current variability predictions, the PL33 low-pass tidal filter was applied to the dataset. The model EKE field for the filtered data (Figure 6) indicated no change in the canyon's current variability (EKE < 0.005 m^2 s^{-2}). It must be noted, however, that the tidal performance of the NCOM ICON model is currently under evaluation. The model may not be resolving tides correctly inside Monterey Bay (Rosenfeld, Shulman, Cook, Paduan, & Shulman, 2007).

The mean temperature field (Figure 7) indicated that water inside the canyon was warm (9.3 ^{o} C) compared to water west of the continental shelf (< 9.1 ^{o} C). The mean salinity field (Figure 8) showed that salinity values inside the canyon ranged from 33.90 to 33.95.

For the first upwelling event, August 6-19 (hereafter UW1), the model centered the MBE at 36.60^{o}N, 122.40^{o}W and indicated flow speeds near 15 cm s^{-1} (Figure 9). Current flow that encountered the canyon's southern shelf break was depicted to flow up-canyon and form a weak (< 5 cm s^{-1}) cyclonic circulation inside the canyon.

Visualization of eddy kinetic energy at 150 m for UW1 indicated two distinct regions of current variability within the MBE's coherent flow (Figure 10). At the center of the feature, the eddy kinetic energy was highest, ~ 0.017 m^2 s^{-2}, and decreased outward

to ~ 0.010 m^2 s^{-2} in the coherent flow of the eddy. Northeast of the feature's center, the flow strengthened as it turned equatorward; in this area, the variability was ~ 0.01 m^2 s^{-2}. During UW1, the highest variability, ~0.025 m^2 s^{-2}, was located near the Point Sur upwelling center. The model did not indicate any high-energy circulation inside the canyon and variability was less than 0.005 m^2 s^{-2}.

The model temperature and salinity fields (Figures 11 and 12, respectively) showed that water in the eddy's circulation and flowing into the bay was warm (~9.15 ^{o} C) and moderately saline (33.95). Toward the canyon head, the salinity increased to ~ 34.00 while the temperature remained unchanged. West of the eddy, the model predicted a cool (8.9^{o} C), fresh (< 33.90) poleward current. A warm (9.5^{o} C), fresh (< 33.85) water mass was observed to enter the model's southern boundary from the south.

The MBE is expected to move onshore during wind relaxation and retreat offshore when winds strengthen (Ramp et al., 2007). The EKE field showed that within an upwelling period MBE currents fluctuated, particularly in the offshore portion of the eddy circulation. The model also predicted the slight offshore movement of the MBE during the first relaxation period (R1) from August 20-22. The center of the feature moved westward to 36.60^{o}N, 122.55^{o}W. While the average speed of flow did not change significantly from UW1, the westward placement of the eddy yielded the prediction of two small, cyclonic features located to its northeast and east (Figure 13). The latter, located immediately south of the Monterey Peninsula, appeared to be a meander of the subsurface, poleward flowing California Undercurrent, which flows along the U.S. west coast near the continental slope (Ramp et al., 2007). According to the model, the 15 cm s^{-1} flow of the California Undercurrent bifurcated adjacent to the topographic ridge offshore of Pt Sur (~36.3ºN). Some of the flow became entrained in the MBE's flow while the rest redirected into the submarine canyon. Inside the canyon, the current flowed cyclonically and weakened to about 5 cm s^{-1}.

The variability of current flow during the R1 period (Figure 14) was weak (< 0.005 m^2 s^{-2}) relative to that observed during upwelling. There were two regions of relatively low eddy kinetic energy (~ 0.01 m^2 s^{-2}): one within the cyclonic feature next to

the Peninsula and the other at the western limb of the MBE. The variability inside the canyon was consistent with that during UW1.

During this wind relaxation, water temperature in the canyon was ~ 9.4^{o}, consistent with the temperature of the water contained within the eddy's circulation (Figure 15). The salinity inside the canyon (33.95) matched that of the MBE's southeastern region (Figure 16). Temperature and salinity values inside the canyon may have been influenced by the onshore movement of the eddy.

For the second upwelling period (UW2) from August 23-31, the model predicted a northwestward displacement of the MBE with its circulation center located at 36.70^{o}N, 122.60^{o}W. The model also forecasted a weak, cyclonic feature to develop between the anticylonic flow of the Monterey Bay Eddy and the poleward flow of the California Undercurrent, which was predicted to have maintained its structure across the mouth of the canyon. The presence of this feature appeared to force weak (~ 7 cm s^{-1}) anticyclonic circulation inside the canyon (Figure 17).

During UW2, the variability of current flow within the canyon was again minimal (Figure 18). The variability visualization, however, indicated relatively energetic (~ 0.01 m^{2} s^{-2}) regions along the slope associated with the location of the California Undercurrent.

The model temperature and salinity fields (Figures 19 and 20, respectively) indicated the poleward advection of the fresh (33.85), warm (> 9.4^{o} C) water mass that entered the model domain from the south. Flow from this body of water filled the bay, whose temperature and salinity values matched that of the water mass.

The second wind relaxation (R2) occurred September 1-3. For this period, the model forecasted the slight onshore movement of the MBE with its circulation centered near 36.70^{o}N, 122.55^{o}W (Figure 21). This eastward displacement of the eddy eliminated the closed cyclonic feature described in UW2. Additionally, the poleward flow of a coastal undercurrent was no longer apparent; it had been replaced by a relatively strong (10-15 cm s^{-1}) equatorward coastal current. The model predicted that the MBE and the

equatorward current would induce fast (~ 10 cm s^{-1}) currents flowing into and out of the canyon. Near the canyon head, flow was weaker (~ 5 cm s^{-1}), but maintained an anticyclonic course.

Unlike the other upwelling and relaxation periods where the model expected negligible current variability inside the canyon, the eddy kinetic energy calculation for R2 indicated a region of high variance (0.009 m^2 s^{-2}) relative to the surrounding area (Figure 22). This pocket of higher energy was located off the canyon's southern shelf.

Temperature and salinity plots showed that the eddy's anticyclonic circulation carried cool, fresh water into the canyon. In this brief wind relaxation period, water near the canyon's north and south edges was ~ 9.2^o and water in the middle of the canyon was even cooler at ~ 9.0^o (Figure 23). Salinity near the canyon's northern edge was ~33.90 and slightly fresher (~ 33.85) near the canyon's middle and southern shelf (Figure 24).

During the final upwelling event from September 4-6 (UW3), the model predicted the offshore movement of the MBE to 36.61^o N, 122.60^{o}W. Moving the eddy eastward enabled the formation of a weak, anticyclonic circulation center immediately northeast of the Monterey Peninsula (Figure 25). Under this arrangement of circulation features, currents entering and exiting the canyon retained weak, clockwise flow. Variability for this period was minimal (Figure 26).

The model's mean temperature field indicated that water inside the canyon was warm (~ 9.3^o C) with one cooler (~ 9.0^o C) pocket at the canyon head (Figure 27). The mean salinity field showed that fresh (~ 33.85) water forced southward along the coast by the eddy decreased the canyon's overall salinity to ~ 33.85 (Figure 28).

The mean current and current variability fields predicted by the model showed that the Monterey Bay submarine canyon was a region of consistently weak flow and low energy regardless of the prevailing atmospheric conditions. Beyond the offshore edge of the canyon, stronger, more variable currents were observed. For this reason, the submarine canyon may provide a favorable habitat for krill swarms because its reduced currents enable euphausiids to reduce their swimming energy output (Croll et al., 2005).

2. Model Currents, Temperature, and Salinity at 10 m

For the thirty day period from August 6, 2003 to September 6, 2003, the model's mean currents showed the presence of the Monterey Bay Eddy (MBE). Within the model current field, the MBE did not appear to be a meander of the California Current (CC) (Figure 29). The average position of the CC may have been further offshore, beyond the model's boundary. An upwelling favorable wind regime dominated the AOSN II experiment period; only six of the thirty days were characterized by wind relaxation (Ramp et al., 2007). The surface current pattern corroborated circulation driven by predominately northwesterly winds and exhibited persistent equatorward flow. The EKE field (Figure 30) showed the highest current variability (~ 0.06 m^2 s^{-2}) along the coast between the Monterey Peninsula and the Point Sur upwelling center. Overall variability in the bay was minimal (< 0.01 m^2 s^{-2}).

The PL33 low-pass tidal filter was also applied to the near-surface model data. The filtered current variability field (Figure 31) indicated a slight decrease in EKE in the high-energy region along the coast between the Peninsula and Point Sur. In this area, the maximum variability decreased from ~ 0.060 m^2 s^{-2} to ~ 0.047 m^2 s^{-2}. There was no observable change in variability inside the bay.

The model temperature and salinity fields (Figures 32 and 33) indicated cold (< 12^{o}C), saline (> 33.40) water originating near the Point Año Nuevo and Point Sur upwelling centers and being advected southward along the coast. Upwelled water from the north filled the bay and was retained in the bay's northern corner. Offshore water circulating in the MBE's anticyclonic flow was markedly warmer (> 16^o C) and fresher (< 33.10) than coastal water.

During UW1, the model current field (Figure 34) indicated that the MBE was located far enough offshore to allow a strong (~ 0.5 m s^{-1}) equatorward current to form between the eddy and the coast. This current was most energetic (EKE ~ 0.05 m^2 s^{-2}) along the coast of Big Sur, just north of the Point Sur upwelling center (Figure 35). Temperature and salinity plots (Figures 36 and 37) concurred that upwelling was more intense at Point Sur (SST < 11.5^o C and salinity > 33.60) than at Point Año Nuevo (SST ~ 12.5^o and salinity ~ 33.50). Water from the latter upwelling center flowing southward

into the bay appeared to be contained in the northern region of the bay, near Santa Cruz. The mean current field showed weak cyclonic rotation in this region of the bay which likely encircled the upwelled water in the bay's corner.

When the winds relaxed during R1, the mean current field (Figure 38) indicated that the MBE moved slightly onshore. This shoreward displacement of the eddy eliminated the strong equatorward current that was evident during UW1. Under this wind regime, a poleward current developed along the coast and flowed north into the bay. The EKE field (Figure 39) indicated that this current was not energetic (< 0.02 m^2 s^{-2}) compared to the prevailing eddy kinetic energy of the region. A stronger current (EKE ~ 0.04 m^2 s^{-2}) flowed from the north into the bay.

Between upwelling events, the water in the center of the bay was cool and salty (SST < 12^o C and salinity > 33.60). Temperature and salinity depictions (Figures 40 and 41) showed that cold, saline water located near Point Sur turned seaward and became entrained in the circulation of the MBE.

During the second upwelling event (UW2), the MBE moved offshore and continuous equatorward flow was again observed between the eddy and the coast (Figure 42). This southerly flow was most energetic near the Point Año Nuevo (EKE ~ 0.04 m^2 s^{-2}) and Point Sur (EKE ~ 0.06 m^2 s^{-2}) upwelling centers (Figure 43). Cold (< 12^o C) water flowed from the northern upwelling region into the bay (Figure 44). This upwelled water, however, was less saline (33.40) than the water upwelled during UW1 (Figure 45). Again, the inflowing water was retained in the bay's northern corner.

The mean current field for R2 (Figure 46) predicted the significant displacement of the MBE; it moved to the north and closer to the coast. Current flow from the eddy, upon encountering the bight at Point Año Nuevo, became divergent: a filament of strong (~ 20 cm s^{-1}) flow forced more defined cyclonic circulation in Monterey Bay. While EKE inside the bay was small (< 0.01 m^2 s^{-2}), equatorward flow from Point Año Nuevo was moderately energetic (~ 0.03 m^2 s^{-2}) (Figure 47). The mean temperature and salinity fields (Figures 48 and 49) showed cool (~ 13^o C) and comparatively fresh (33.30) water entering the bay from the north and encircling a pocket of cooler (~ 12^o C), saltier (33.40) water in the bay's northern corner.

September 4-6 was the last upwelling period of the AOSN II experiment. During this time, the MBE moved southward and the split flow into the bay dissipated. A small cyclonic feature developed along the coast north of the Point Sur upwelling center. Circulation from this feature (~ 20 cm s^{-1}) directed water from the upwelling region northward and into the bay (Figure 50). Current variability for this wind regime was negligible (< 0.02 m^2 s^{-2}) throughout the entire region (Figure 51). The mean temperature and salinity fields (Figures 52 and 53) substantiated the influx of comparatively fresh (33.30), cool (13^o C) water into the bay from the south; water in the area of the bay sheltered from incoming flow by the Monterey Peninsula remained slightly warmer (14^o C) and more saline (33.40).

The near-surface model current fields showed that during upwelling events, cool, salty water originating from the Point Año Nuevo upwelling center flowed southward and into the bay. Monterey Bay's location downstream from an upwelling center makes it an attractive environment for euphausiids because they feed in nutrient-rich surface water (Croll et al., 2005; Howard, 2005).

3. Threshold Current Analysis

Classified as plankton, krill cannot swim forcibly against ocean currents (Garrison, 2001, p. 247). They generally swim 0.2 to 1.0 body lengths per second (Ignatyev, 1999). (Adult krill of the species *T. spinifera* and *E. pacifica* are between 15 and 20 mm long (Howard, 2005).) In the Monterey Bay submarine canyon, euphausiids have been observed to aggregate in regions of weak currents (< 2 cm s^{-1}), probably to reduce their swimming energy output during schooling (Croll et al., 2005).

To discern whether current speeds inside the canyon were consistently weak enough to support krill accumulations, the model's current velocity field at 150 m was analyzed to determine for what percentage of each defined upwelling or relaxation period the current speed was less than or equal to a pre-determined threshold. The first threshold velocity considered was 5 cm s^{-1} because the model's mean current output at 150 m predicted currents of about that speed inside the canyon. The second threshold current velocity examined was 2 cm s^{-1} to represent the flow speed in which krill have been observed to accumulate.

Over the thirty day period from August 6 to September 6, the model current threshold field at 150 m (Figure 54) indicated that mean current speed inside the canyon was $\leq$ 5 cm s^{-1} about 35% of the time. In the canyon's northeastern corner, current speed did not exceed 5 cm s^{-1} for nearly 50% of the time. Equatorward flow along the continental shelf was less than or equal to the threshold speed for ~35% of the time over the thirty day period. Within the coherent flow of the Monterey Bay Eddy, the mean current speed was not observed to be less than the threshold. Inside the canyon, flow speed was $\leq$ 2 cm s^{-1} for ~ 20% of the month-long period (Figure 55). At the surface, the model did not predict the mean current speed to fall below 5 cm s^{-1} (Figure 56).

During the first upwelling period, mean current speed inside the canyon was $\leq$ 5 cm s^{-1} for roughly half of the time (Figure 57). Near the Point Sur upwelling center, the currents were less than the threshold speed for about 35% of the fortnight-long upwelling event. After decreasing the threshold current speed to 2 cm s^{-1}, the model indicated that mean flow speed was observed below the limit for ~ 10% of the period (Figure 58).

The model predicted that currents in the canyon's center were $\leq$ 5 cm s^{-1} for about 80% of the first wind relaxation (Figure 59). Toward the mouth of the canyon, current speed did not exceed 5 cm s^{-1} about 45% of the time. At the 2 cm s^{-1} threshold, the model showed that currents were less than the limit ~ 30% of the time at a small region near the canyon's mouth (Figure 60).

In the middle of the canyon, flow speed was $\leq$ 5 cm s^{-1} for nearly half of the second upwelling event and $\leq$ 2 cm s^{-1} for less than 10% of it (Figures 61 and 62). Within the shoreward region of the MBE's circulation, current speed was less than the 5 cm s^{-1} threshold speed for ~ 40% of the period.

During the second wind relaxation, the mean current speed of the eddy's southward flow was $\leq$ 5 cm s^{-1} more than 60% of the time (Figure 63). The model also showed that currents inside the canyon were less than the threshold for about 40% of the relaxed wind regime. The speed of circulation inside the canyon fell below 2 cm s^{-1} during ~ 15% of this period (Figure 64).

Mean current speed at the canyon's middle was $\leq$ 5 cm s^{-1} for about 75% of the third upwelling event (Figure 65). Flow within the warm, fresh water mass along the

coast south of Big Sur was weak for more than 80% of the period. The model predicted that this body of water had currents ≤ 2 cm s^{-1} for ~ 30% of the upwelling period (Figure 66). Flow inside the canyon was less than this threshold for ~ 30% of the three-day wind event.

4. Diffusivity from Model EKE

While diffusion describes the net movement of particles from an area of higher concentration to an area of lower concentration until equilibrium is reached, diffusivity describes the rate at which particles move away from their initial position. A master's thesis by Giannetti (1993) codified diffusivity values for several regions of the northeast Pacific Ocean including open ocean, upwelling filaments, and the eastern boundary current. Giannetti (1993) concluded that average diffusivities scale with the eddy kinetic energy of the mean current field; diffusivity is greater in regions of higher energy (p. 49). Tables 1 and 2 below were compiled from the EKE values predicted by the NCOM ICON model (as described in sections 1 and 2 above) and from the diffusivity values based on EKE in Giannetti's thesis (p. 57).

At 150 m depth (Table 2), EKE inside the canyon was less than 0.005 m^2 s^{-2} (or 50 cm^2 s^{-2}) for all wind regimes between August 6 and September 6, 2003. The corresponding average diffusivity inside the canyon was 1.7 x 10^7 cm^2 s^{-1}. Current flow beyond the canyon mouth was more energetic with EKE values as high as 160 cm^2 s^{-2} and the resultant average diffusivity exceeding 6.0 x 10^7 cm^2 s^{-1}.

During the prolonged upwelling period from August 6-19, the model predicted that the most energetic flow was contained within the anticyclonic circulation of the Monterey Bay Eddy. The average diffusivity at the eddy's core surpassed 6.0 x $10^7 cm^2$ s^{-1} but diminished to ~ 3.1 x $10^7 cm^2$ s^{-1} at the anticyclone's perimeter. When the winds relaxed, the average diffusivity inside the eddy decreased to 4.2 x 10^7 cm^2 s^{-1}. For UW2, R2, and UW3, the highest average diffusivity (> 6 x 10^7 cm^2 s^{-1}) within the model domain was located near the Point Sur upwelling center.

Near the surface (Table 3), model-predicted EKE values inside Monterey Bay were less than 100 cm^2 s^{-2} between August 6 and September 6. The associated average diffusivity for the bay was less than 4.2 x 10^7 cm^2 s^{-1}. Outside the bay, the model

expected more energetic flow (EKE > 400 cm^2 s^{-2}) and higher average diffusivity (> 6 x 10^7 cm^2 s^{-1}) for all periods except UW3. During the third upwelling event, the highest EKE (~ 100 cm^2 s^{-2}) was associated with the outer circulation of the MBE; the average diffusivity for this area was 4.2 x 10^7 cm^2 s^{-1}.

Low rates of diffusivity suggest particle retention in regions of low eddy kinetic energy. Accordingly, planktonic organisms would be expected to accumulate in less-energetic areas, such as Monterey Bay and its submarine canyon.

Optical backscatter is a measure of particles suspended in the water column. During the AOSN II experiment, the MBARI Dorado AUV collected ocean optical backscatter (676 nm) data in Monterey Bay from the surface to 255m. Although the identity of the floating particles was not reported, zooplankton and phytoplankton are likely constituents of the suspended particulate matter. From August 6 to September 6, the AUV data indicated regions of higher optical backscatter at the surface in the northern and southern portions of the bay (Figure 67). Along the coast from Santa Cruz to Moss Landing, backscatter values ranged from 0.005 m^{-1} to 0.007 m^{-1}; from Marina to Monterey, backscatter values reached 0.0082 m^{-1}. In the center of the bay, backscatter values were slightly lower, ~ 0.0035 m^{-1}. Around 150 m depth (Figure 68), optical backscatter was highest inside the canyon (0.0018 m^{-1} to 0.0028 m^{-1}) and over the continental shelf north of the canyon (up to 0.0032 m^{-1}). Toward the open ocean, observed backscatter decreased to 0.0013 m^{-1}. The Dorado AUV data support the premise that floating matter accumulates in regions of low energy and low diffusivity.

Depth = 150 m	Max EKE ($cm^2 sec^{-2}$) inside Bay	Diffusivity (10^7 cm^2 s^{-1}) inside Bay	Max EKE ($cm^2 sec^{-2}$) outside Bay	Diffusivity (10^7 cm^2 s^{-1}) outside Bay
6 AUG – 6 SEP	< 50	< 1.7	160	> 6
UW1	< 50	< 1.7	170	> 6
R1	< 50	< 1.7	100	4.2
UW2	< 50	< 1.7	100	4.2
R2	< 50	< 1.7	< 50	< 1.7
UW3	< 50	< 1.7	< 50	< 1.7

Table 2. Maximum EKE and Diffusivity values at 150 m.

Depth = 10 m	Max EKE ($cm^2 sec^{-2}$) inside Bay	Diffusivity (10^7 cm^2 s^{-1}) inside Bay	Max EKE ($cm^2 sec^{-2}$) outside Bay	Diffusivity (10^7 cm^2 s^{-1}) outside Bay
6 AUG – 6 SEP	< 100	< 4.2	600	> 6
UW1	< 100	< 4.2	500	> 6
R1	< 100	< 4.2	400	> 6
UW2	< 100	< 4.2	700	> 6
R2	< 100	< 4.2	500	> 6
UW3	< 100	< 4.2	100	4.2

Table 3. Maximum EKE and Diffusivity values at 10 m.

5. Model Water Mass Analysis

Two distinct locations (see Figure 3) within the NCOM ICON model domain were analyzed for temperature, salinity, and density because plankton accumulate at convergence zones and at boundaries between water types (Sverdrup et al., 2005, p. 398). Location 1 (36.71° N, 122.20° W) was outside of Monterey Bay in a region where currents were strong (> 20 cm s^{-1}) at the surface and at 150 m. Location 2 (36.79° N, 121.99° W) was in the submarine canyon, a region of weak current flow (< 10 cm s^{-1}) at

the surface and at depth. The currents speeds at the two locations were determined from the model's mean current fields at both 10 m and 150 m.

Time series for temperature at both locations (Figure 69) showed that at Location 1 water temperature at the surface ranged from 13-16^{o} C during the first upwelling event through the end of the first wind relaxation. At the onset of the second upwelling regime, the water temperature increased to ~ 18^{o} before decreasing to ~ 13.5^{o} during the second wind relaxation. At 150 m depth, the water temperature ranged between 8.5 and 9.5 degrees. Water temperature was the highest (> 9^{o} C) during R1. Time series for salinity at both locations (Figure 70) indicated that the water at Location 1 was most saline at 150 m with salinity values ranging from 33.80 to 34.00. The surface water was fresher (32.90 to 33.50) than the deep water. An influx of comparatively salty water (> 33.20) occurred during each of the three upwelling events.

At Location 2, sea surface temperature (SST) ranged from 10.5 to 15.5 ^{o}C, cooler than SST outside the bay. Surface water temperature was the lowest (< 12^{o} C) after UW1. At 150 m, the water temperature was between 9.0 and 9.8 ^{o}C. Surface salinity values ranged from 33.10 to 33.60. The water was most saline (> 33.45) during UW1. At depth, the water inside the canyon was very salty (> 33.81) for the entire record with the highest salinity values (> 34.00) during UW1.

Temperature and salinity (T-S) scatter plots with isopycnals were created to analyze the interaction of the water masses at Locations 1 and 2 over the entire period and during the upwelling and wind relaxation events (Figures 71 to 76). At 150 m, the interaction between distinct water masses was apparent. During UW1, cool (8.6^{o} to 9.4^{o} C), less saline (33.85 to 34.00) water from outside the bay mixed with warmer (8.8^{o} to 9.7^{o} C), more saline (33.85 to 34.05) water inside the bay. The density anomaly of both water masses was ~ 26.9 kg m^{-3}. T-S diagrams for the two wind relaxation periods indicated that two water masses of discrete temperature and salinity characteristics existed at Locations 1 and 2. The model's T-S data for third upwelling event did not show the interaction of water from outside the bay with water inside the bay. Although both water masses were of similar salinity (33.81 to 33.90) and density anomaly (~ 26.9

kg m^{-3}), they were different in temperature. The water at Location 1 was colder (8.8° to 9.0° C) than the water at Location 2 (9.2° to 9.4° C).

Near the surface (10 m), water masses with distinct temperature, salinity, and density characteristics were observed to mix during upwelling events and to separate during wind relaxations (Figures 77 to 82). Throughout the first upwelling period, warmer (10.5° to 16.5° C) fresher (32.90 to 33.50) less dense (< 25.2 kg m^{-3}) water from Location 1 mixed with cooler (10.0° to 15.5° C) saltier (33.20 to 36.60) more dense (> 25.1 kg m^{-3}) water from Location 2. During the first wind relaxation, the water outside the bay was distinct from water inside the bay. The water mass at Location 1 was warmer (> 13° C), fresher (< 33.50), and less dense (< 25.1 kg m^{-3}); the body of water at Location 2 was cooler (< 13° C), saltier (> 33.50) and more dense (> 25.1 kg m^{-3}). T-S scatter plots for UW2 and UW3 and for R2 also indicated the interaction of warm, fresh water from outside the bay with cool, salty water inside the bay during upwelling and the separation of these water masses during wind relaxation.

Vertical T-S plots for all depths at both Location 1 (Figure 83) and Location 2 (Figure 84) were created to analyze the entire water column for differences in temperature, salinity, and density. The water mass outside the bay (Location 1) was less stable than that inside the bay (Location 2). At Location 1, the most variability occurred in less dense (< 26.04 kg m^{-3}) water where temperature values ranged from 8° to 20° C and salinity values from 32.60 to 33.51. At Location 2, the water mass was more stable; moderate variability in temperature and salinity occurred when the density anomaly was < 25.09 kg m^{-3}. Temperature values ranged from 10° to 19° C and salinity values from 33.10 to 33.60. The consistency of water properties at Location 2 suggests that water inside Monterey Bay experiences less flushing than water outside the bay.

B. BIOLOGICAL FACTORS

1. Primary Production

As recounted in Garrison (2001, p. 250-255) and Sverdrup et al. (2005, p. 374-376), phytoplankton is a descriptive term referring to the myriad plant-like species that live suspended in the water column. These organisms comprise the autotrophic

component of marine food webs because they create their own energy. Their cells contain the pigment chlorophyll which ensnares solar energy for use in photosynthesis, the process by which carbon dioxide and water are converted into organic compounds and water ($6\ H_2O + 6\ CO_2 \rightarrow C_6H_{12}O_6 + 6\ O_2$). The term *primary productivity* describes the rate at which biomass (grams of organic carbon per unit area) is created from photosynthesis. Primary producers are integral to marine food webs because they provide food energy to higher trophic levels; the primary consumers that feast upon phytoplankton are eaten by secondary consumers, which, in turn, are devoured by tertiary consumers, and so on.

2. Upwelling and Primary Production

Regions characterized by wind-driven upwelling are twice as productive as coastal areas and six times more productive than the open ocean (Sverdrup et al., 2005). Additionally, wind-forced oceanographic events are connected with increases in chlorophyll concentration at the surface (Croll et al., 2005). Service et al. (1998) concluded that upwelling affects phytoplankton distribution in Monterey Bay. Along the Northern California coast, upwelling occurs when northwesterly along-shore winds coupled with Ekman transport move surface water away from the land so that cold, nutrient-rich water can rise from below (Enriquez & Friehe, 1995). The upwelled water, fortified with the inorganic nutrients (nitrogen and phosphorus compounds) required for primary production, becomes entrained in the southerly flow of the California current (Fiedler et al., 1998). Cold surface water that has been upwelled north of Monterey Bay moves equatorward and across the mouth of the bay at about 20 cm s^{-1}; when the water reaches the bay, it has been in the euphotic zone for two to four days and its biomass production rate is high (Pennington & Chavez, 2000). Phytoplankton blooms, or periods of high productivity and rapid reproduction, have been observed to occur six to ten days after an upwelling event (Service et al., 1998; Fiedler et al., 1998). The high level of primary production in upwelled waters might explain the prevalence of krill, which eat phytoplankton and undersized zooplankton (Fiedler et al., 1998).

The Regional Navy Coastal Ocean Model (~ 9 km horizontal resolution) modeled chlorophyll concentration, a proxy for phytoplankton abundance (Sverdrup et al., 2005, p.

374), and currents during the AOSN II experiment. During the upwelling event from August 6 to August 19, 2003, the model showed the gradual increase in chlorophyll concentration and the equatorward advection of chlorophyll-laden water from the Point Año Nuevo upwelling center into Monterey Bay. For August 6, the first day of upwelling, the model predicted that the chlorophyll concentration near the upwelling center was about 7 mg m^{-3} and about 1 to 2 mg m^{-3} in the bay (Figure 85). Model runs for the remainder of UW1 predicted the southerly spread (at ~ 50 cm s^{-1}) of increased chlorophyll concentration (3 to 5 mg m^{-3}) along the California coast and into the northwestern portion of Monterey Bay (Figures 86, 87, and 88). The highest values of chlorophyll concentration (~ 10 mg m^{-3}) were observed near the upwelling centers (Point Año Nuevo and Point Sur) on August 12 and 13, approximately six days after the onset of upwelling (Figure 89).

The first wind relaxation began on August 20. On this day, the model indicated that chlorophyll concentration in the bay and along the coast was reduced to only 0.5 mg m^{-3} (Figure 90). Current flow into the bay was from the south at 50 cm s^{-1}. The second upwelling event lasted from August 23 to August 31. During this period, the model forecasted strong current flow (> 50 cm s^{-1}) to enter Monterey Bay from the north. The equatorward advection of increased chlorophyll concentration was again apparent. The amount of chlorophyll in the bay increased from < 1 mg m^{-3} on the first day of upwelling to 1.5 – 3.0 mg m^{-3} by the end of the period.

The higher resolution NCOM ICON model does not predict ecosystem data, but does provide a more accurate depiction of how ocean currents might transport productive water into Monterey Bay. While the Regional NCOM poorly resolved current magnitude and direction inside the bay, NCOM ICON predicted small area circulation patterns. NCOM ICON indicated that strong (~ 50 cm s^{-1}) equatorward flow from Point Año Nuevo contributed to the formation of a weak (< 10 cm s^{-1}) cyclonic feature in the northern portion of the bay during UW1, UW2, and UW3. Southerly flow that did not become part of the feature maintained its course and speed into the southern portion of the bay. During the two wind relaxations, NCOM ICON continued to predict cyclonic circulation (~ 10 cm s^{-1}) in the northern region of the bay. The chlorophyll concentration

fields discussed above indicated that chlorophyll levels were highest in northern portion of Monterey Bay, the region where the cyclonic circulation feature was expected.

The Regional NCOM and the NCOM ICON both predicted strong (~ 50 cm s^{-1}) equatorward flow along the coast from the Point Año Nuevo upwelling center. Cool, nutrient rich water upwelled at this point on August 6 would be expected to flow southward at ~ 26.8 miles day^{-1} (~ 43.2 km d^{-1}). It would reach the northern end of the bay (~ 21 mile transit) in about one day and would reach the southern end of the bay (~ 63 mile transit) after two days. If phytoplankton blooms occur six to ten days after the onset of upwelling (Service et al., 1998; Fiedler et al., 1998), then higher levels of chlorophyll concentration (i.e. primary production) would be expected between August 12 and August 16. The Regional NCOM predicted peak chlorophyll concentration values (3.0 mg m^{-3}) for Monterey Bay beginning August 12.

3. Macronutrient Availability and Primary Production

Ramp et al. (2007) described the use of Autonomous Underwater Vehicles (AUVs) during the AOSN II experiment to collect biogeochemical data. The Dorado AUV from the Monterey Bay Aquarium Research Institute (MBARI) was the largest vehicle used. In August of 2003, the Dorado AUV conducted several canyon axis surveys (from Moss Landing to MBARI's M2 mooring) profiling down to 250 m depth (Figure 91). The vehicle's onboard instrumentation included a fluorometer, a nitrate sensor, and a conductivity, temperature, and depth (CTD) sensor. By following a programmed sinusoidal course through the water column of the survey area, the vehicle collected three-dimensional water temperature, salinity, pressure, dissolved gas concentration, and chlorophyll concentration data.

Sverdrup et al. (2005, p. 380) noted that the abundance of primary producers can be determined from fluorometer data. A fluorometer is an instrument that indicates biomass concentration by measuring the amount of fluorescence attributed to the water's plant-like material. The device produces excitation beams at wavelengths that will cause the chlorophyll pigment to fluoresce. It measures the intensity of the fluorescence to provide a direct measure of the chlorophyll (phytoplankton biomass) in a given body of water. It must be noted, however, that near local apparent noon, fluorometer output may

be reduced (Antal et al., 2001) due to a temporary reduction in photosynthesis caused by the downward migration of phytoplankton cells (Tilzer, 1973).

The availability of dissolved nutrients influences phytoplankton abundance. In addition to sunlight, phytoplankton require the macronutrients nitrate (NO_3^-) and phosphate (PO_4^{3-}), and the micronutrient iron for growth. Nitrogen is important for amino acid and protein synthesis while phosphorus is necessary for energy reactions, cell membrane functionality, and the formation of nucleic acids. During periods of high primary productivity, phytoplankton deplete the ocean's macronutrient supply (Garrison, 2001, p. 251) and, accordingly, maximum nitrate uptake is concurrent with maximum biomass production (Fiedler et al., 1998).

Dorado AUV data from AOSN II showed that the concentration of chlorophyll and of nitrate at the surface changed over the course of the experiment. On August 12 (Figure 92), six days after the onset of the first upwelling event, chlorophyll fluorescence was 0.6 x 10^{-3} rfu (relative fluorescence units) from the surface to ~ 25m depth at the head of the Monterey Bay Submarine Canyon. Toward the continental shelf, chlorophyll fluorescence at the surface ranged from 0.2 x 10^{-3} to 0.4 x 10^{-3} rfu. For all depths greater than ~ 30 m, rfu values were near zero. The lowest levels of nitrate (< 10 μM) corresponded to the areas with the highest chlorophyll fluorescence. Nitrate availability increased with depth and the highest concentration (> 30 μM) was at the greatest depth.

Chlorophyll fluorescence nearest the canyon head ranged from 0.5 x 10^{-3} rfu to 0.8 x 10^{-3} rfu on August 20 (Figure 93), the first day of wind relaxation. Toward the mouth of the canyon, surface chlorophyll fluorescence did not drop below 0.2 x 10^{-3} rfu. The lowest nitrate concentration (< 10 μM) occurred in the areas of the highest chlorophyll concentration. August 26 fell three days after the beginning of the second upwelling event. On this day (Figure 94), the Dorado AUV data showed that chlorophyll fluorescence values at the surface ranged from 0.1 x 10^{-3} to 0.5 x 10^{-3} rfu with the lowest value 0.1 x 10^{-3} rfu nearest the shore. The minimum nitrate concentration (5 μM) corresponded to the region of the lowest chlorophyll fluorescence, possibly indicating that this area had been depleted of its nutrients and, therefore, unable to sustain increased primary productivity.

The AUV data substantiate the theory that the surface waters of Monterey Bay, when imbued with nutrient rich water from nearby upwelling centers, can support high levels of primary production.

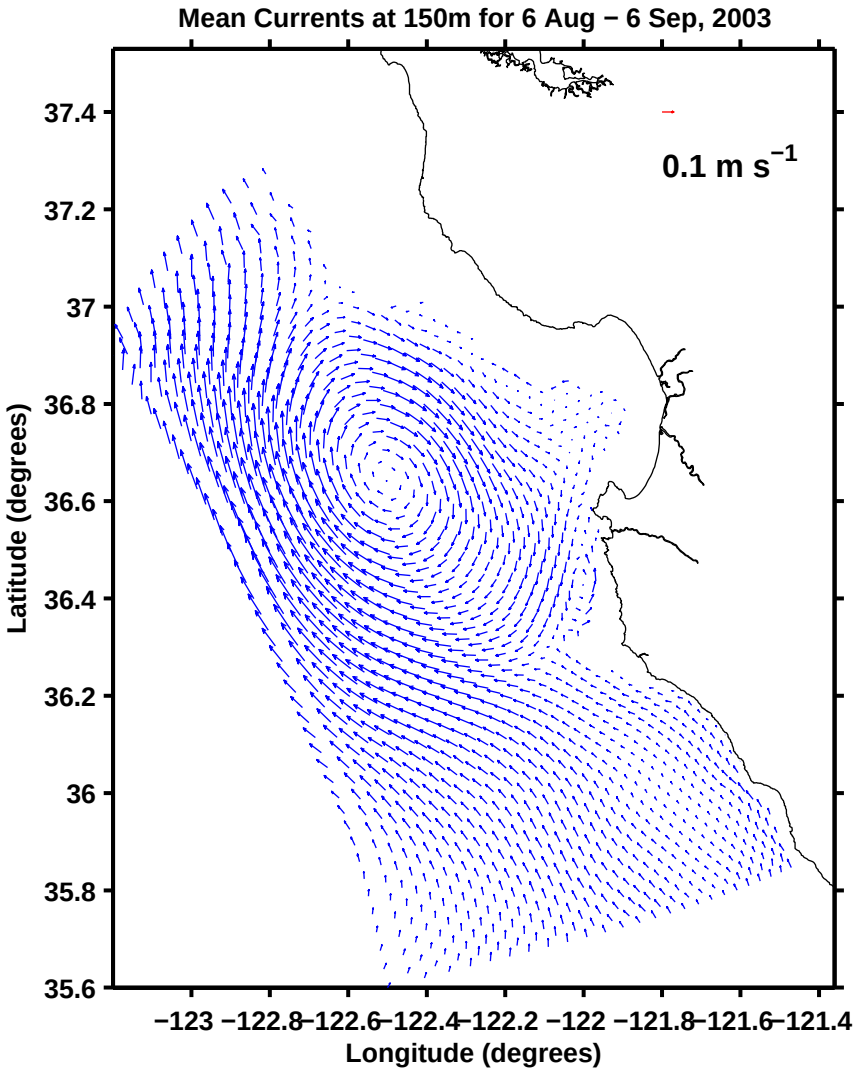

Figure 4. Model mean currents at 150 m for August 6 - September 6, 2003.

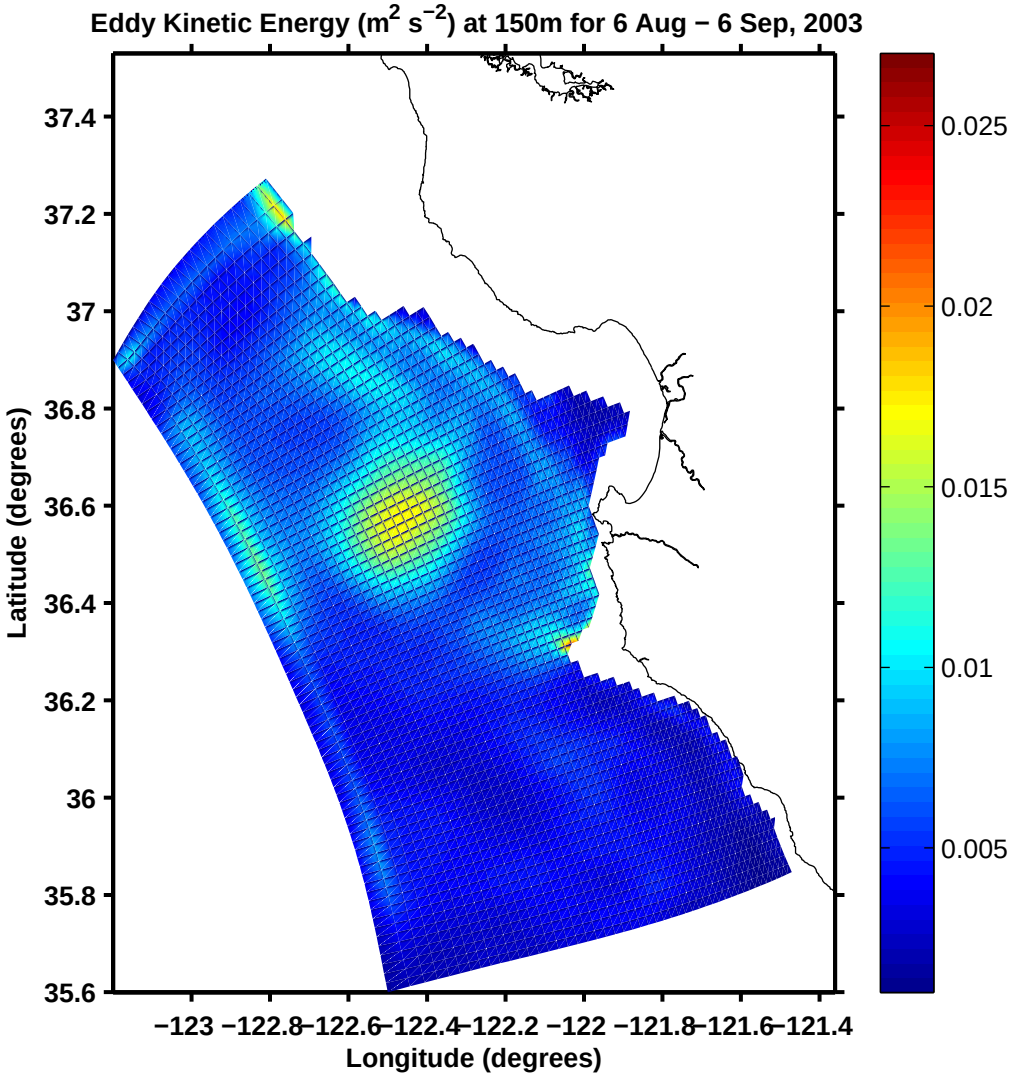

Figure 5. Model EKE at 150 m for August 6 -September 6, 2003.

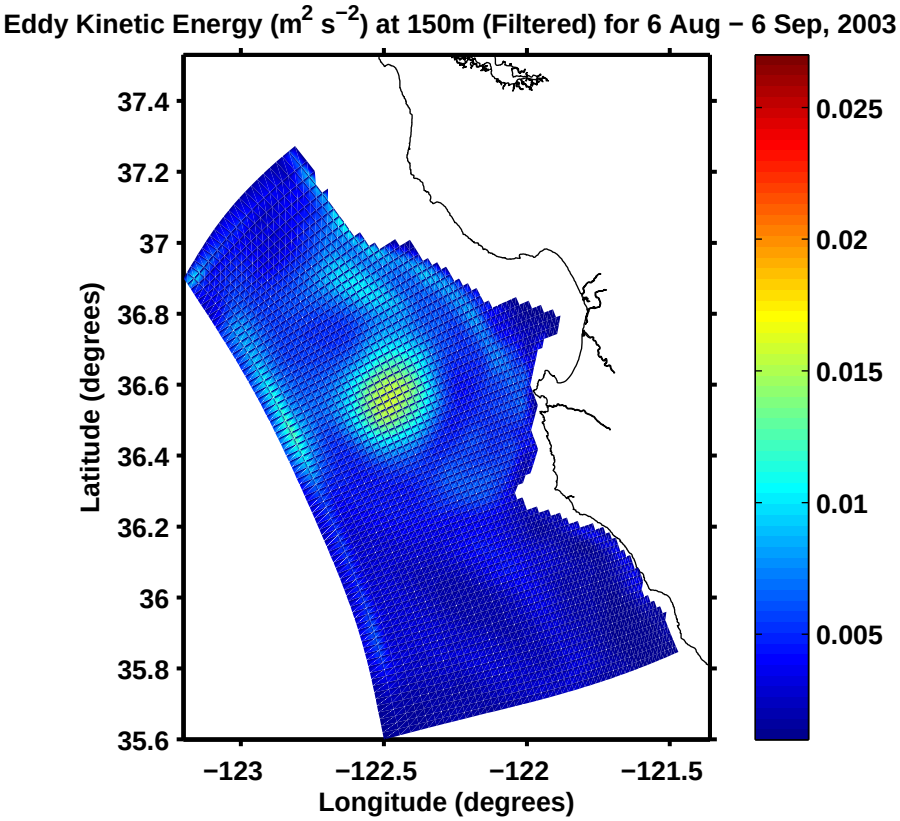

Figure 6. As in Figure 5 except for low-pass tidal filter applied to model data.

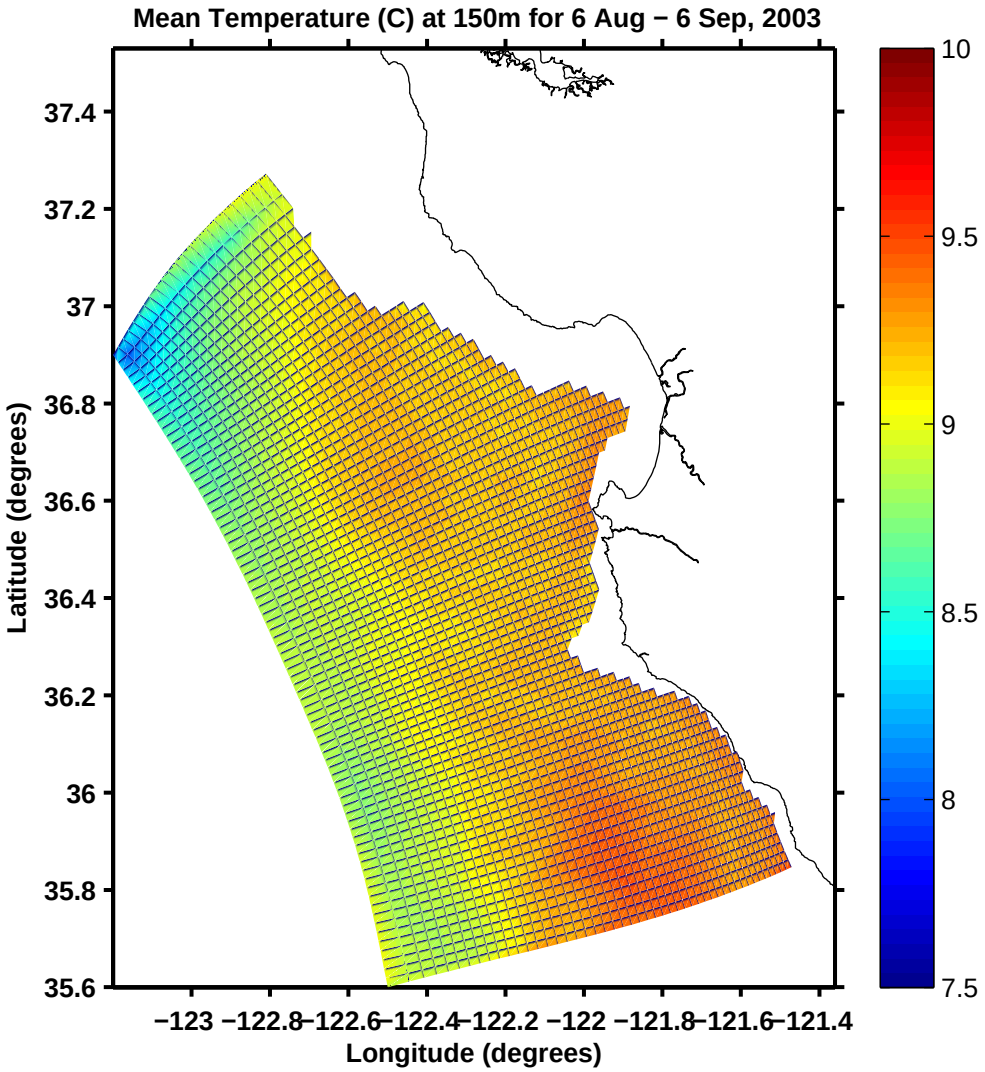

Figure 7. Model mean temperature at 150 m for August 6 - September 6, 2003.

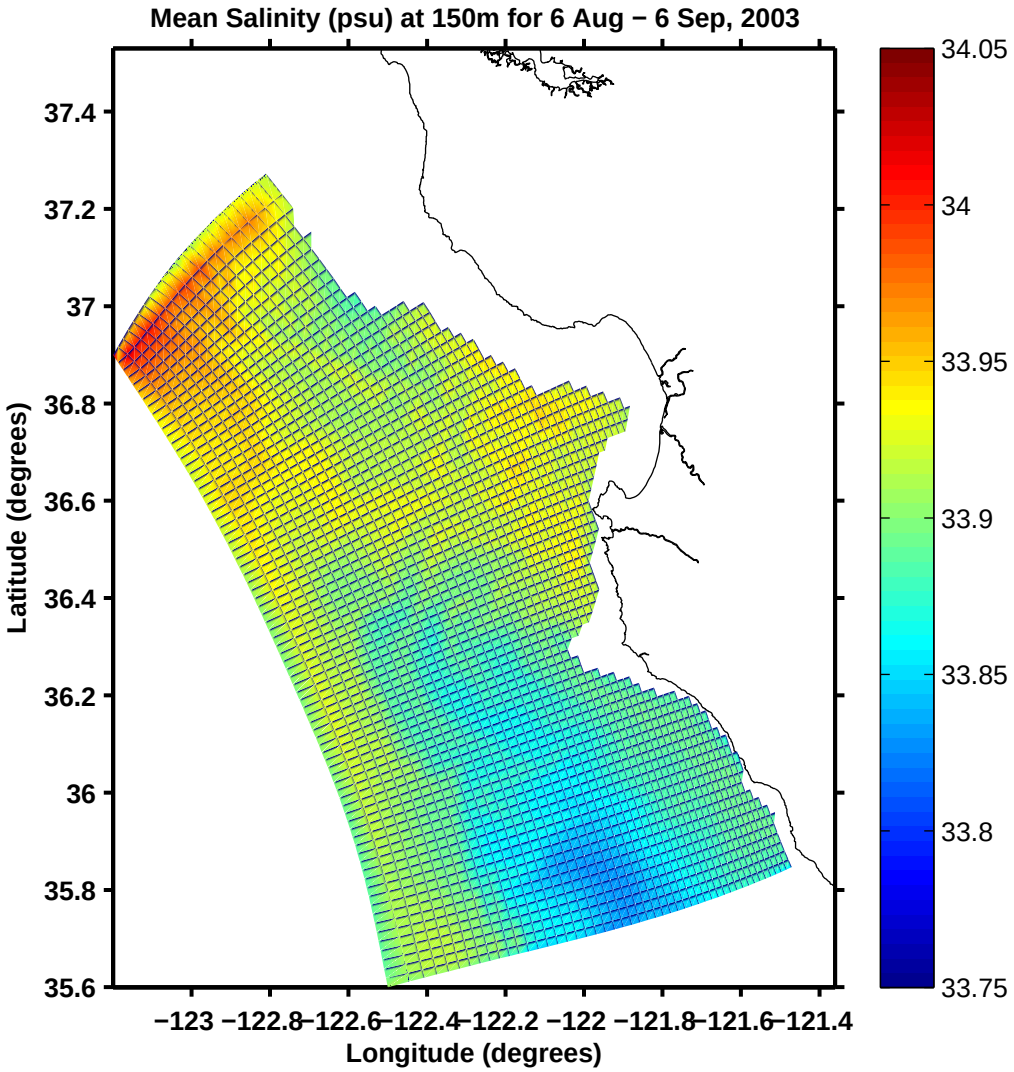

Figure 8. Model mean salinity at 150 m for August 6 -September 6, 2003.

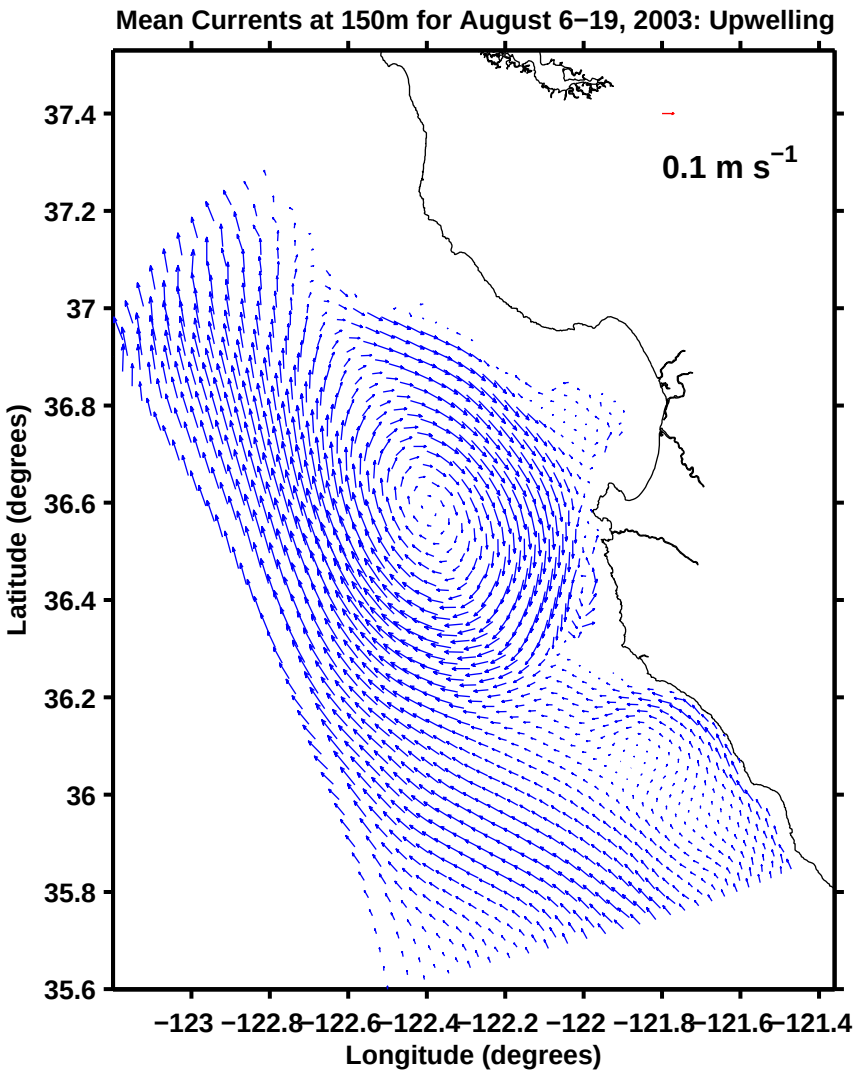

Figure 9. Model mean currents at 150 m for UW1.

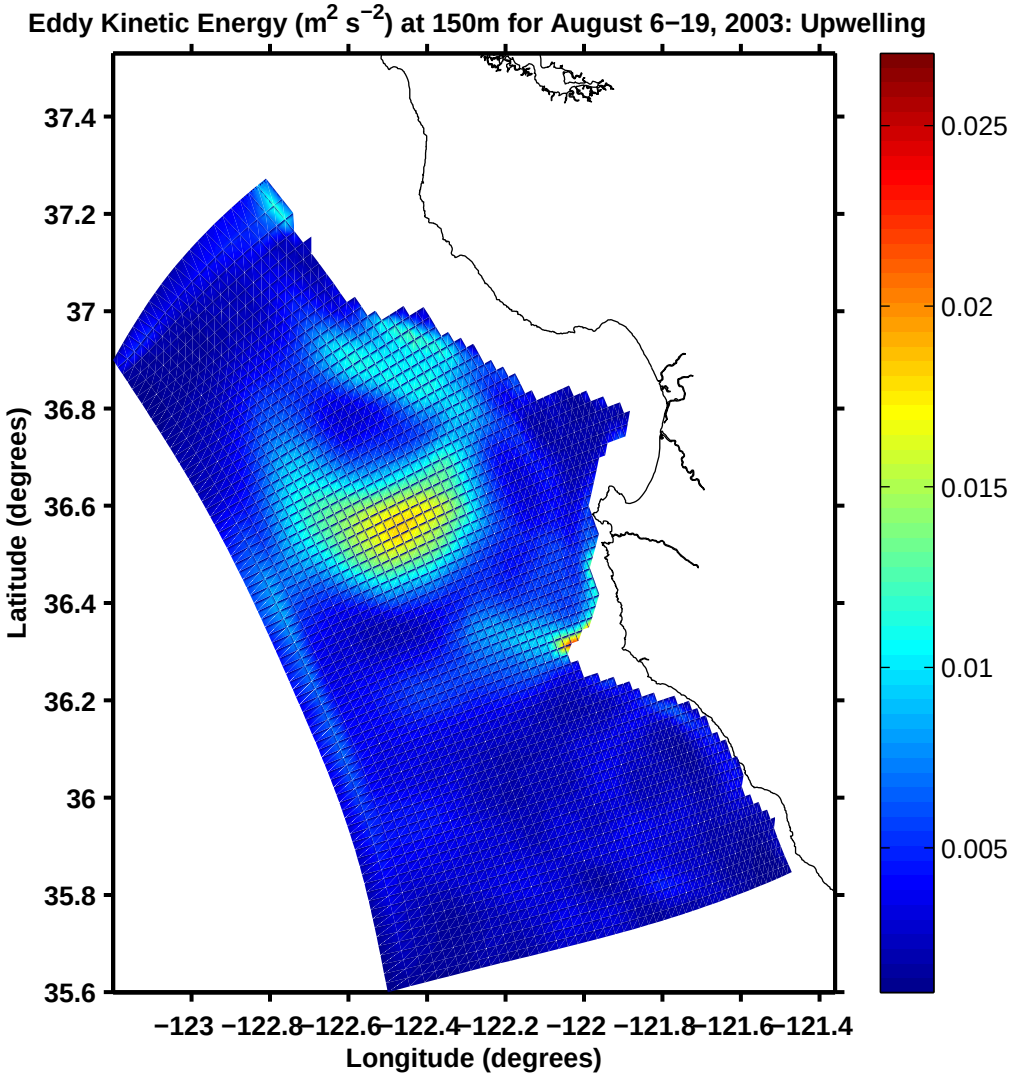

Figure 10. Model EKE at 150 m for UW1.

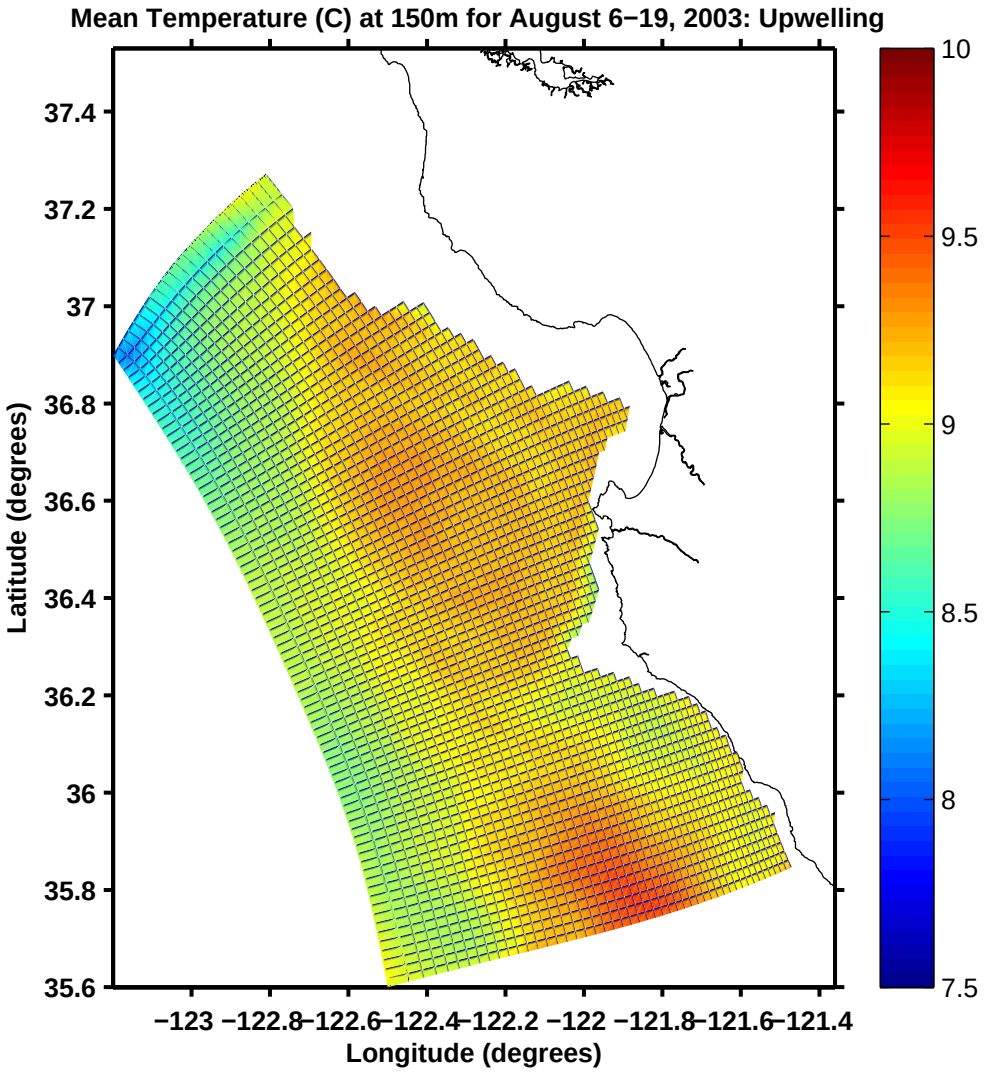

Figure 11. Model mean temperature at 150 m for UW1.

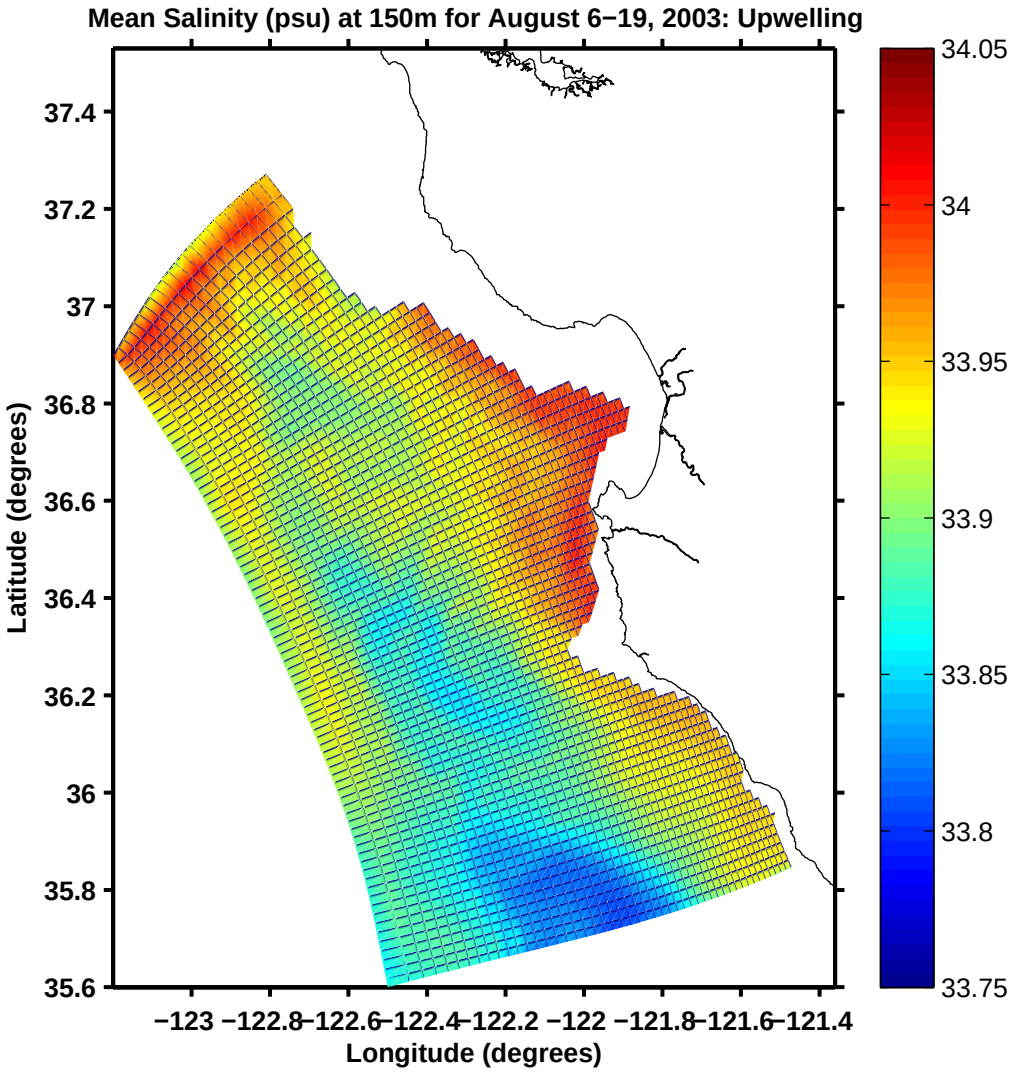

Figure 12. Model mean salinity at 150 m for UW1.

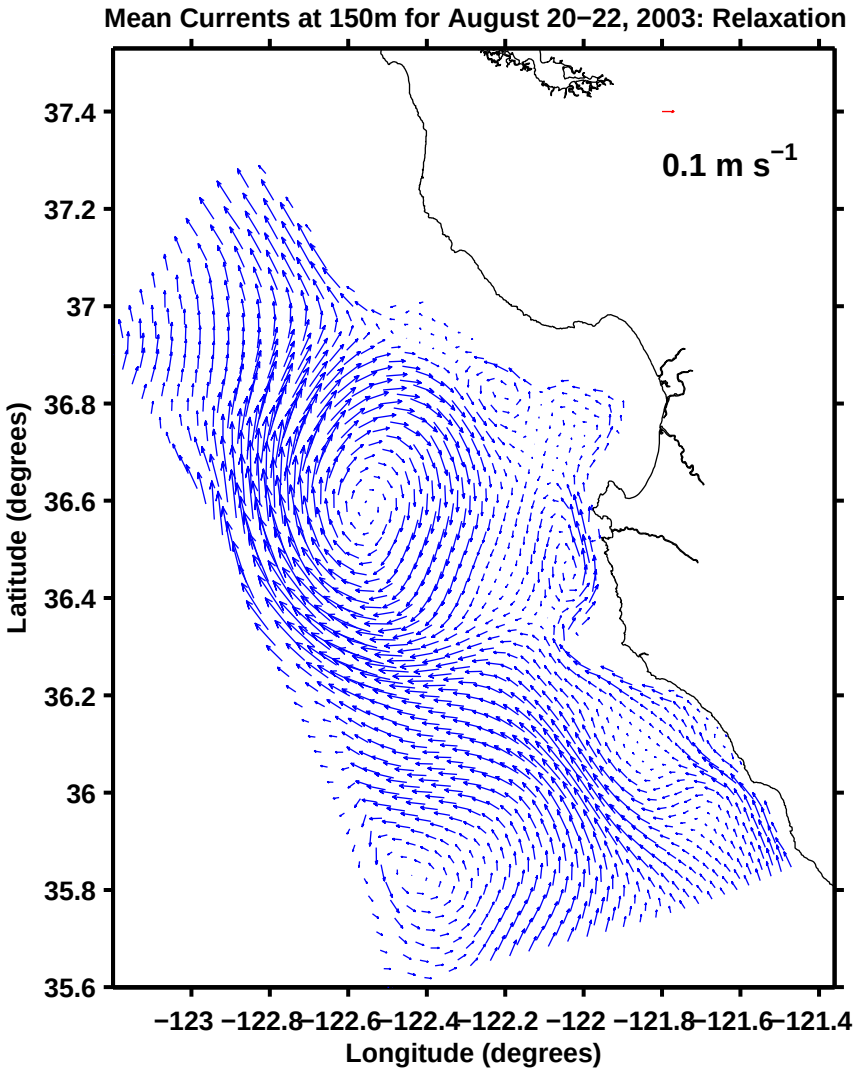

Figure 13. Model mean currents at 150 m for R1.

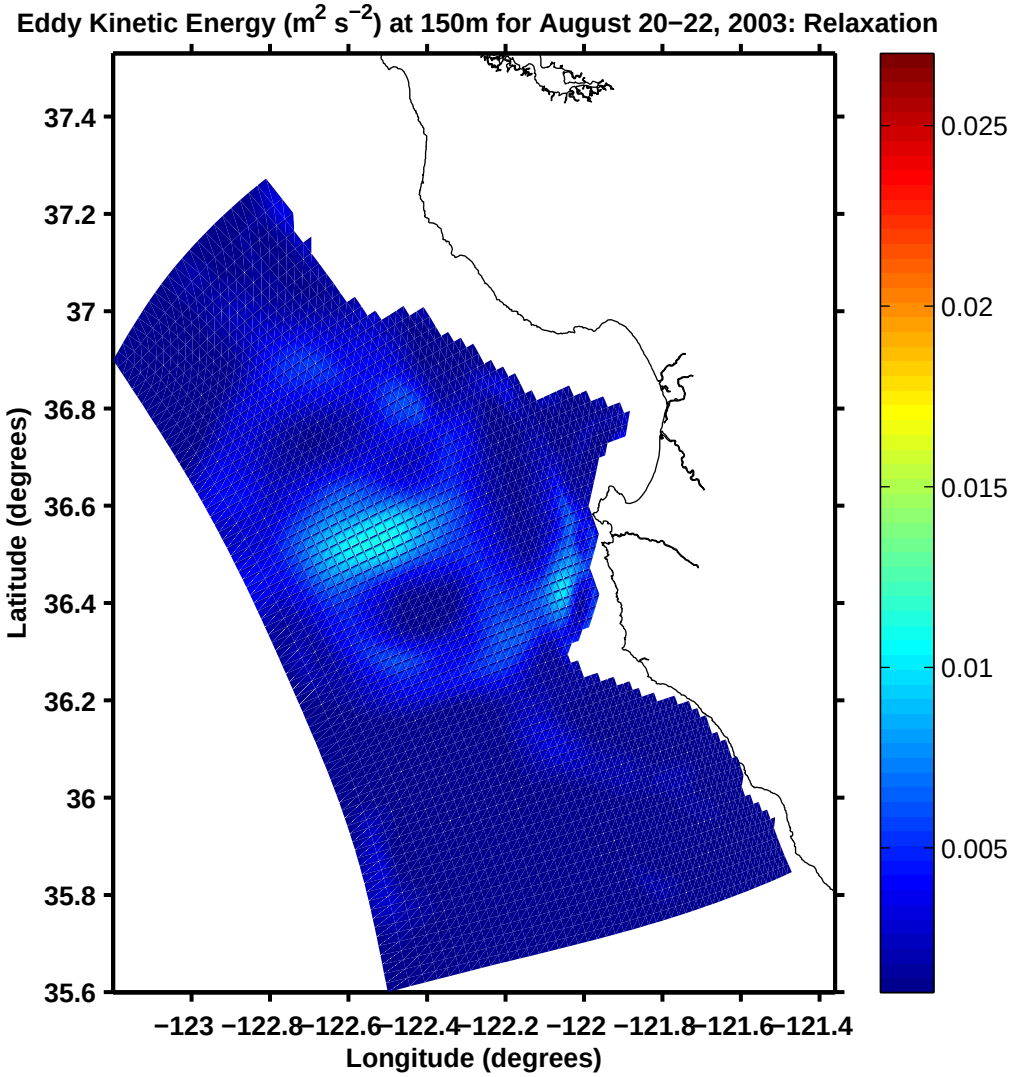

Figure 14. Model EKE at 150 m for R1.

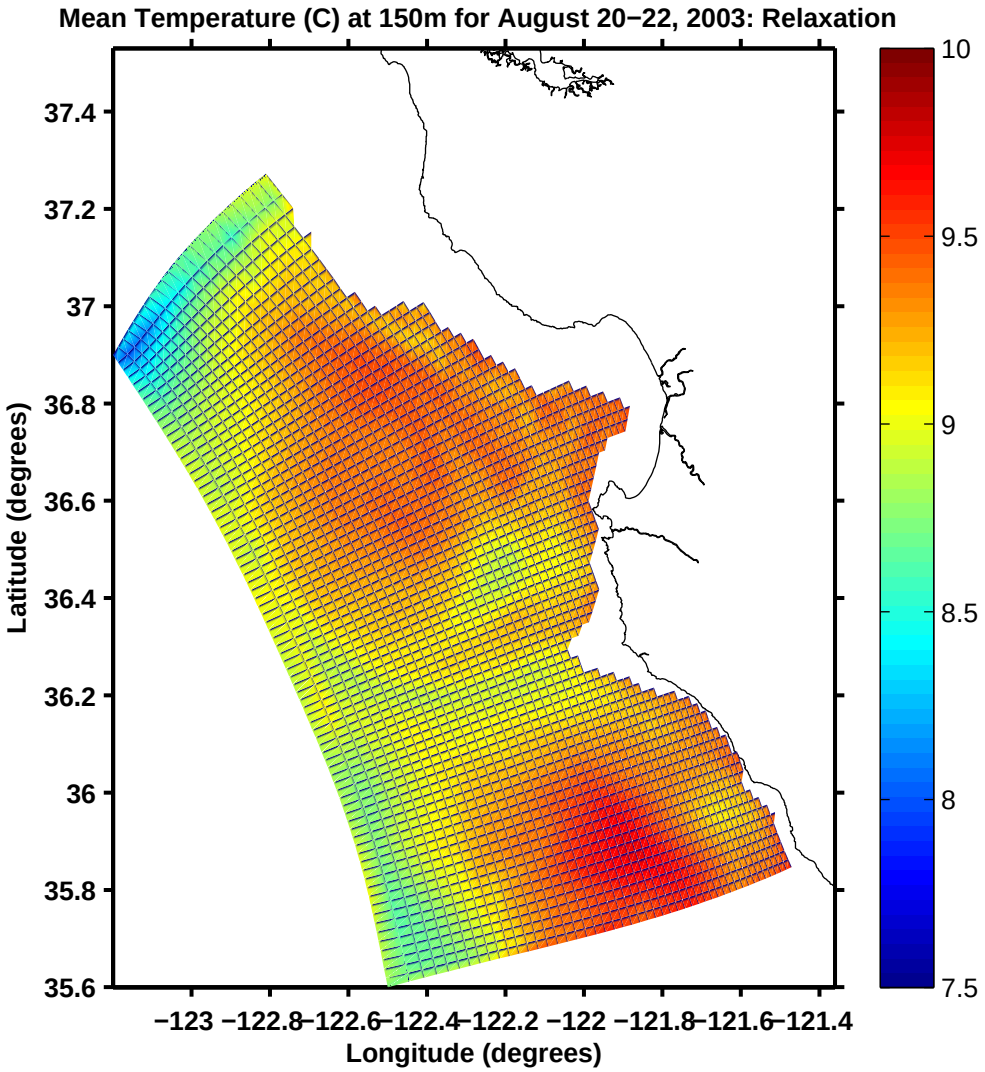

Figure 15. Model mean temperature at 150 m for R1.

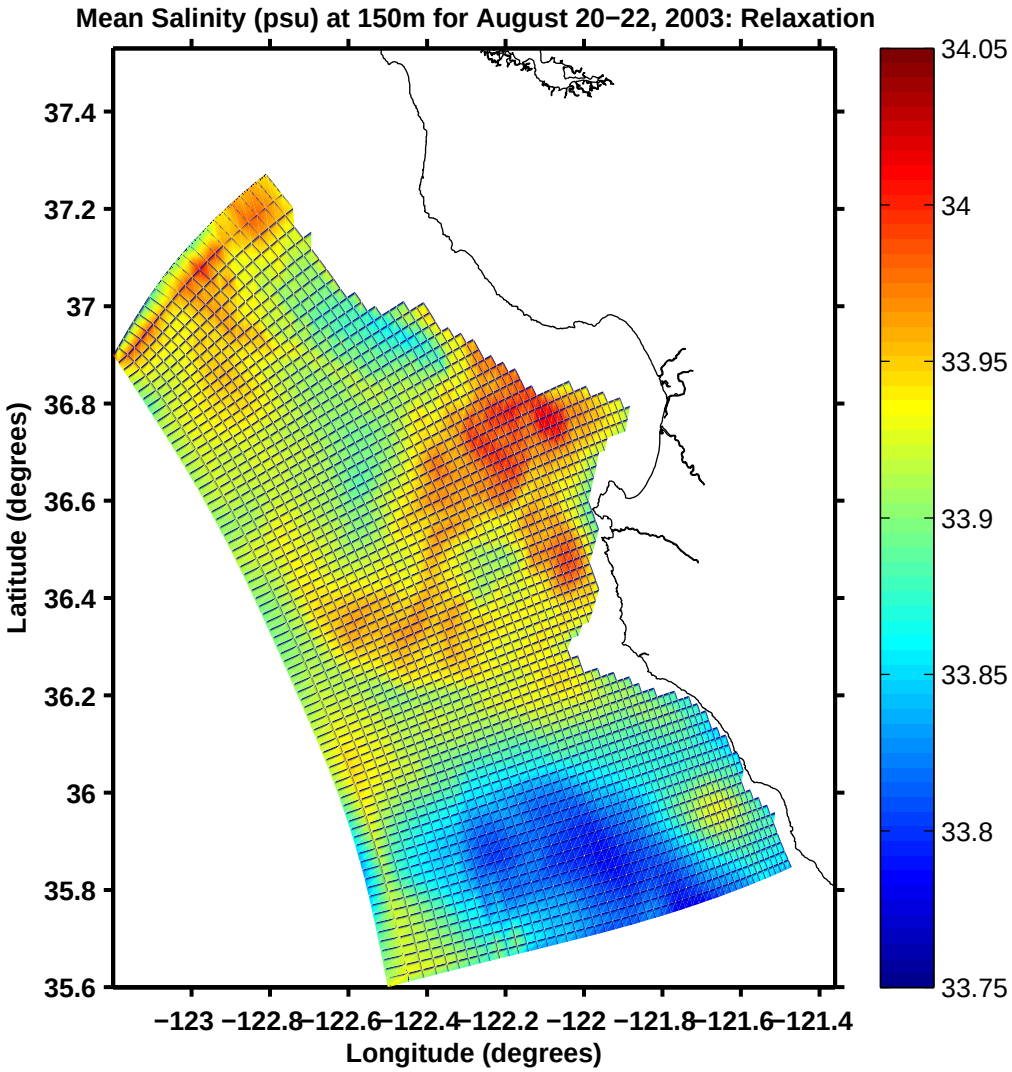

Figure 16. Model mean salinity at 150 m for R1.

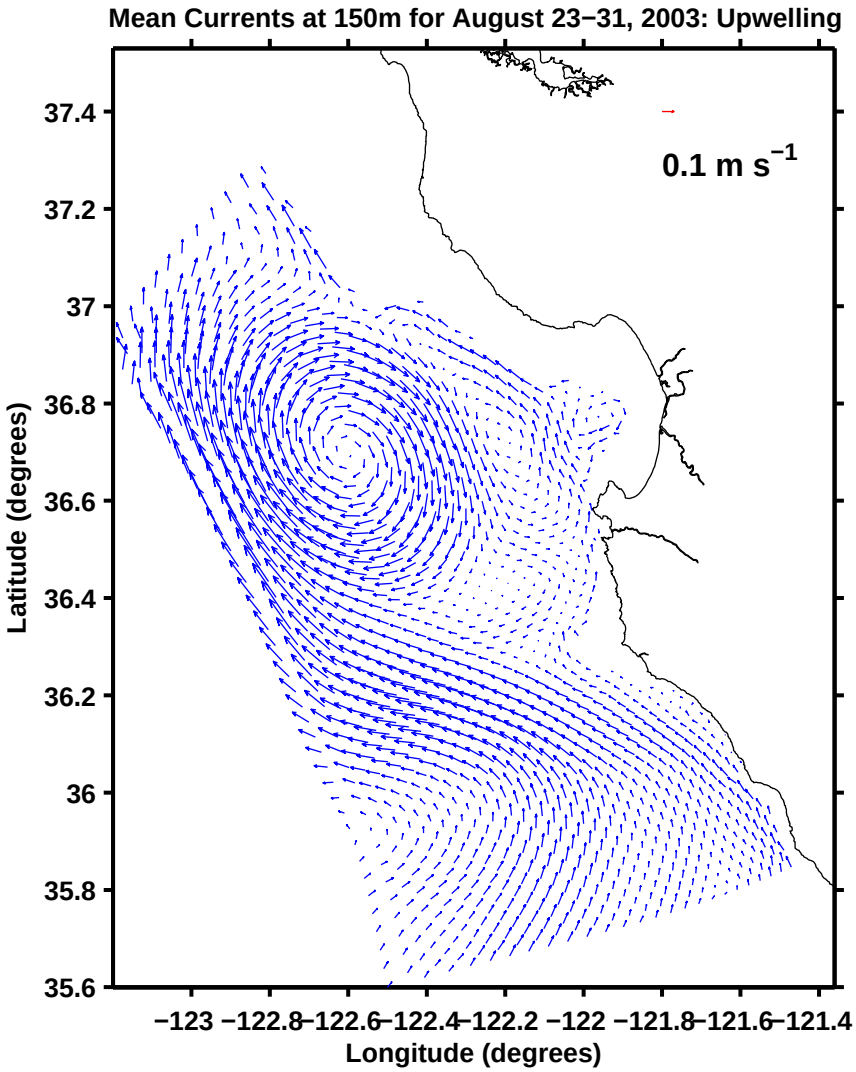

Figure 17. Model mean currents at 150 m for UW2.

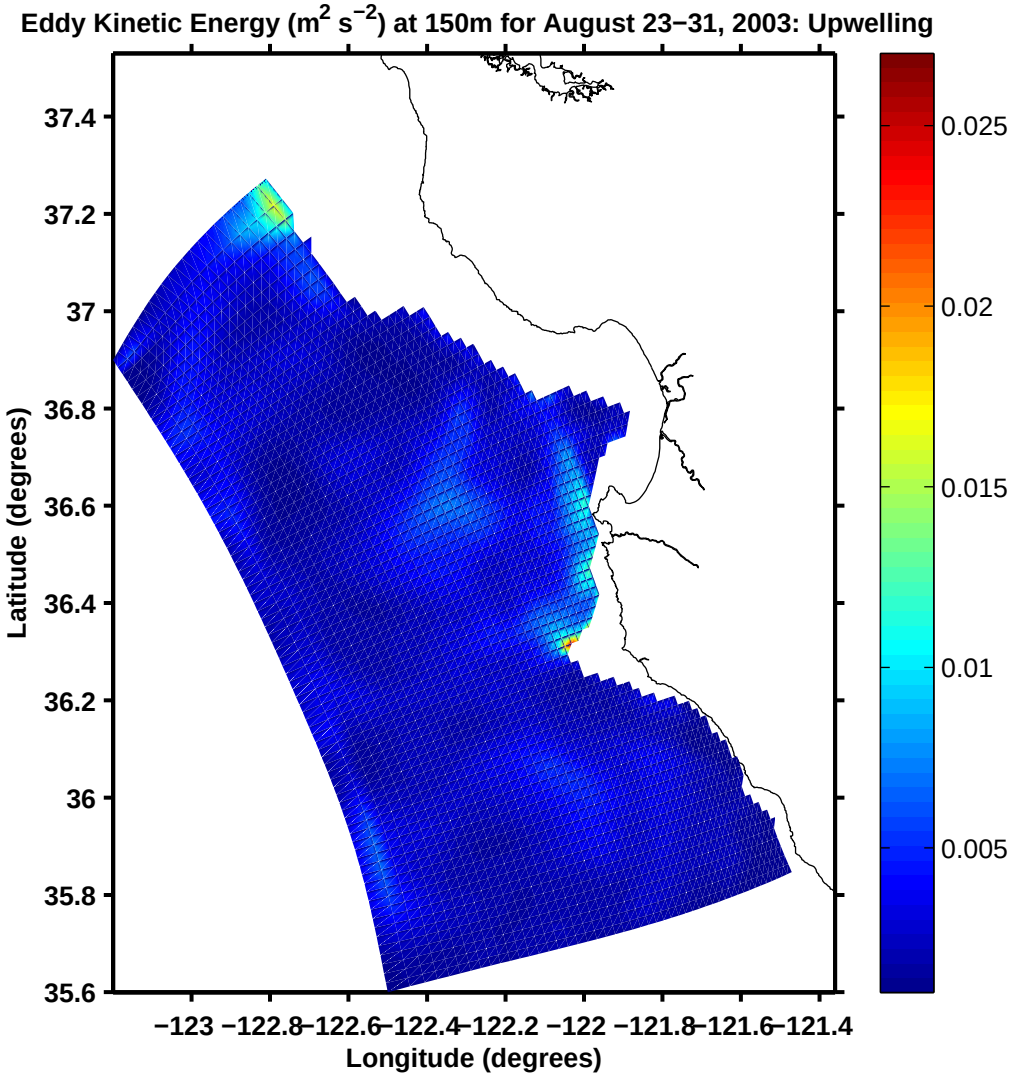

Figure 18. Model EKE at 150 m for UW2.

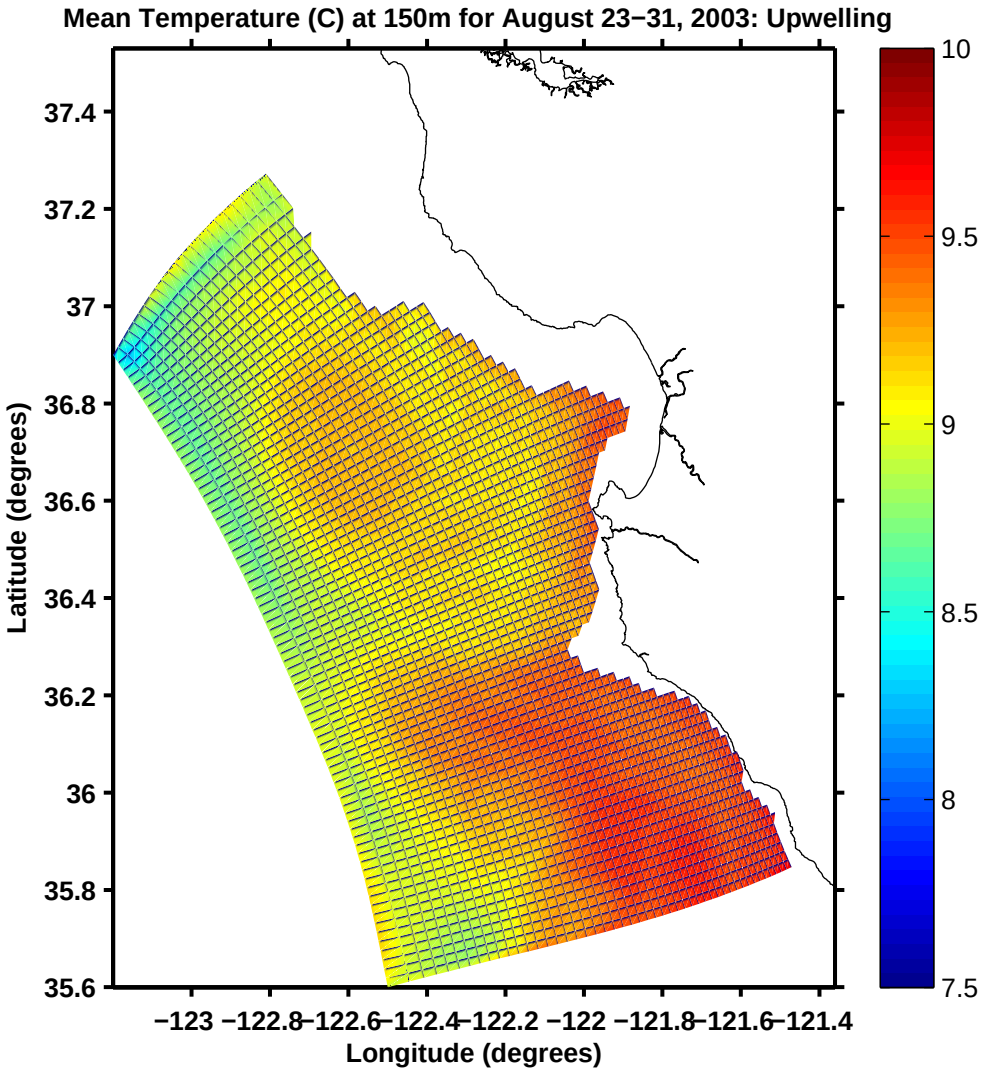

Figure 19. Model mean temperature at 150 m for UW2.

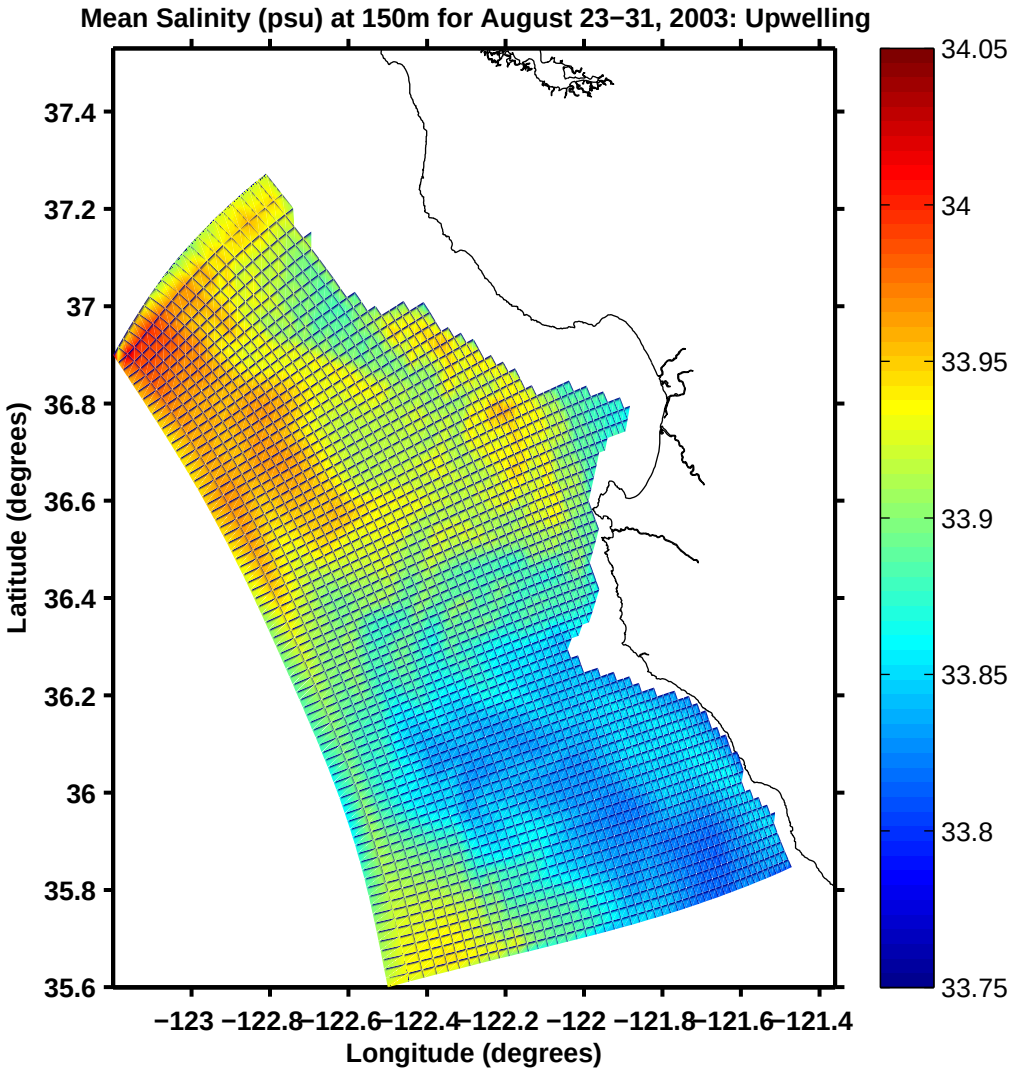

Figure 20. Model mean salinity at 150 m for UW2.

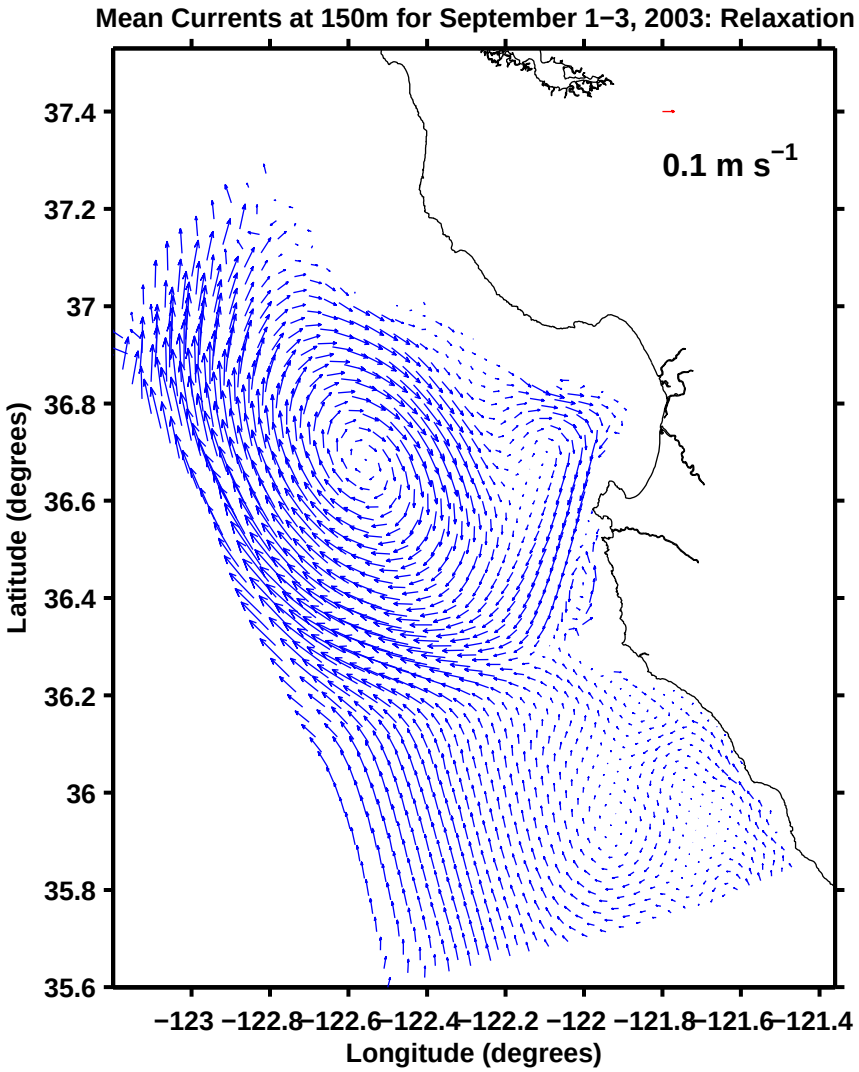

Figure 21. Model mean currents at 150 m for R2.

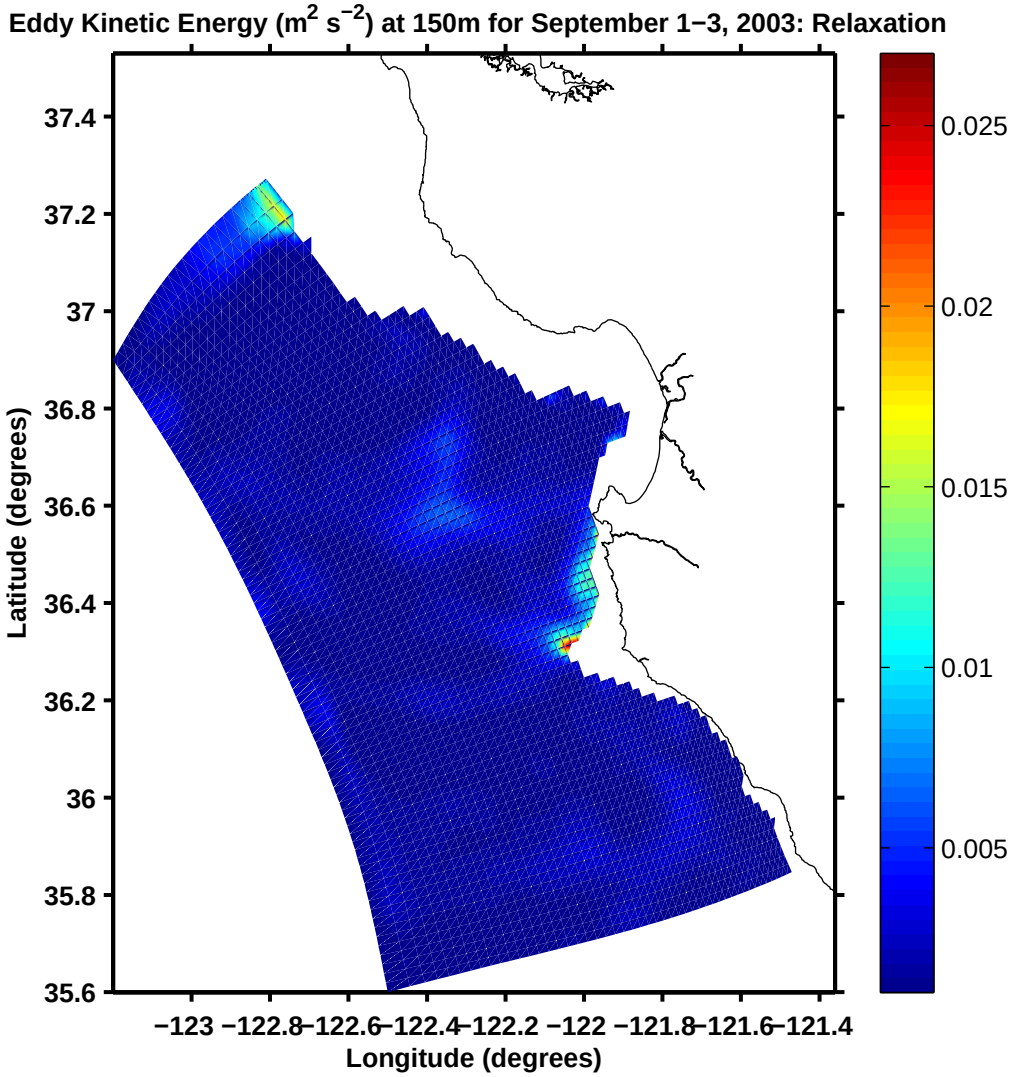

Figure 22. Model EKE at 150 m for R2.

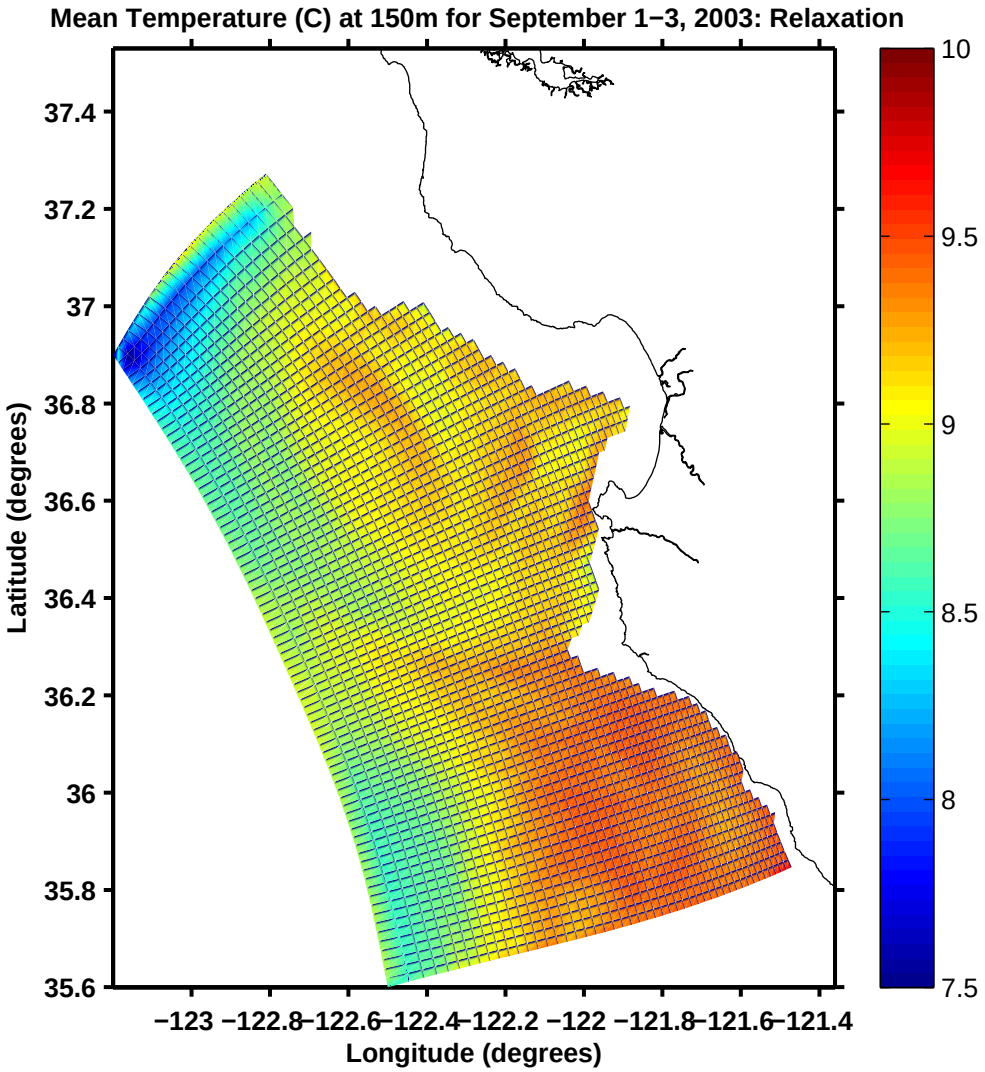

Figure 23. Model mean temperature at 150 m for R2.

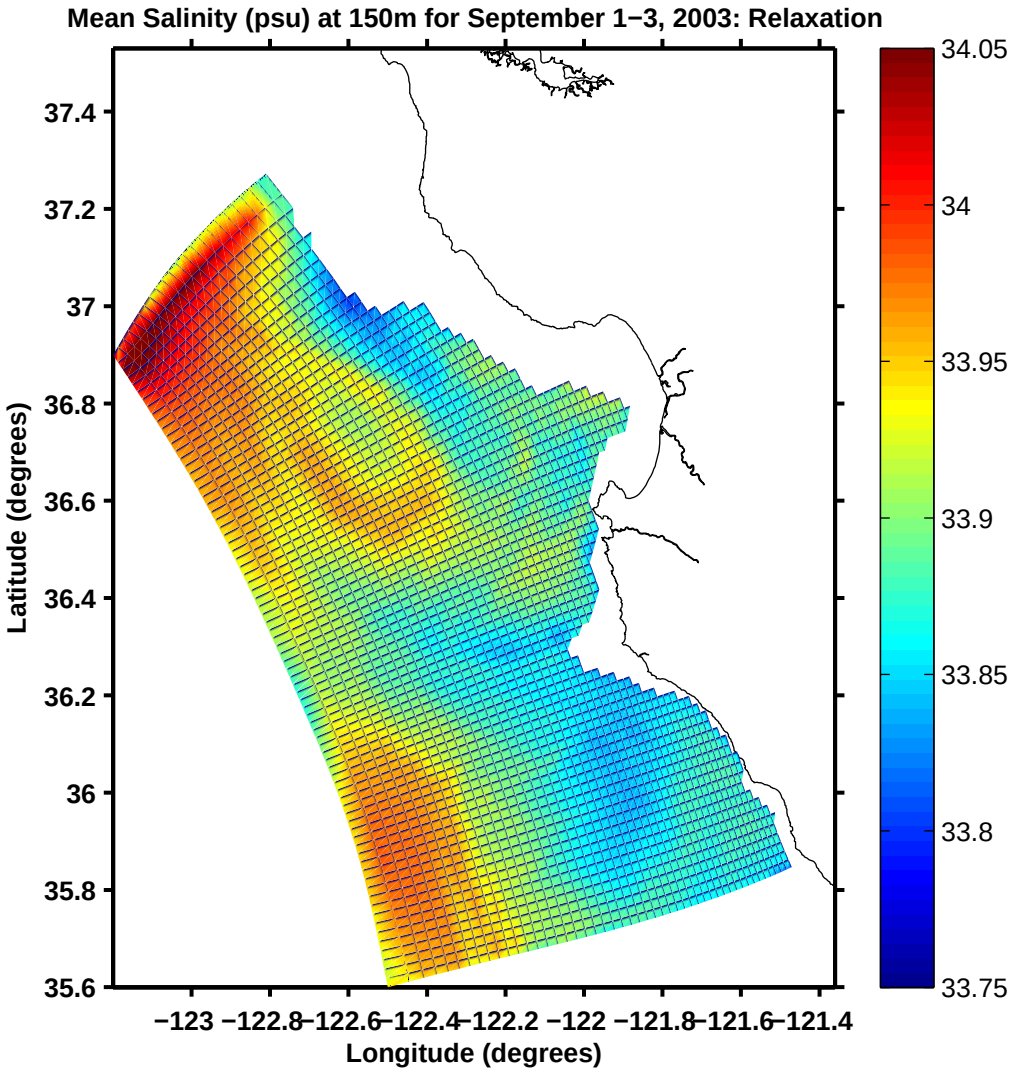

Figure 24. Model mean salinity at 150 m for R2.

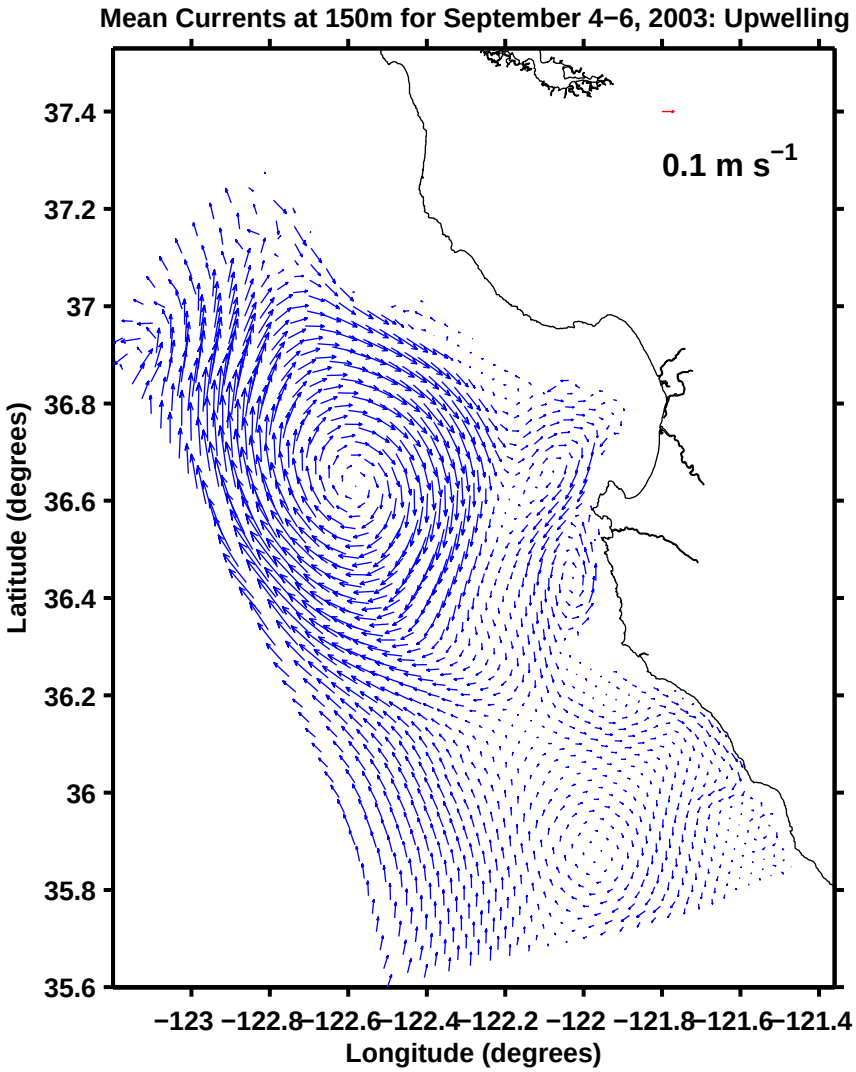

Figure 25. Model mean currents at 150 m for UW3.

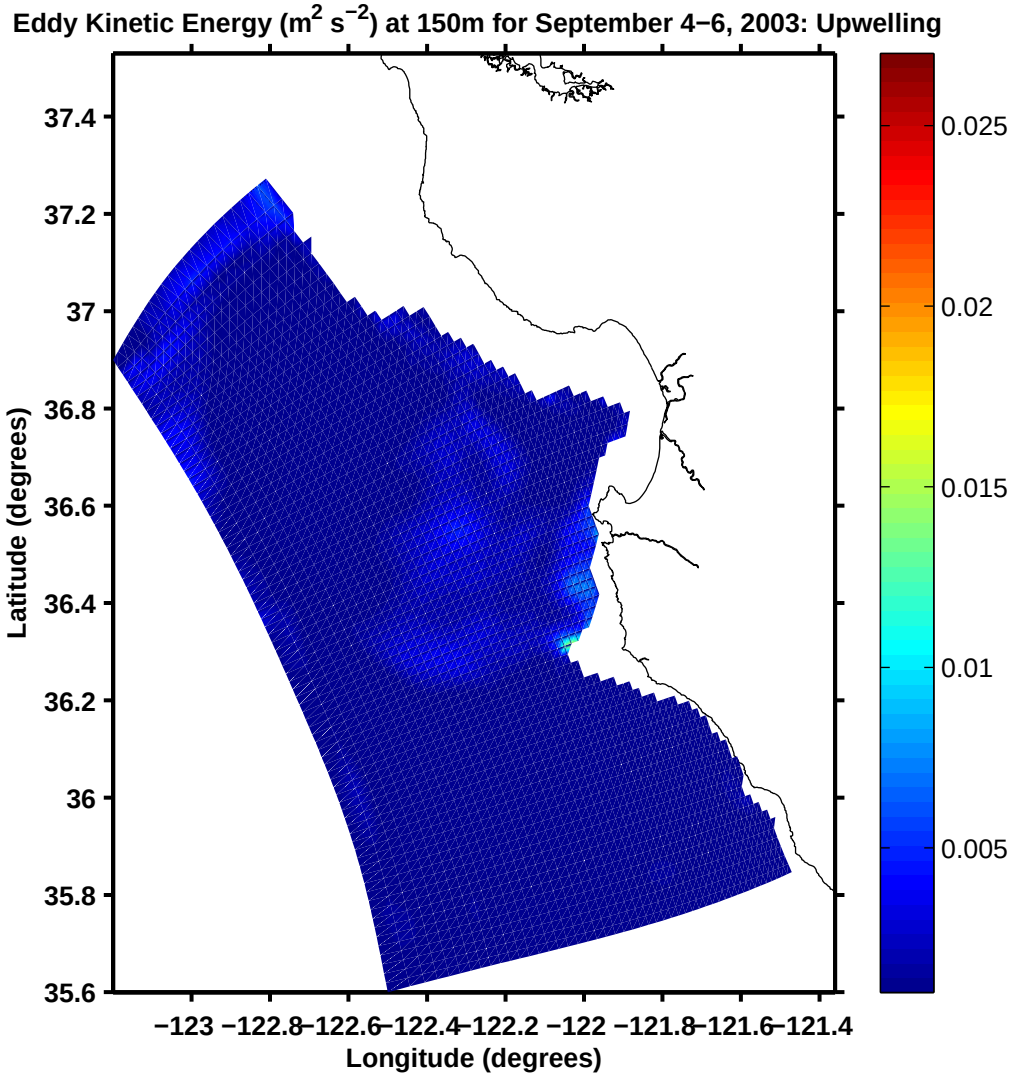

Figure 26. Model EKE at 150 m for UW3.

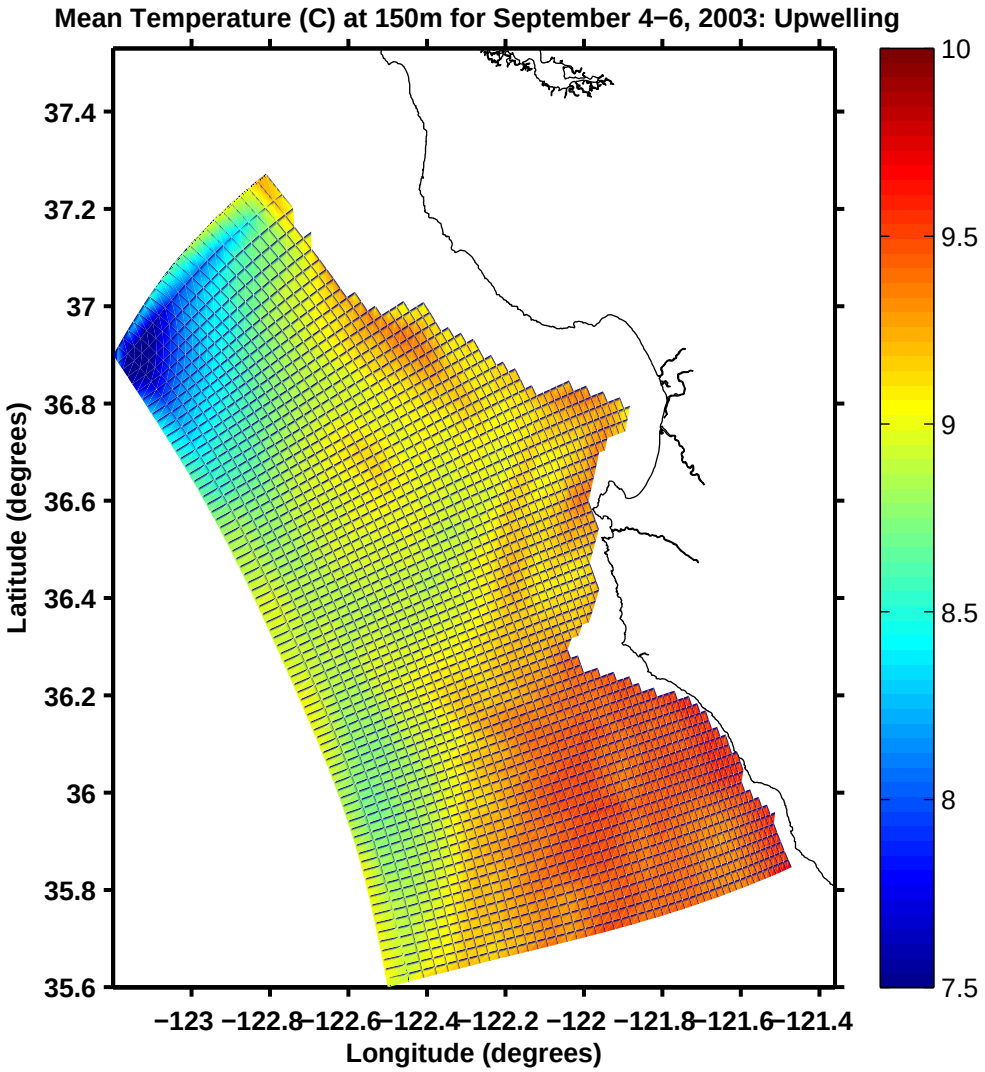

Figure 27. Model mean temperature at 150 m for UW3.

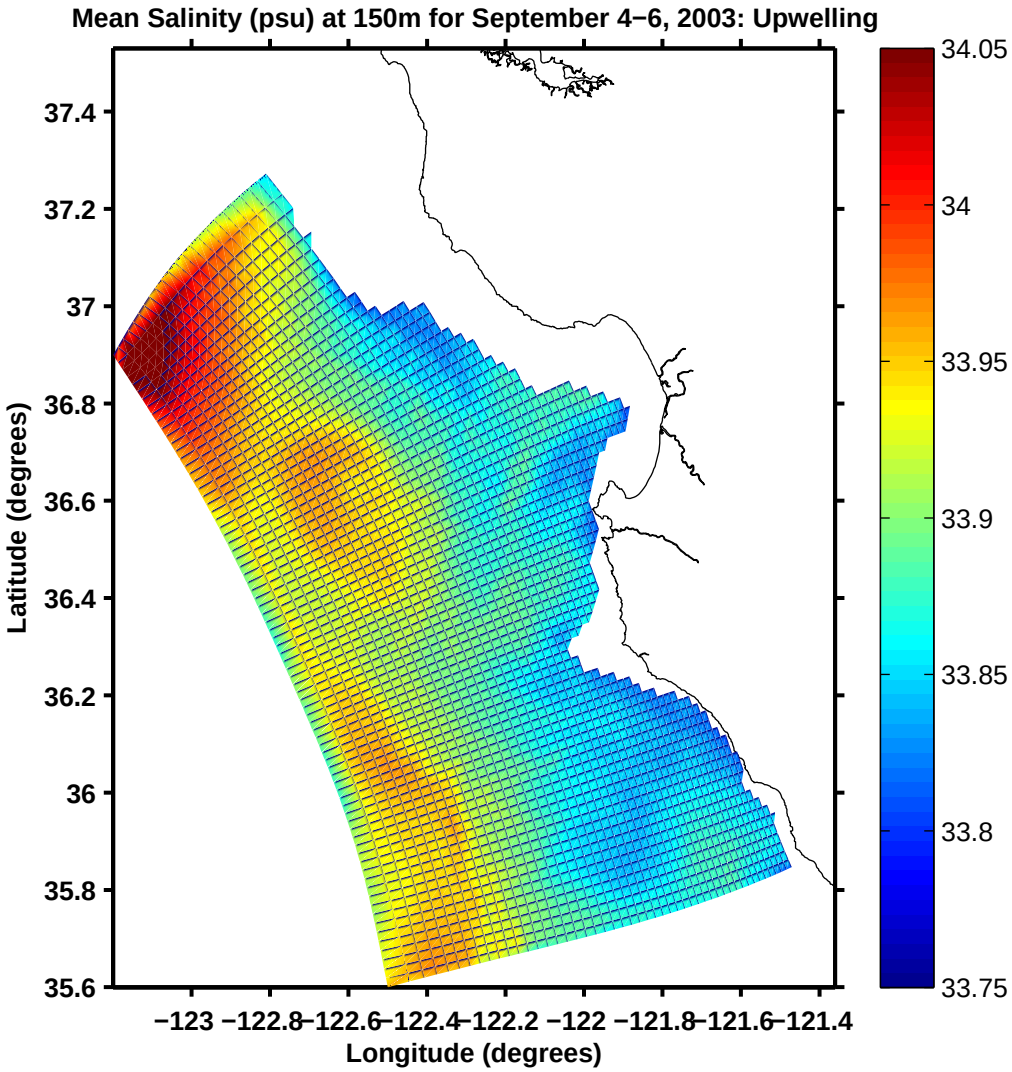

Figure 28. Model mean salinity at 150 m for UW3.

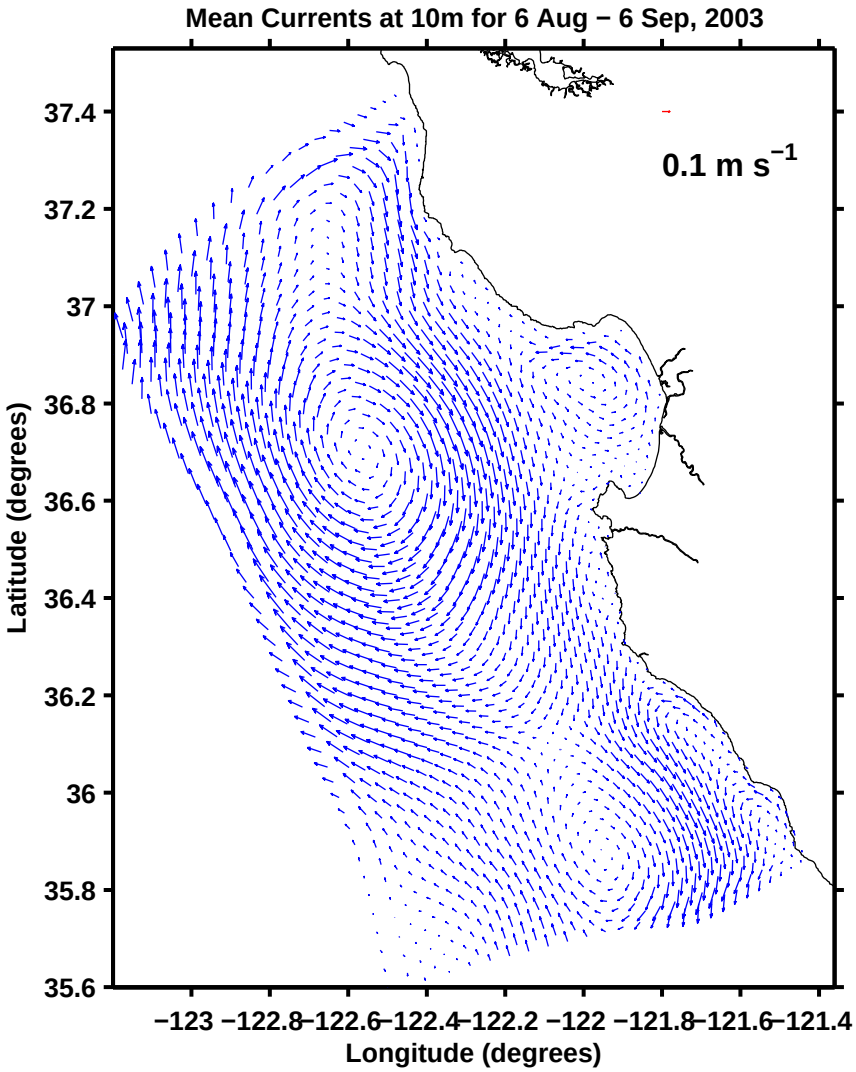

Figure 29. Model mean currents at 10 m for August 6 - September 6, 2003.

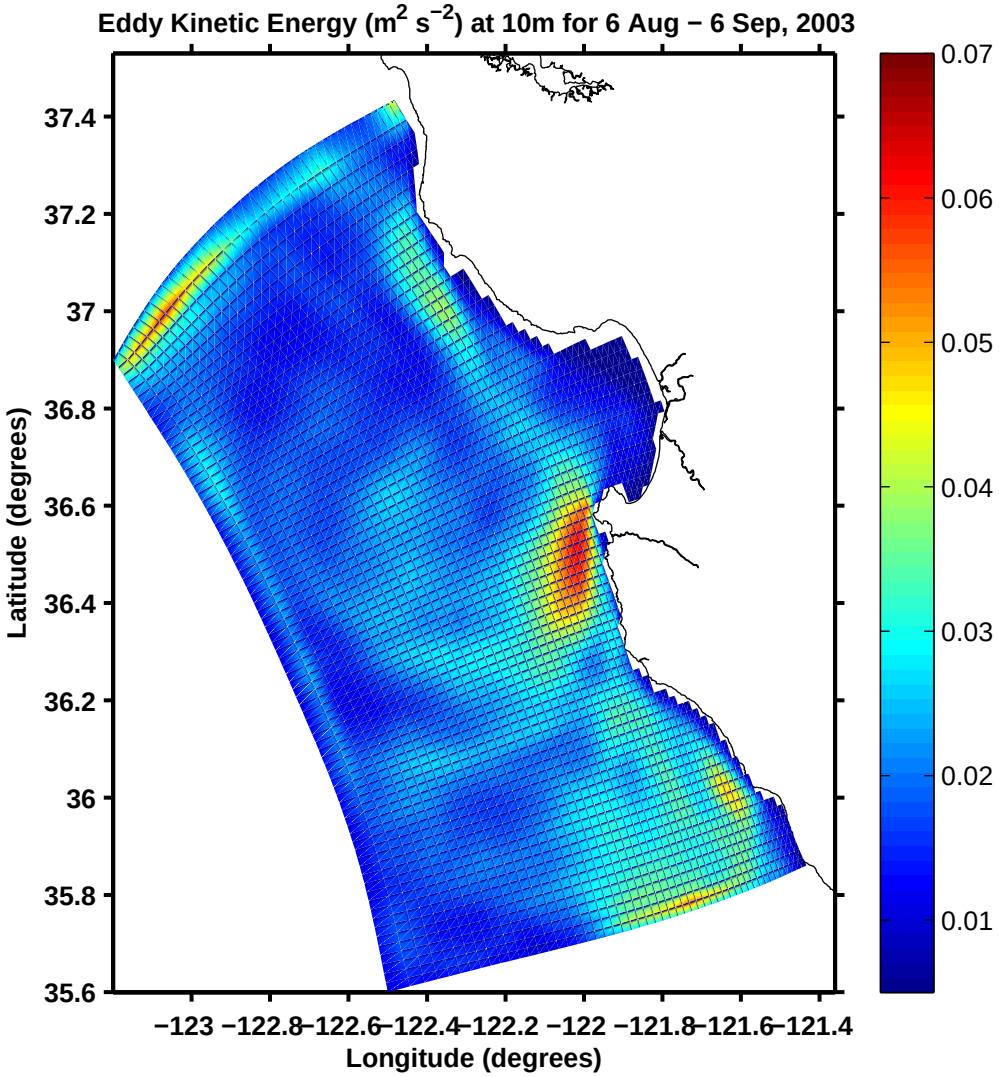

Figure 30. Model EKE at 10 m for August 6 - September 6, 2003.

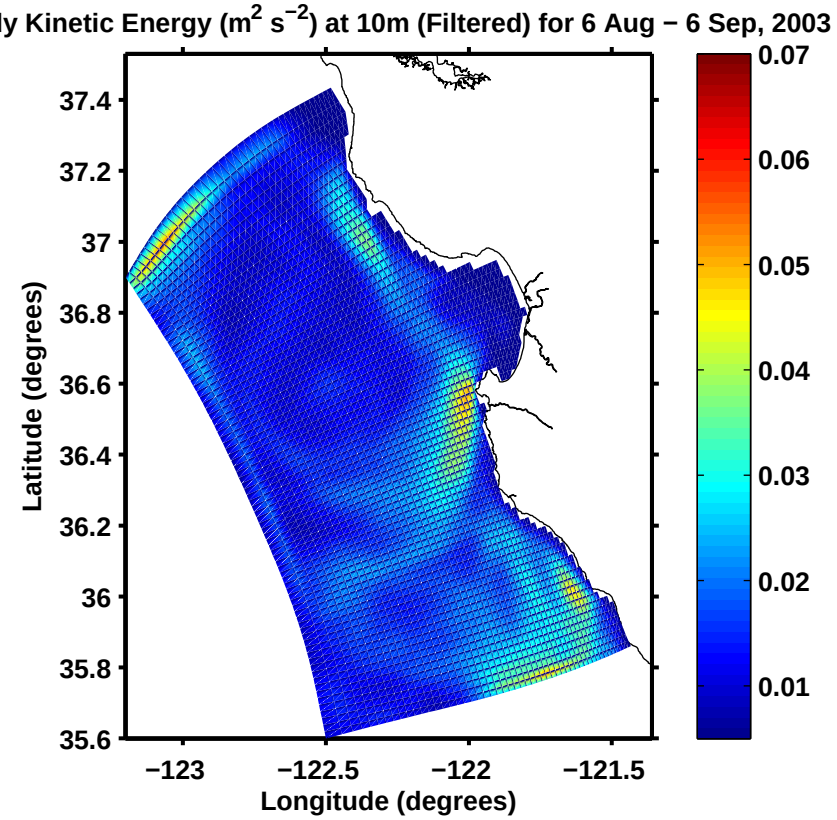

Figure 31. As in Figure 30 except for low-pass tidal filter applied to model data.

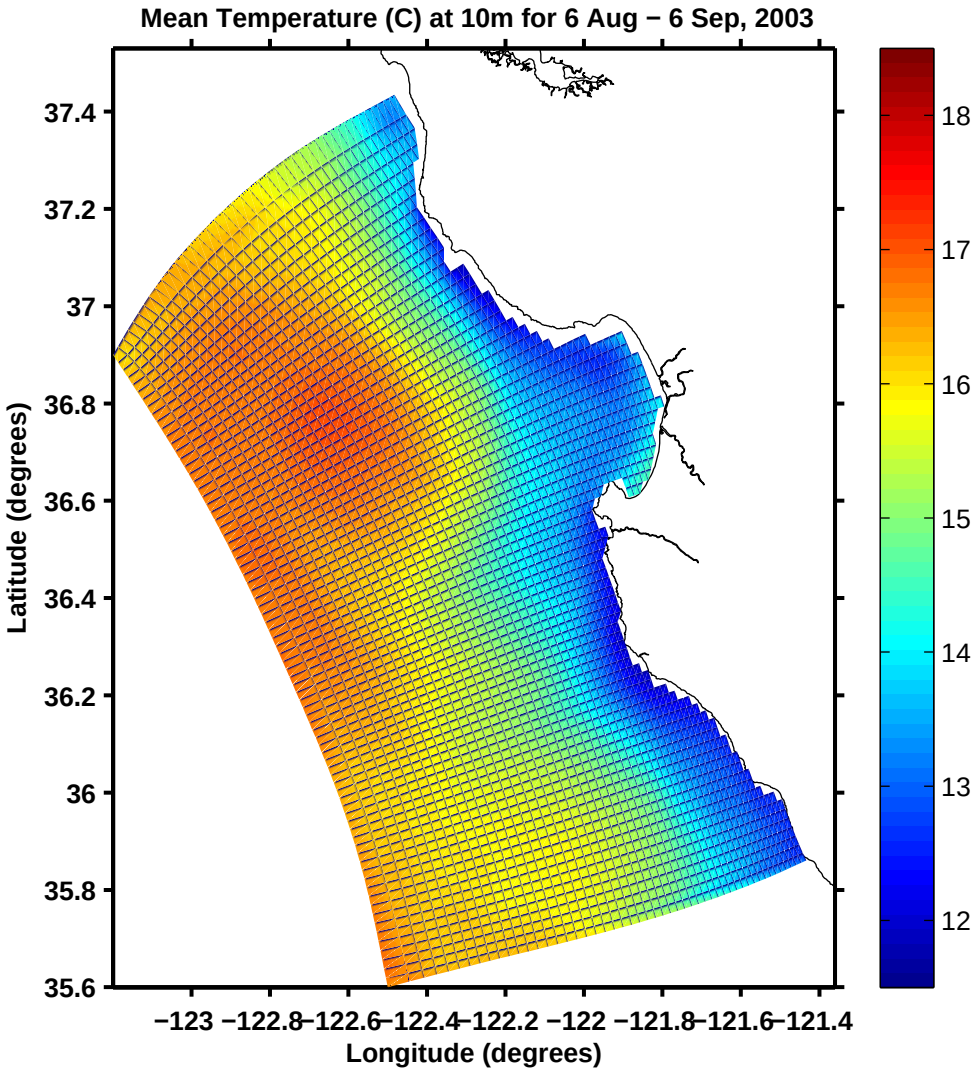

Figure 32. Model mean temperature at 10 m for August 6 - September 6, 2003.

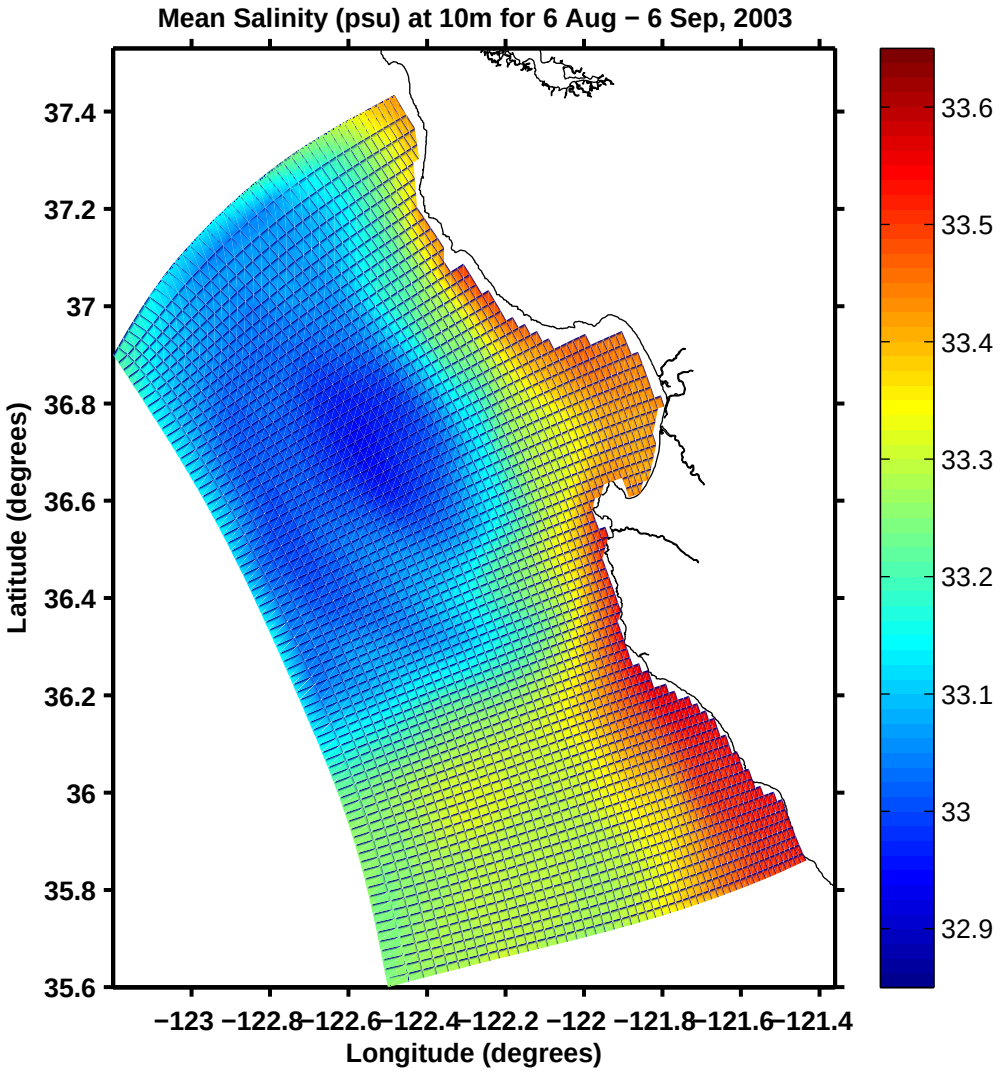

Figure 33. Model mean salinity at 10 m for August 6 - September 6, 2003.

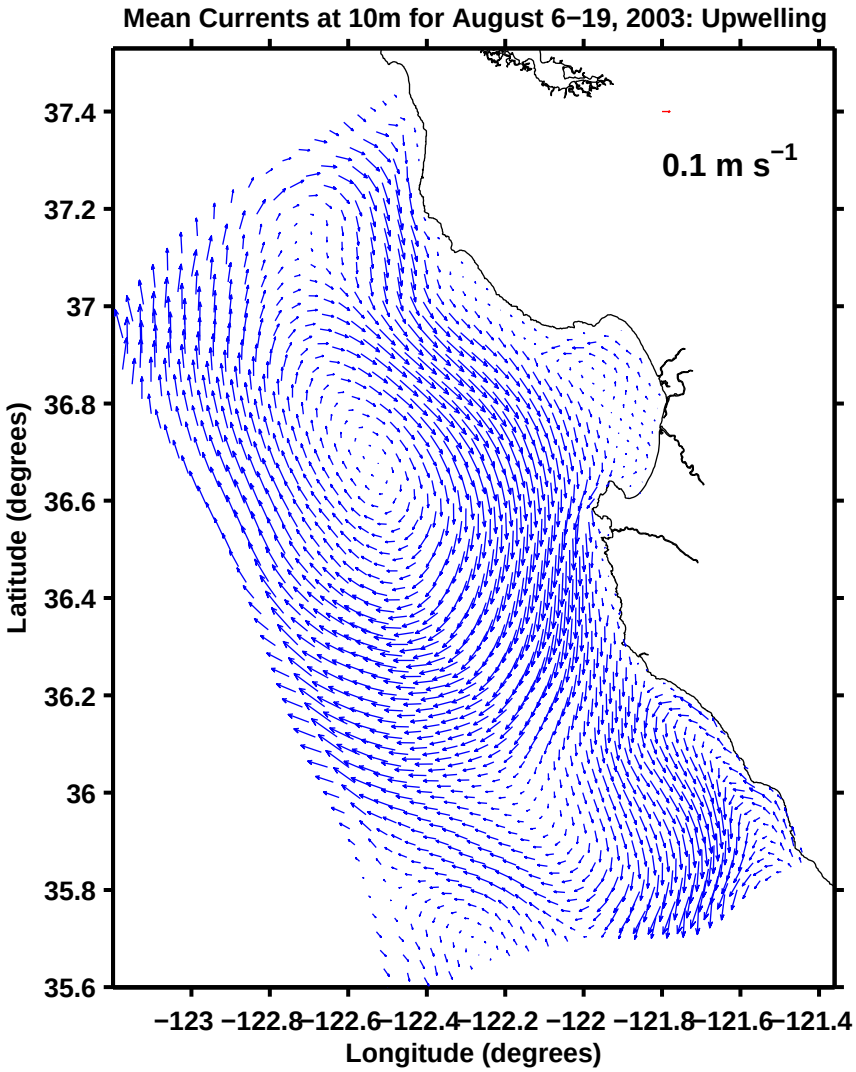

Figure 34. Model mean currents at 10 m for UW1.

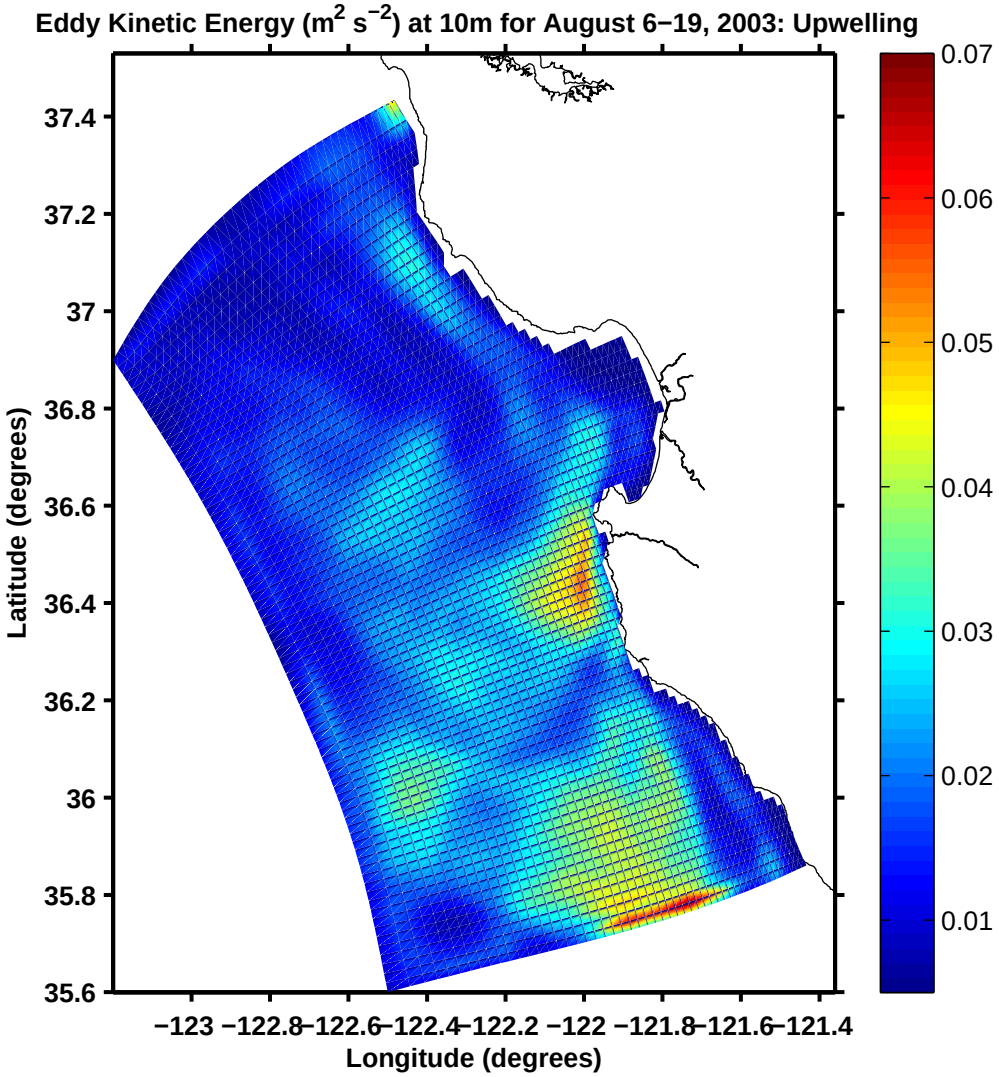

Figure 35. Model EKE at 10 m for UW1.

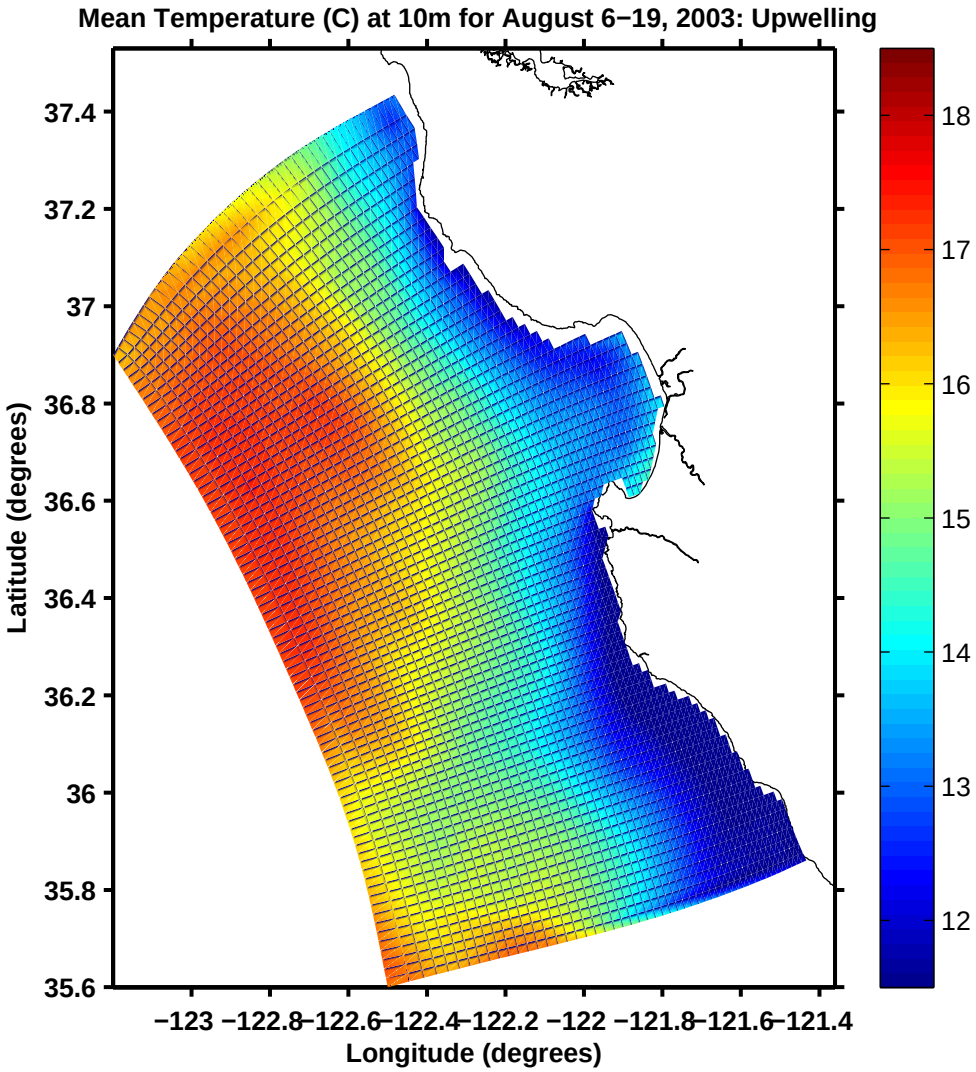

Figure 36. Model mean temperature at 10 m for UW1.

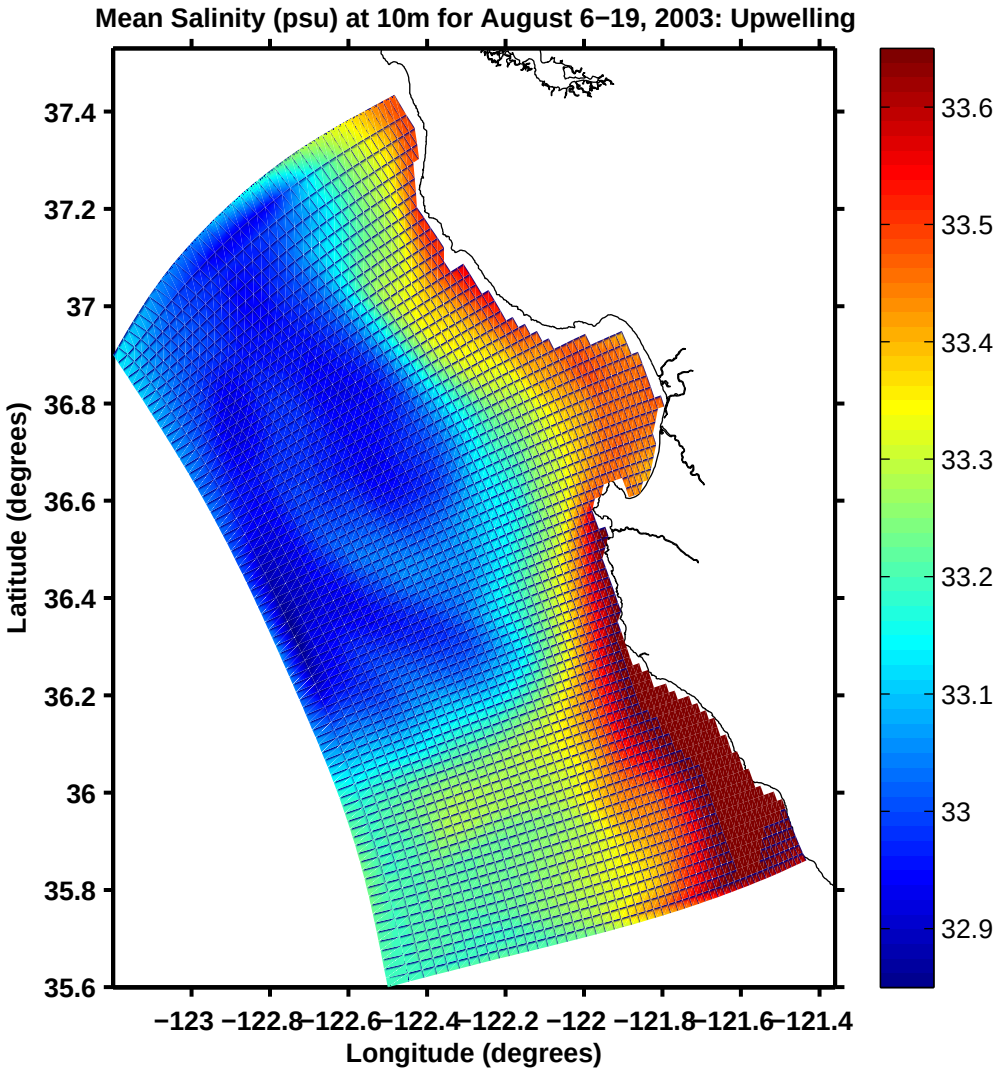

Figure 37. Model mean salinity at 10 m for UW1.

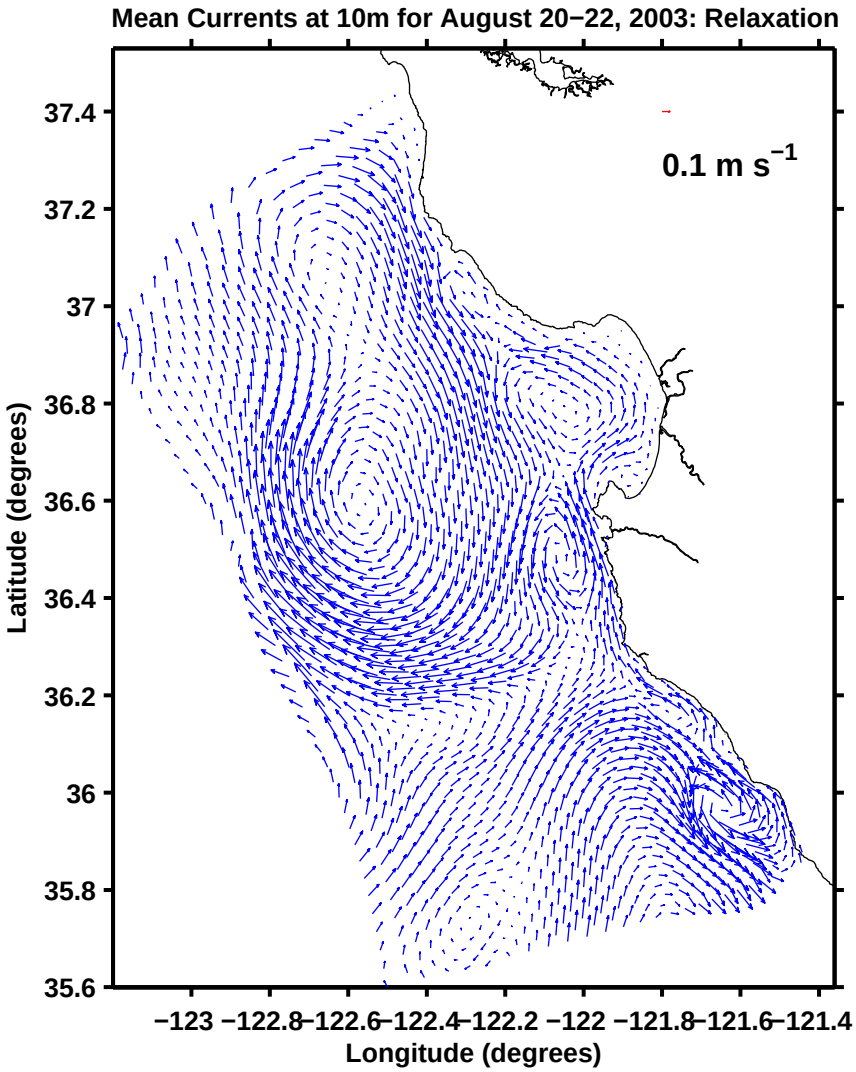

Figure 38. Model mean currents at 10 m for R1.

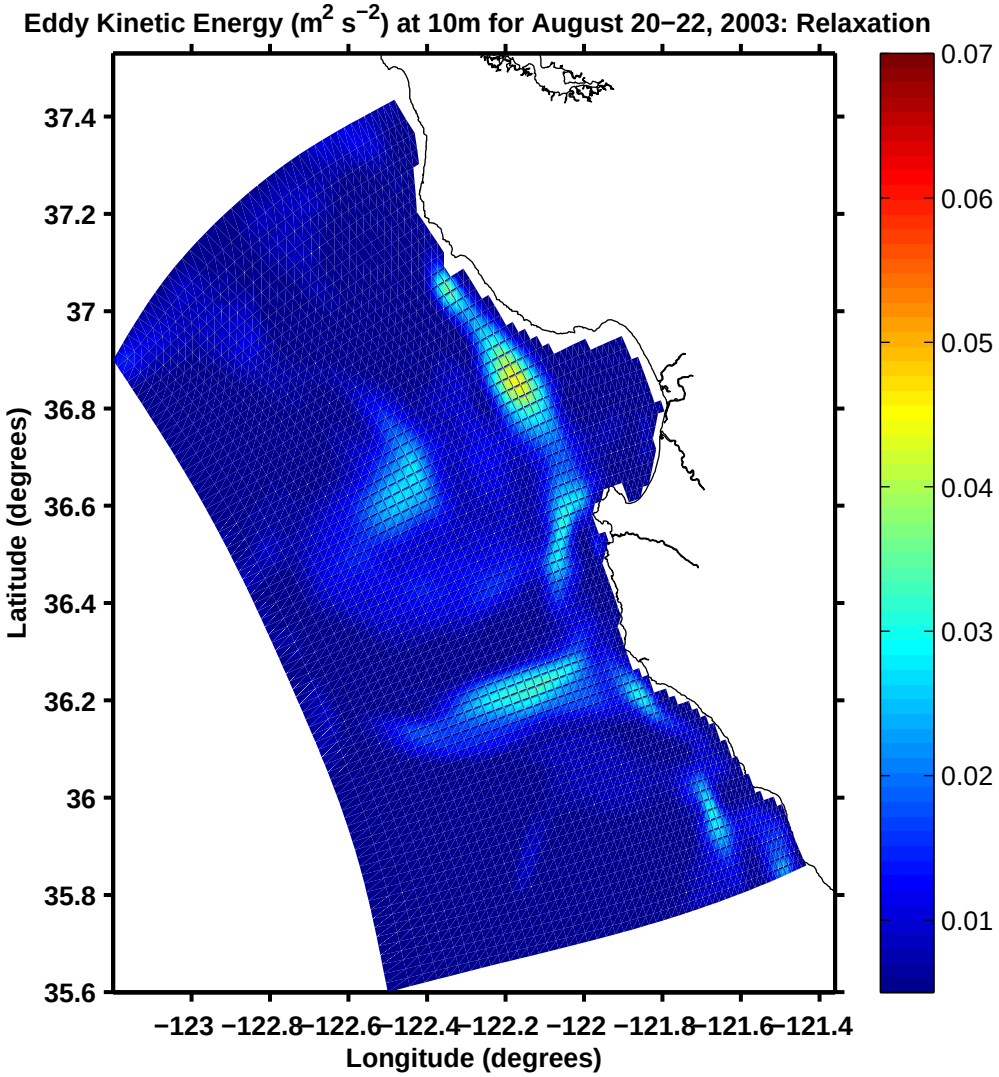

Figure 39. Model EKE at 10 m for R1.

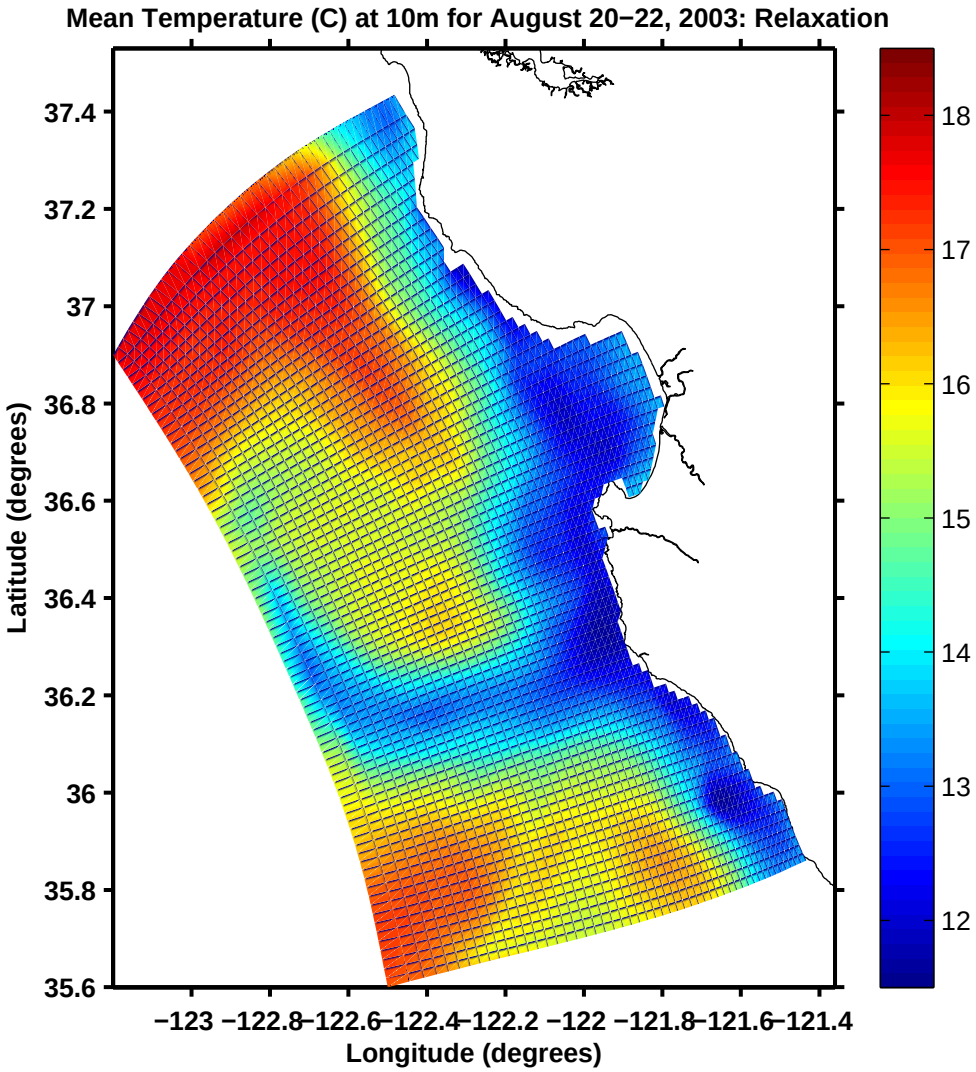

Figure 40. Model mean temperature at 10 m for R1.

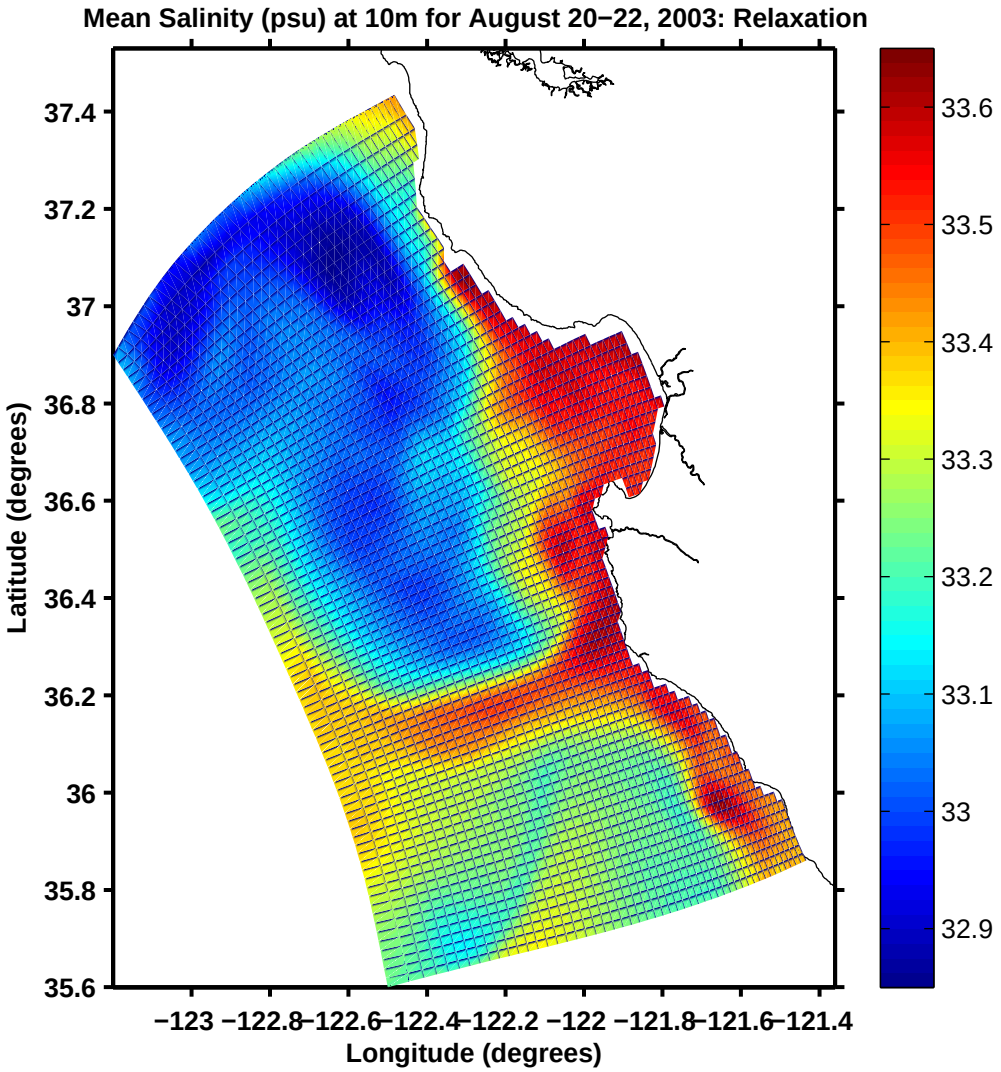

Figure 41. Model mean salinity at 10 m for R1.

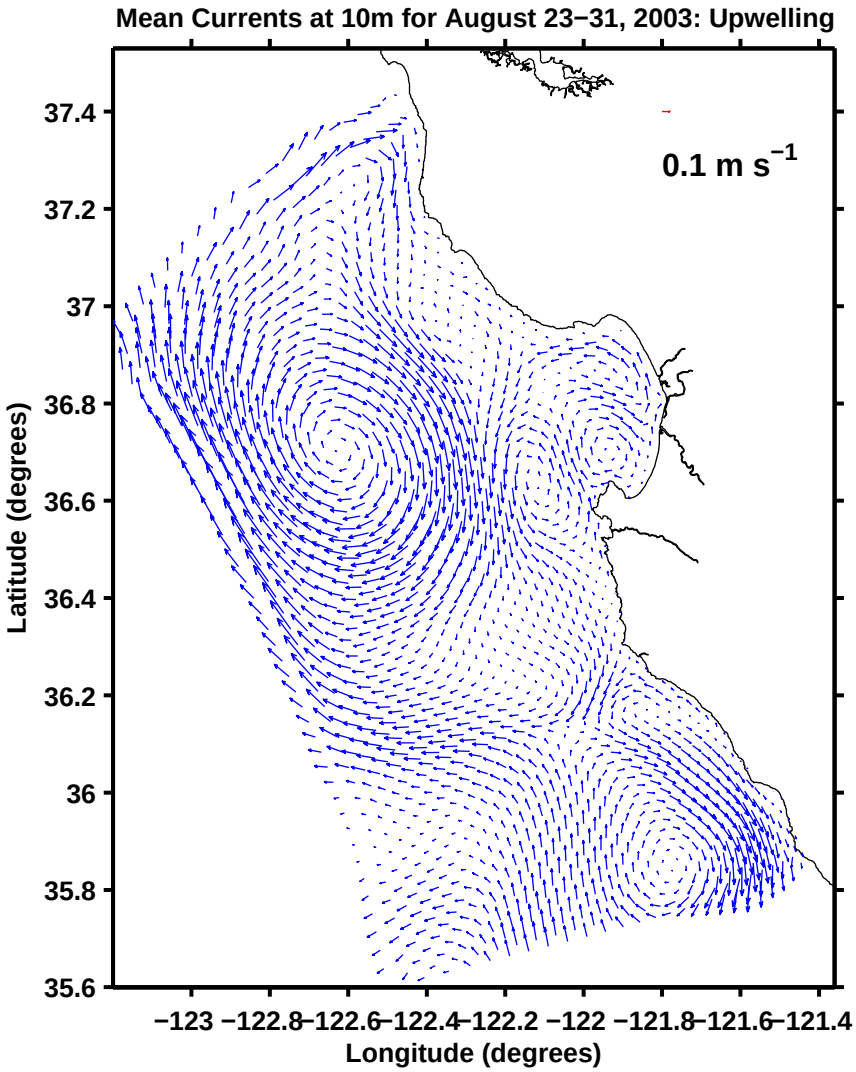

Figure 42. Model mean currents at 10 m for UW2.

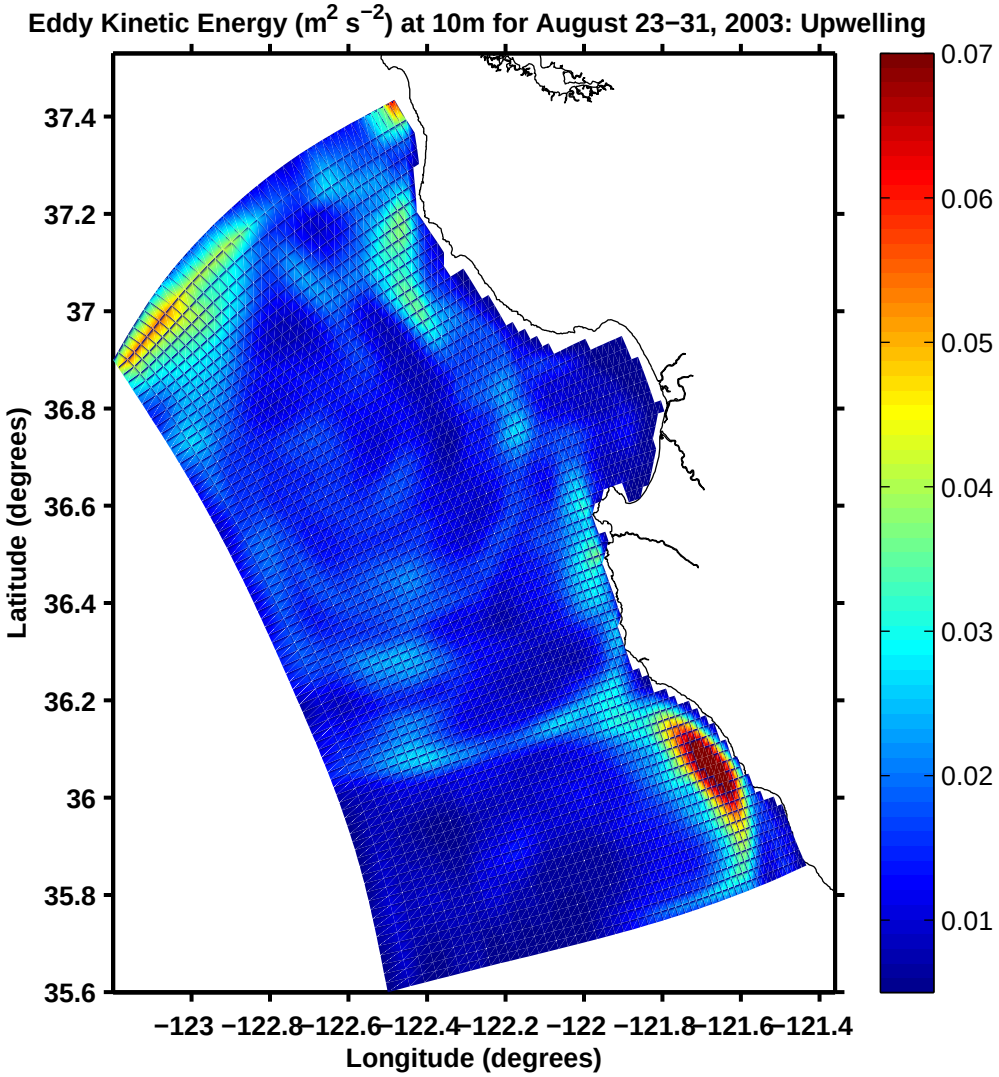

Figure 43. Model EKE at 10 m for UW2.

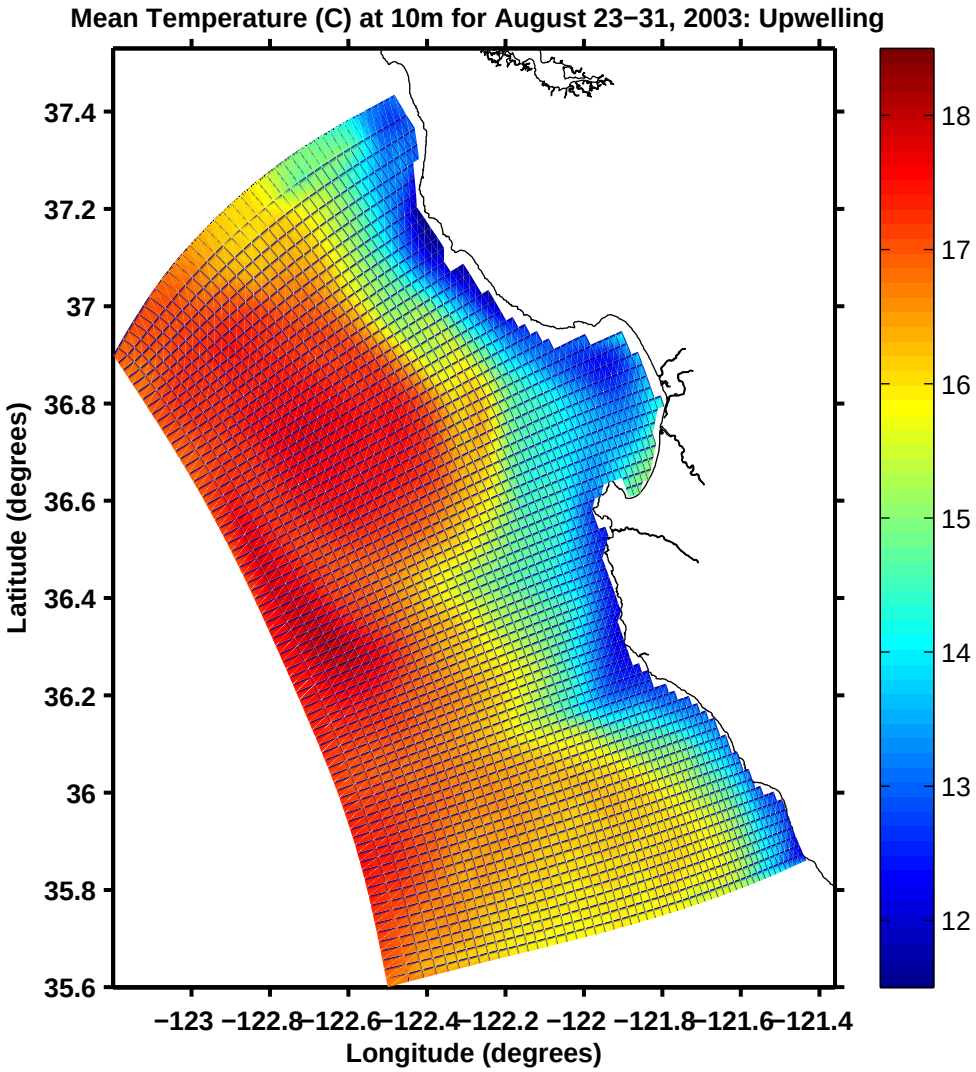

Figure 44. Model mean temperature at 10 m for UW2.

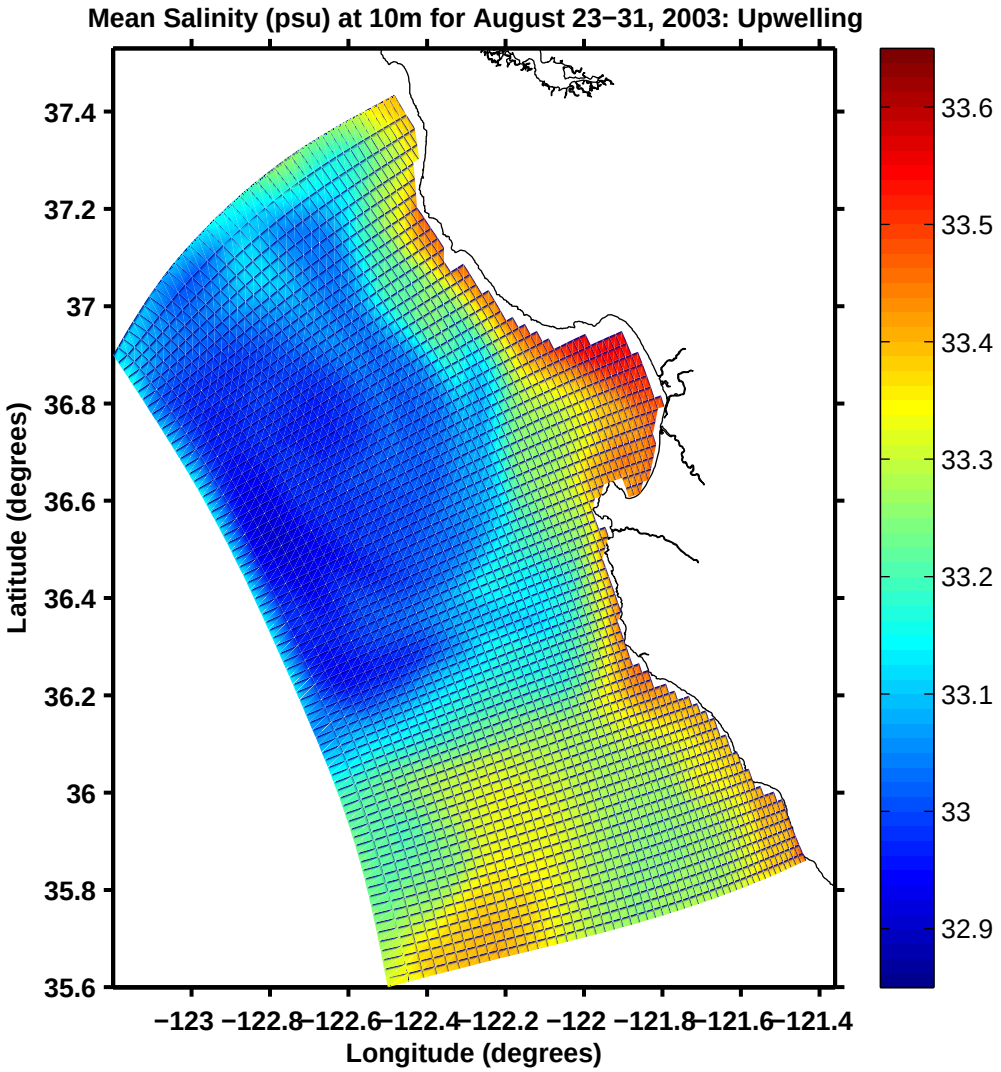

Figure 45. Model mean salinity at 10 m for UW2.

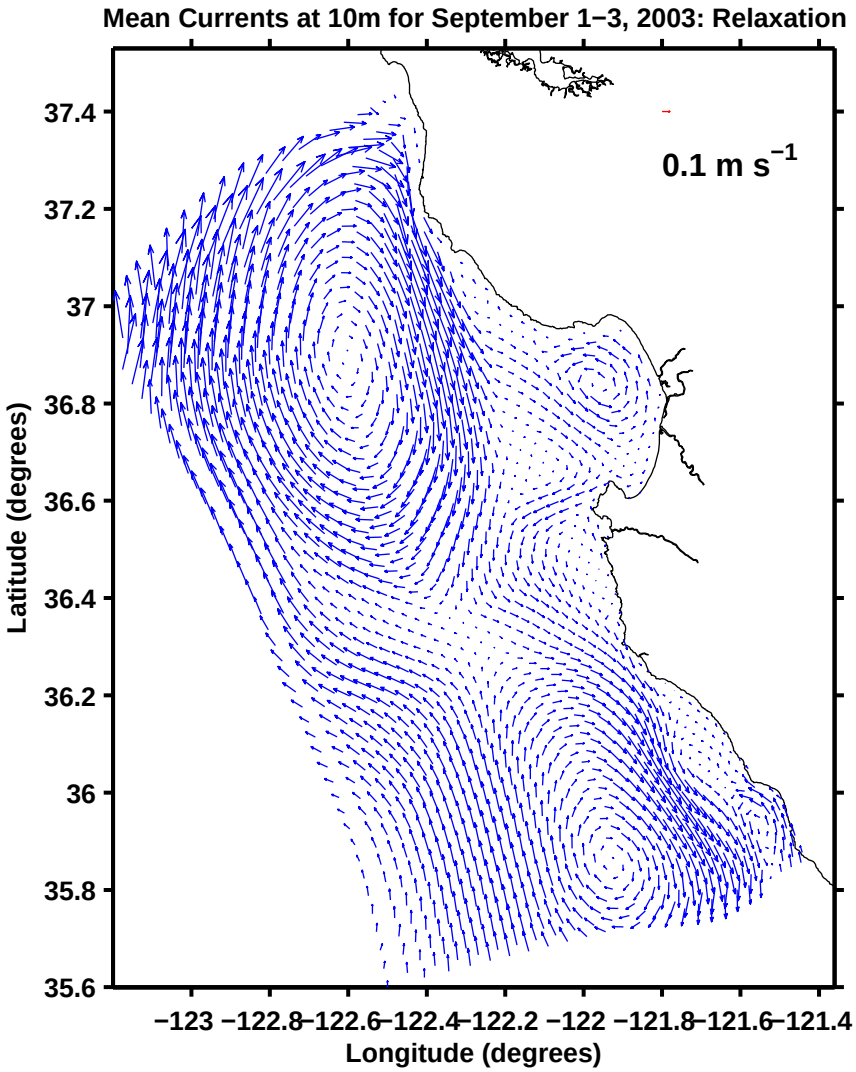

Figure 46. Model mean currents at 10 m for R2.

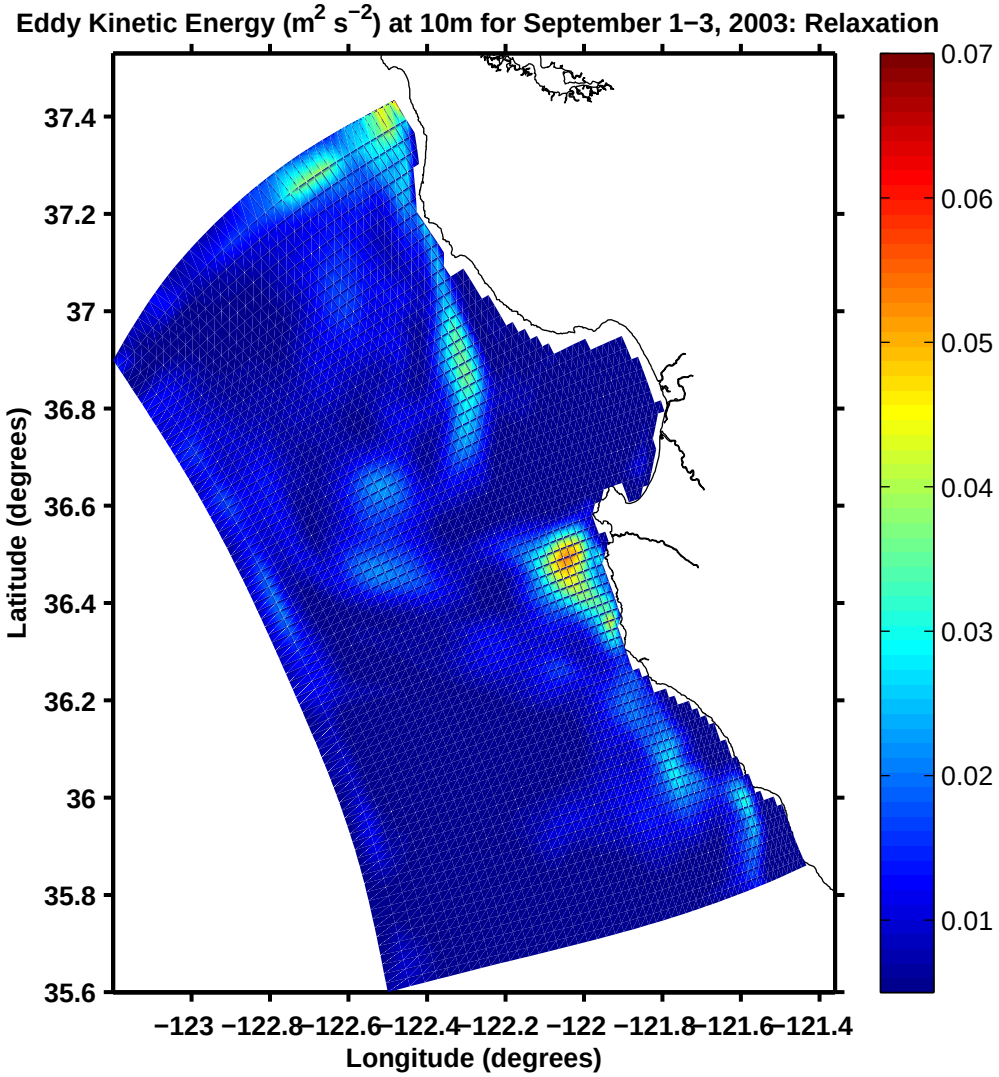

Figure 47. Mean EKE at 10 m for R2.

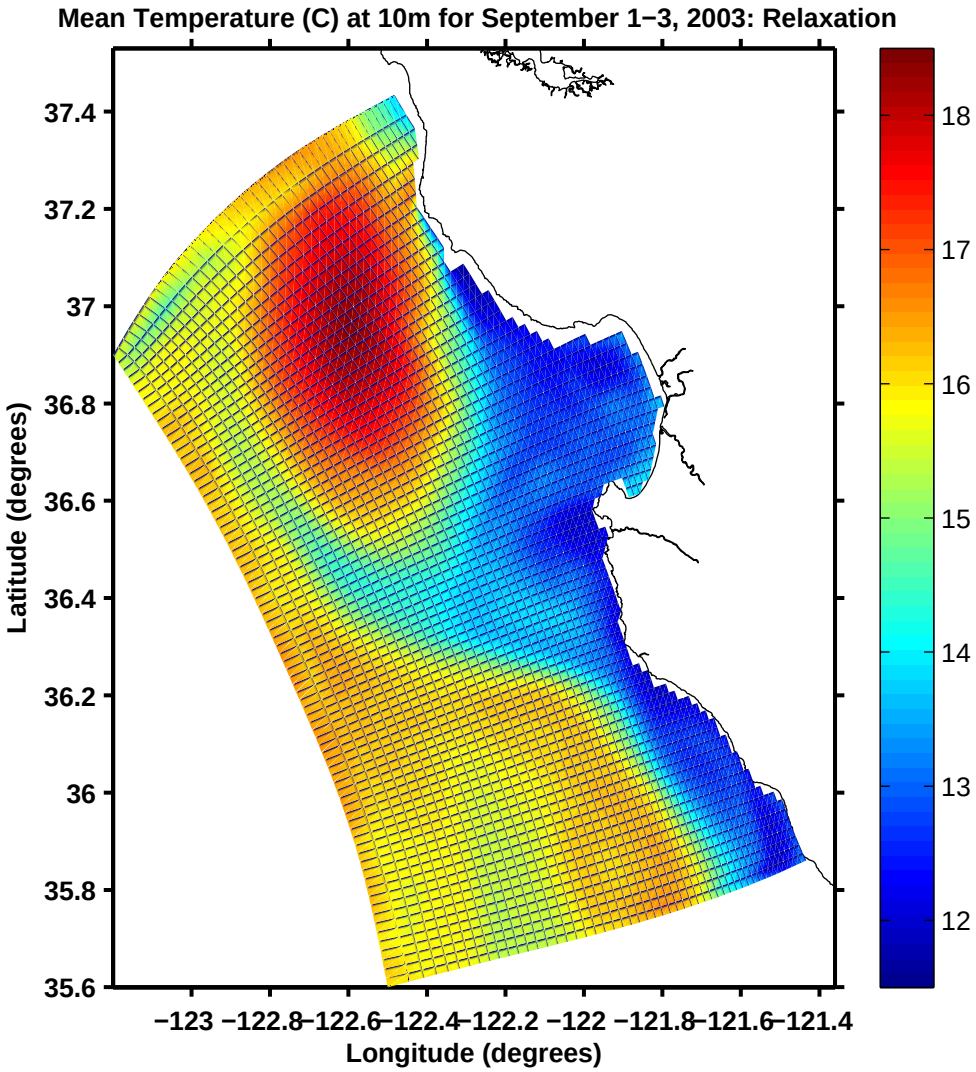

Figure 48. Model mean temperature at 10 m for R2.

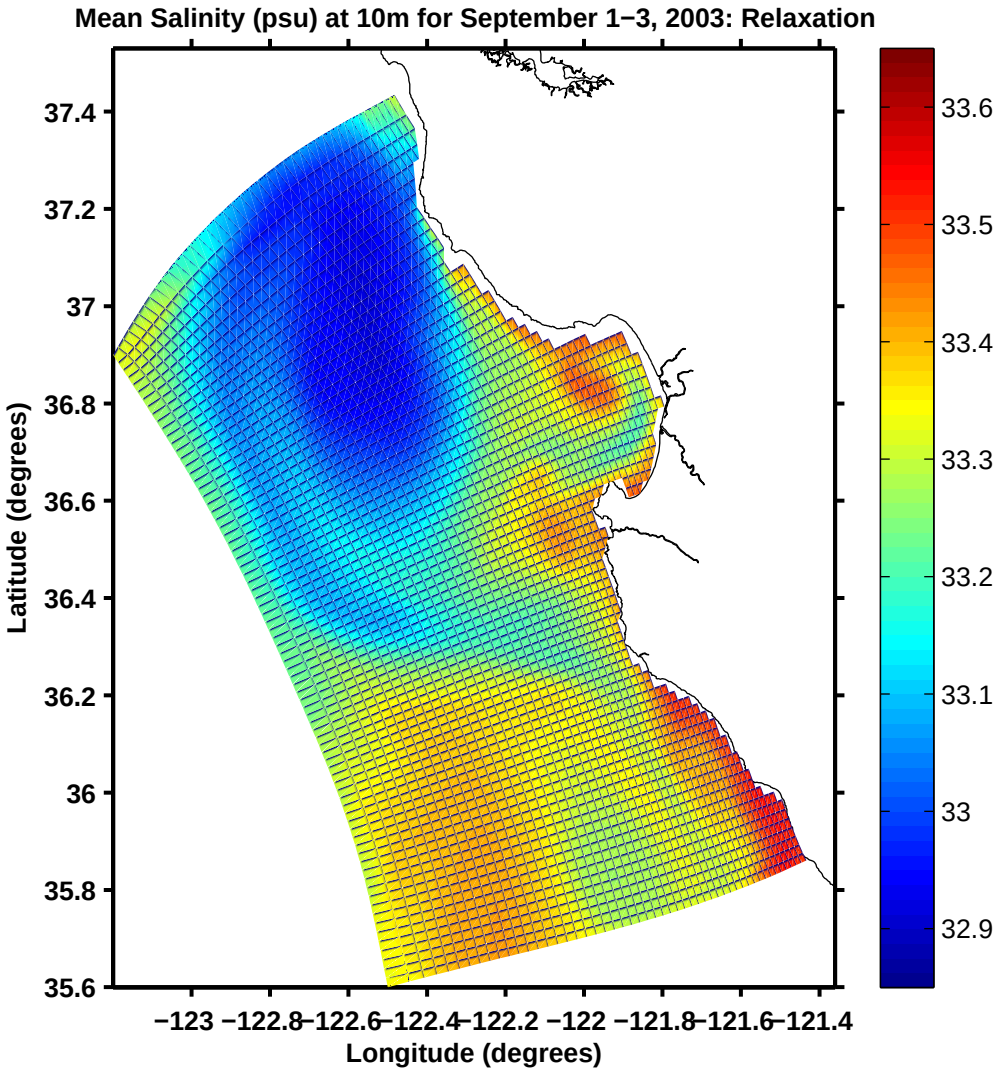

Figure 49. Model mean salinity at 10 m for R2.

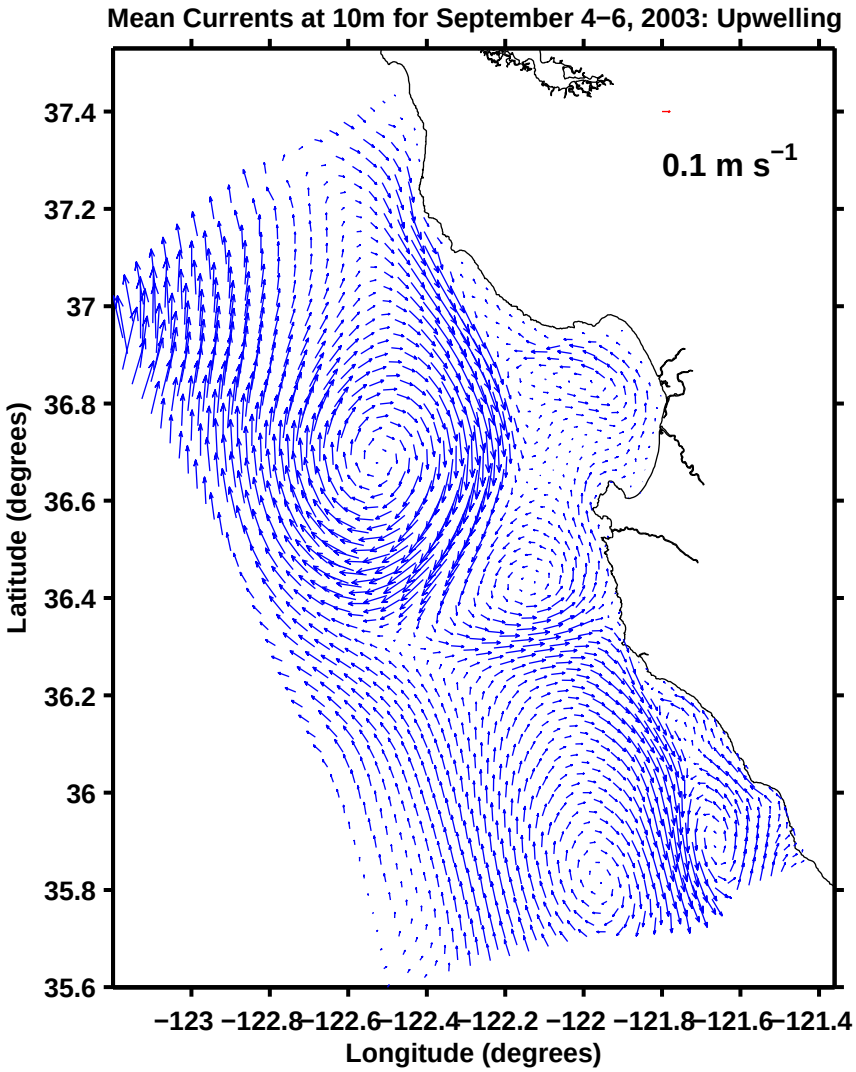

Figure 50. Model mean currents at 10 m for UW3.

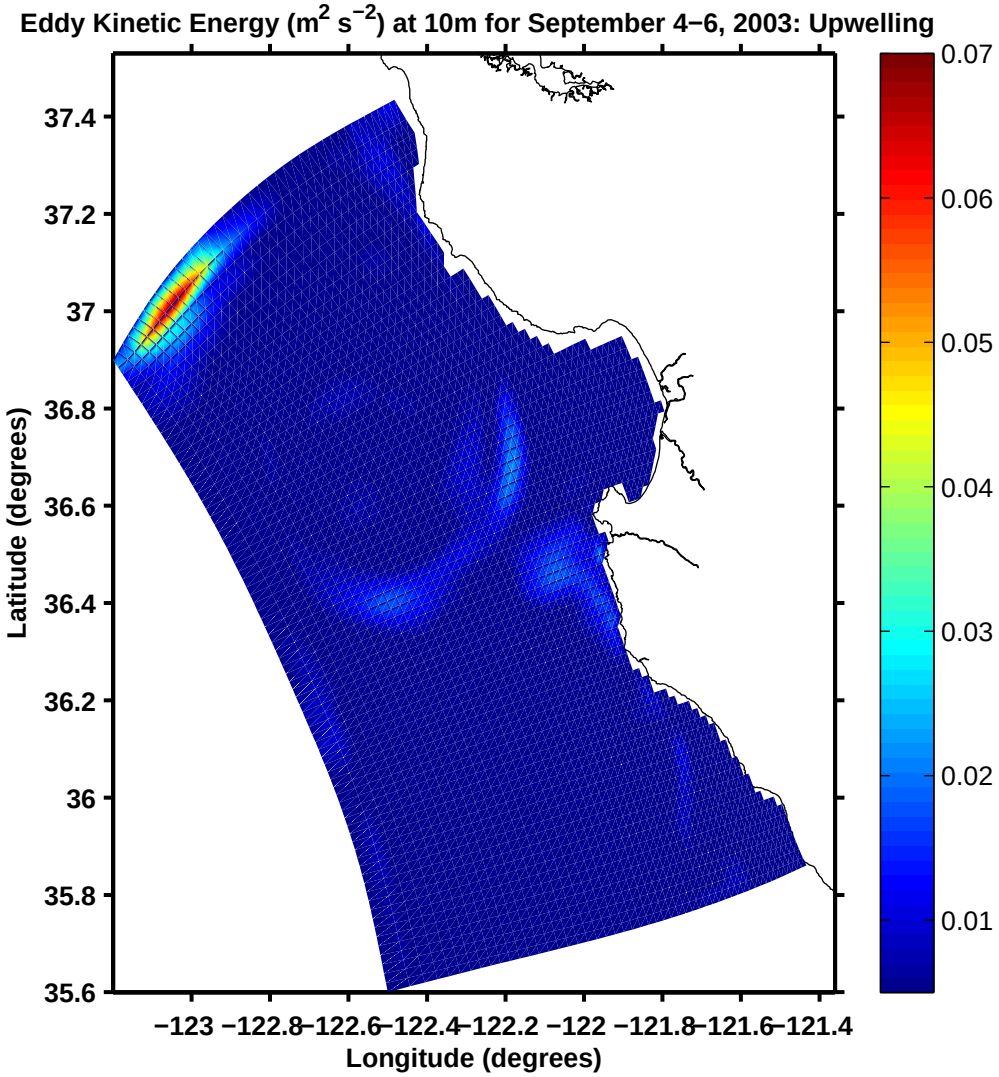

Figure 51. Model EKE at 10 m for UW3.

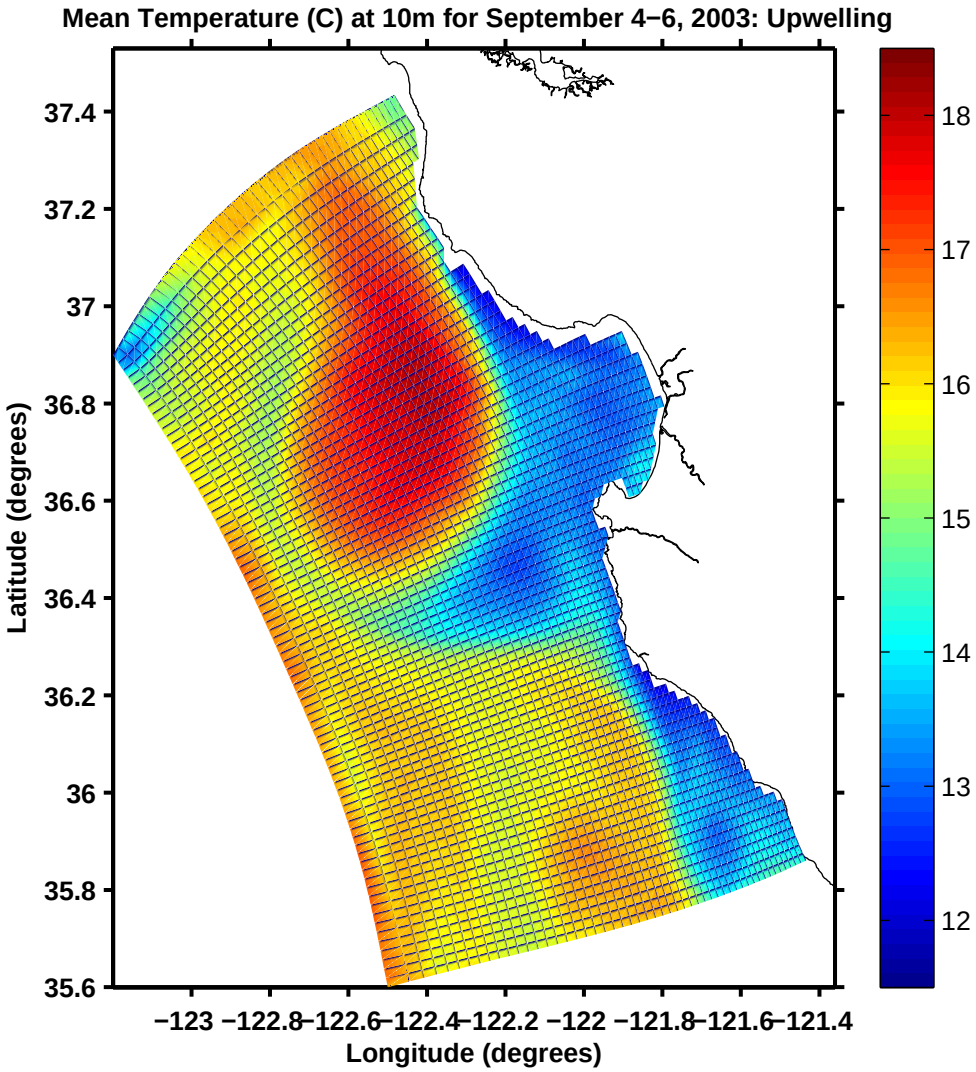

Figure 52. Model mean temperature at 10 m for UW3.

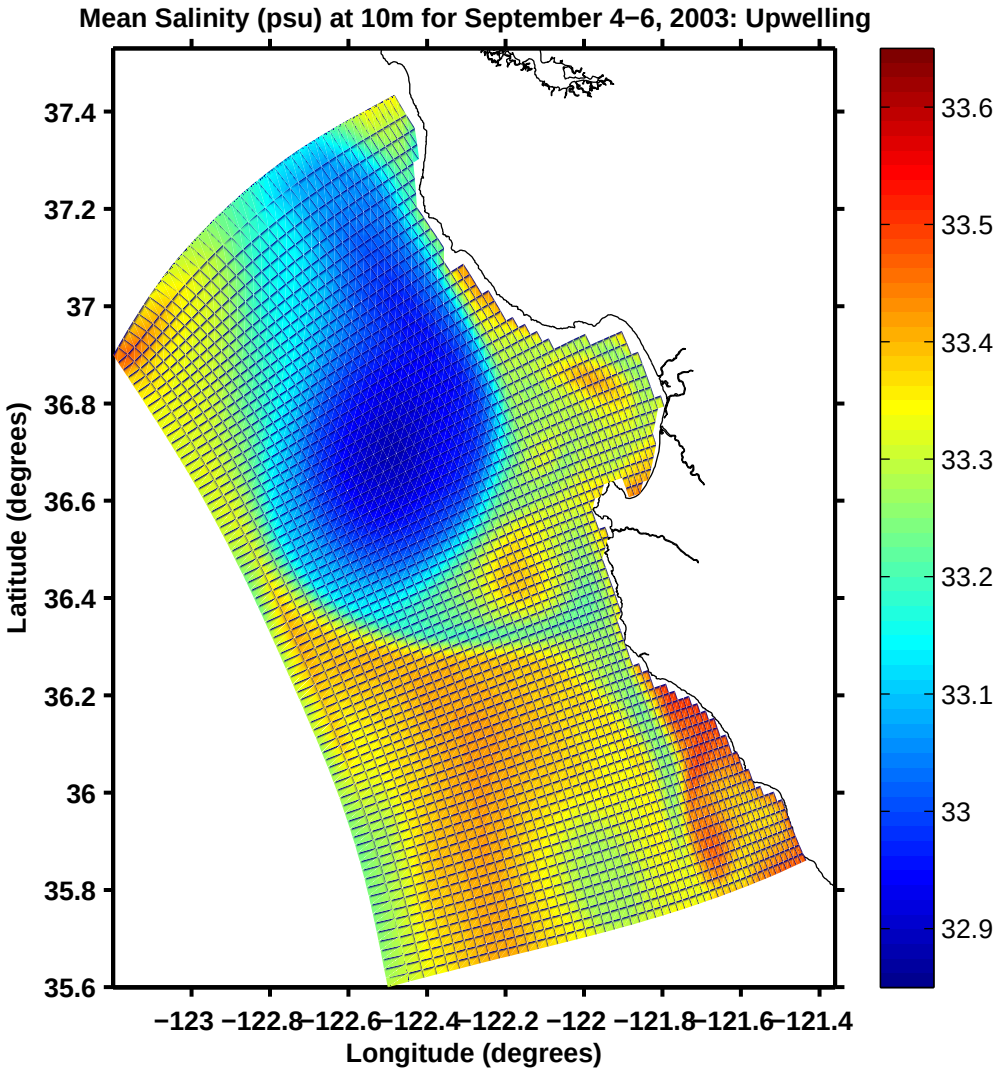

Figure 53. Model mean salinity at 10 m for UW3.

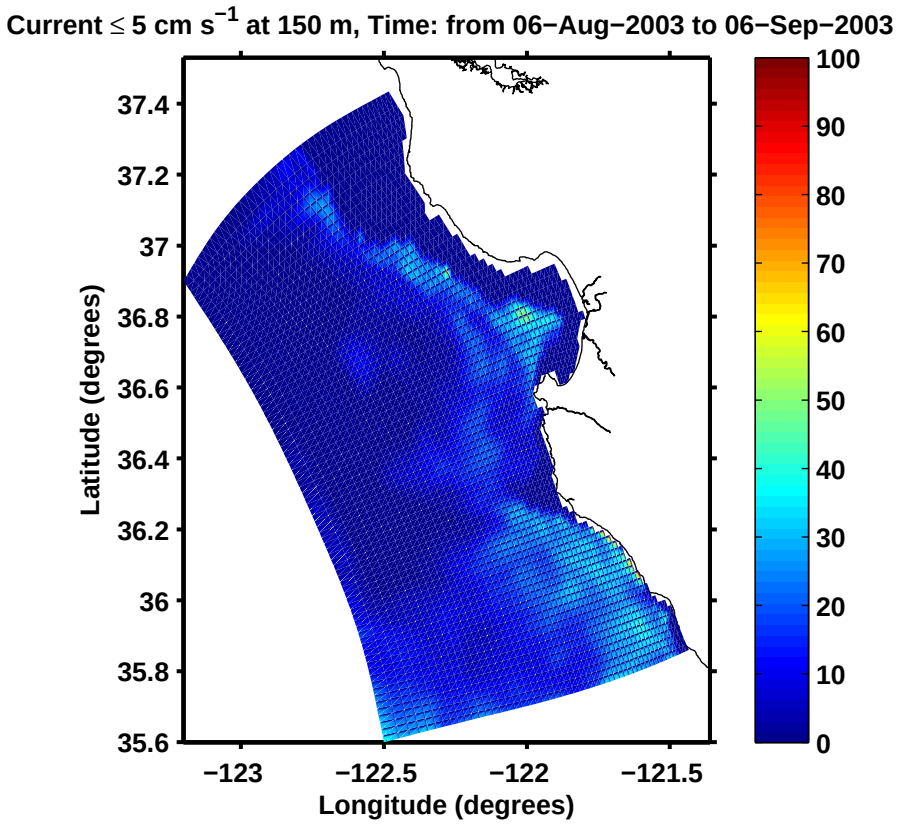

Figure 54. Percent time that model current speed at 150 m is less than or equal to 5 cm/s between August 6 and September 6, 2003.

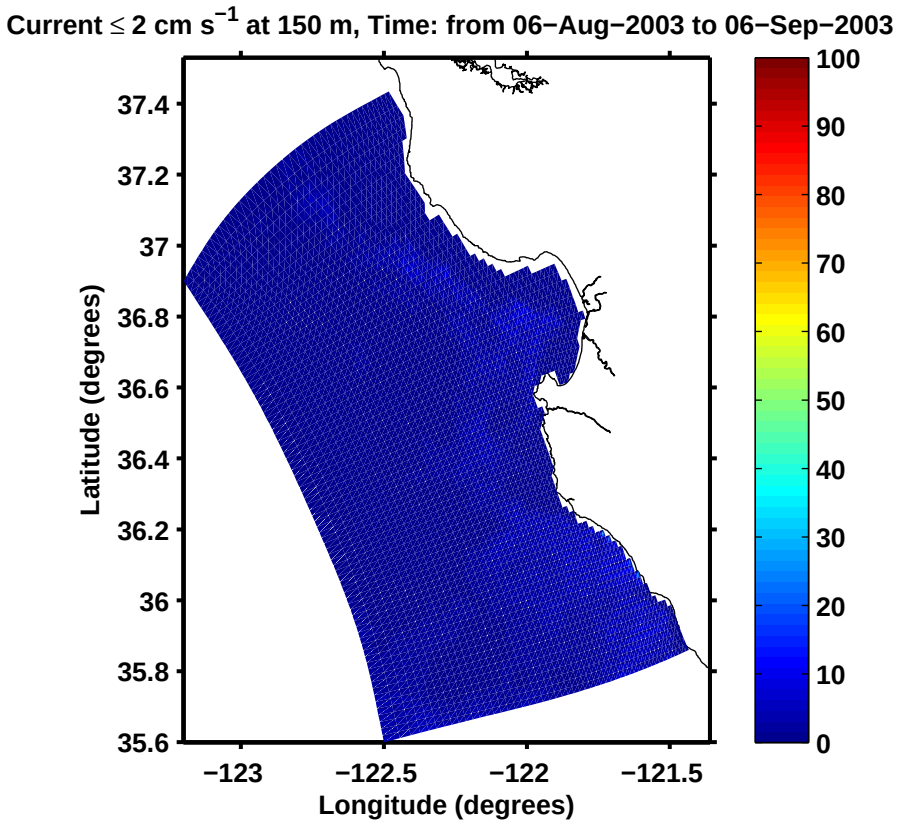

Figure 55. As in Figure 4 except for model current speed less than or equal to 2 cm/s.

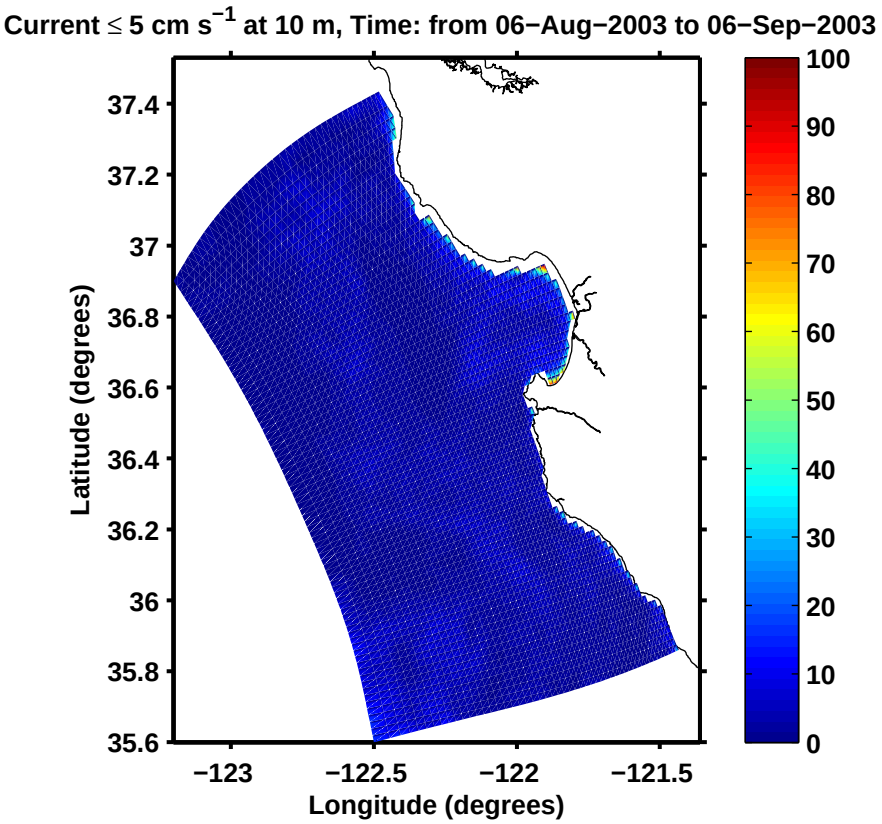

Figure 56. As in Figure 54 except for at 10 m.

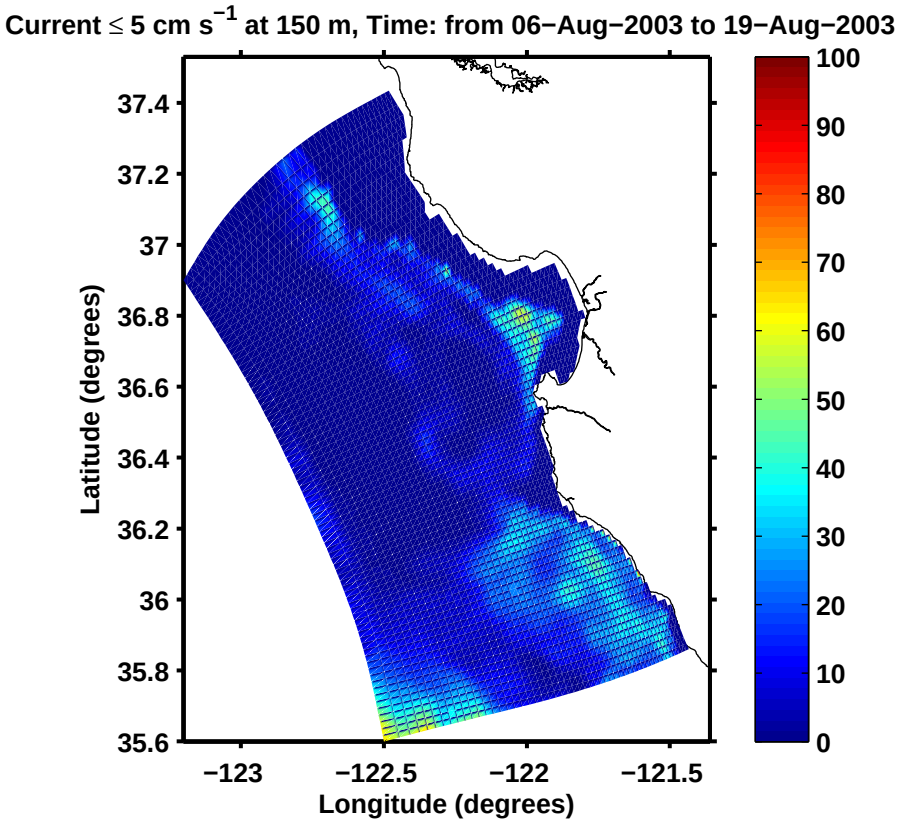

Figure 57. Model current speed threshold of 5 cm/s at 150 m for UW1.

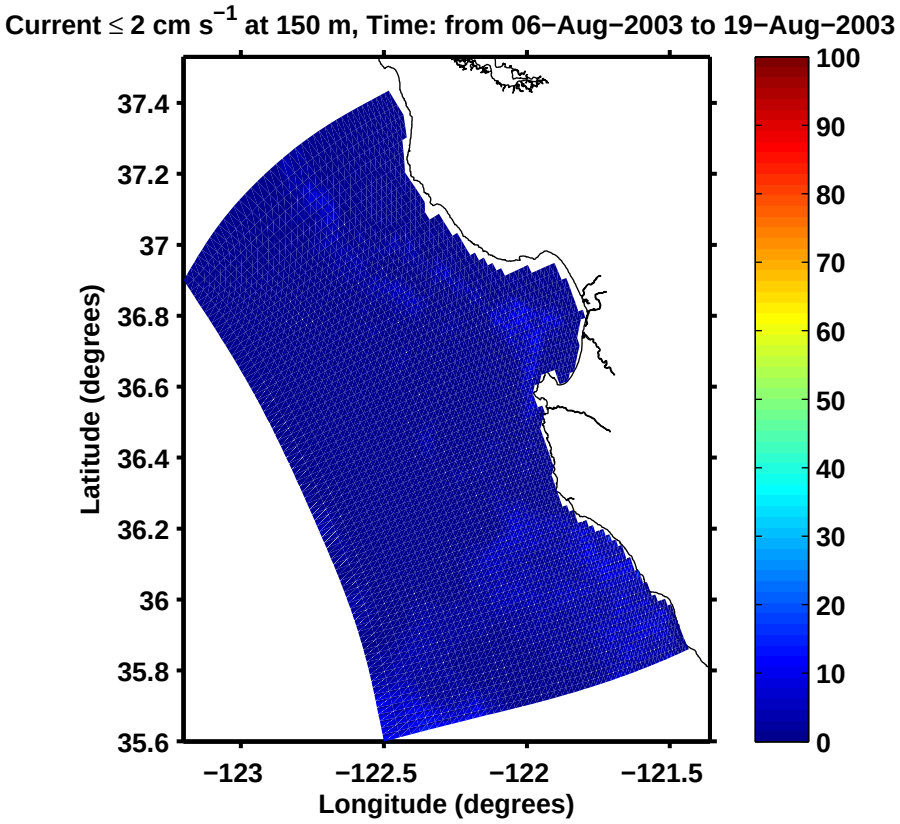

Figure 58. Model current speed threshold of 2 cm/s at 150 m for UW1.

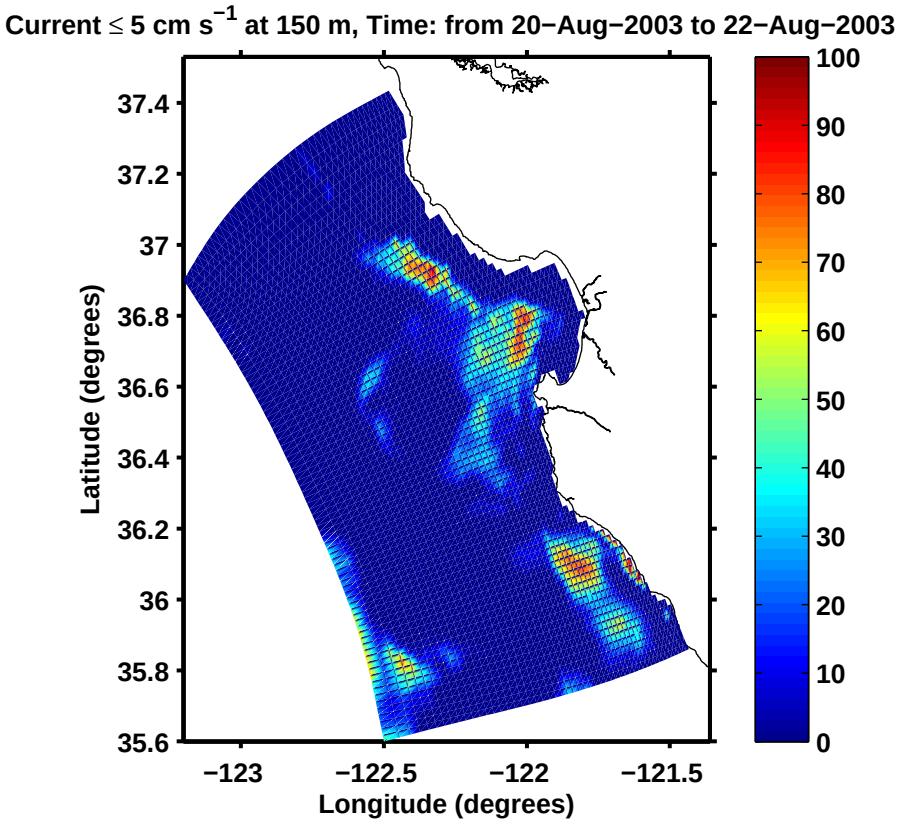

Figure 59. Model current speed threshold of 5 cm/s at 150 m for R1.

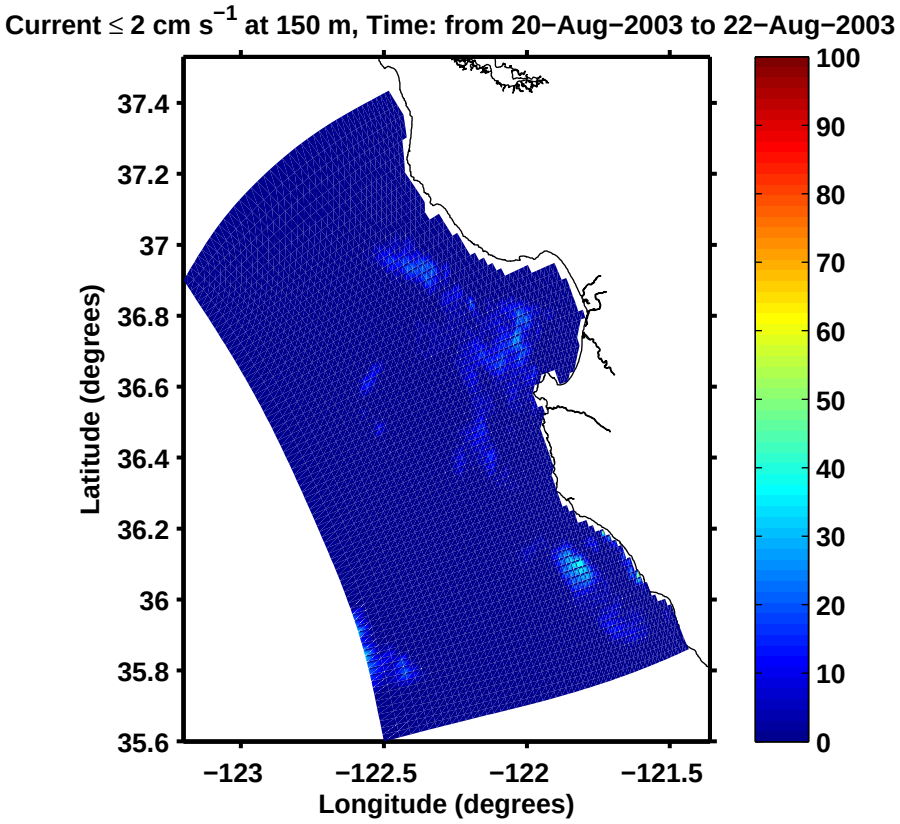

Figure 60. Model current speed threshold of 2 cm/s at 150 m for R1.

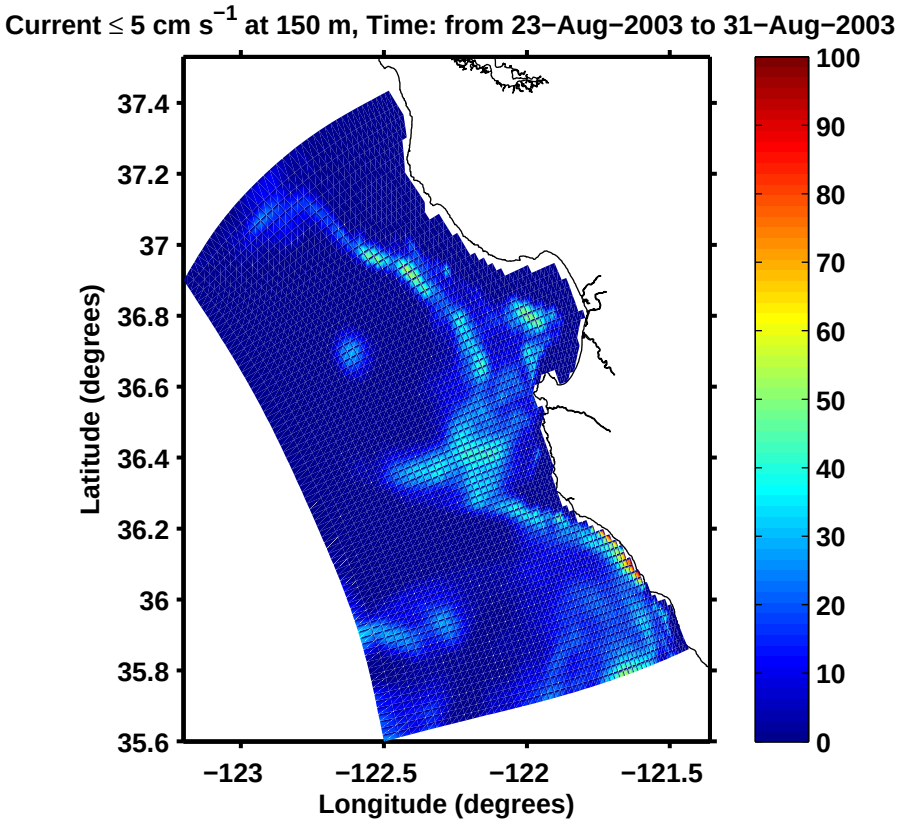

Figure 61. Model current speed threshold of 5 cm/s at 150 m for UW2.

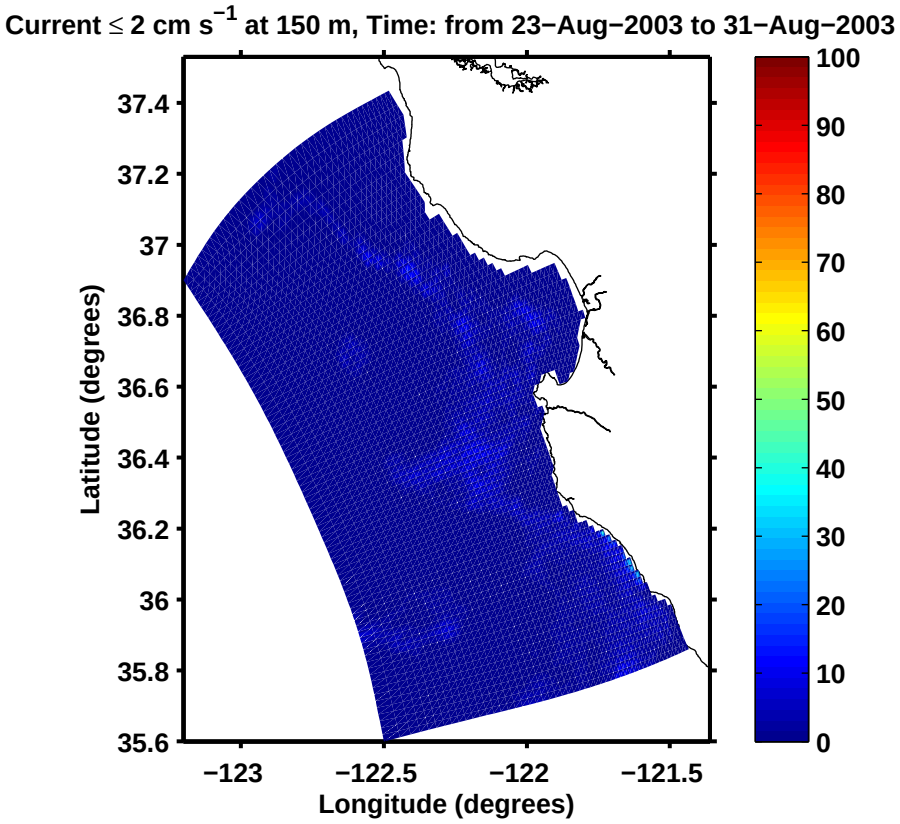

Figure 62. Model current speed threshold of 2 cm/s at 150 m for UW2.

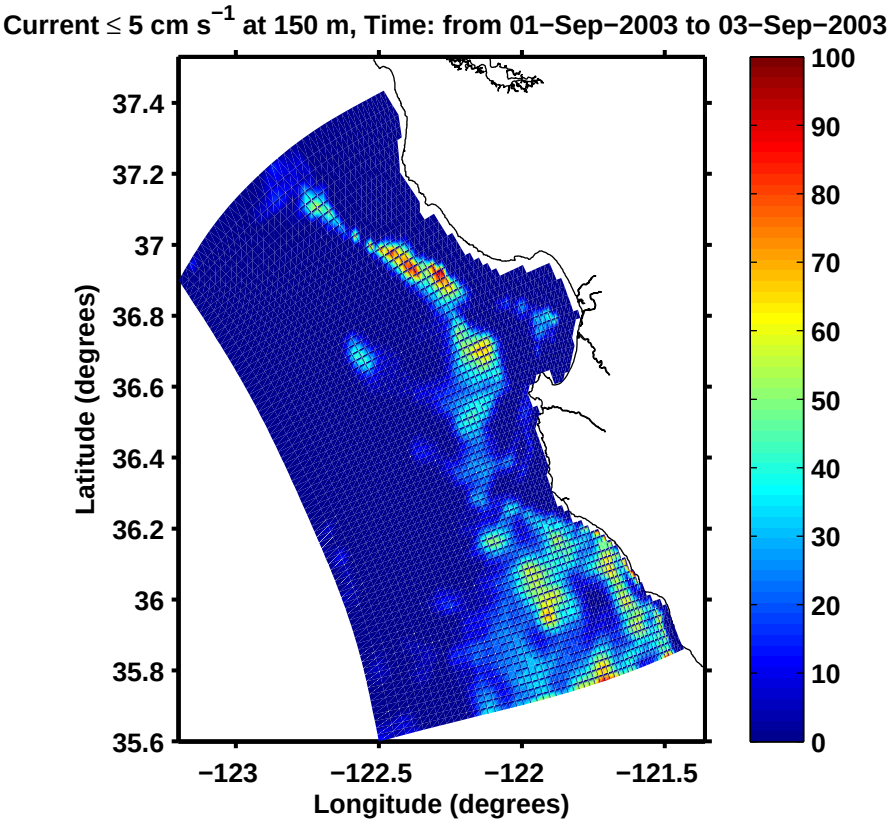

Figure 63. Model current speed threshold of 5 cm/s at 150 m for R2.

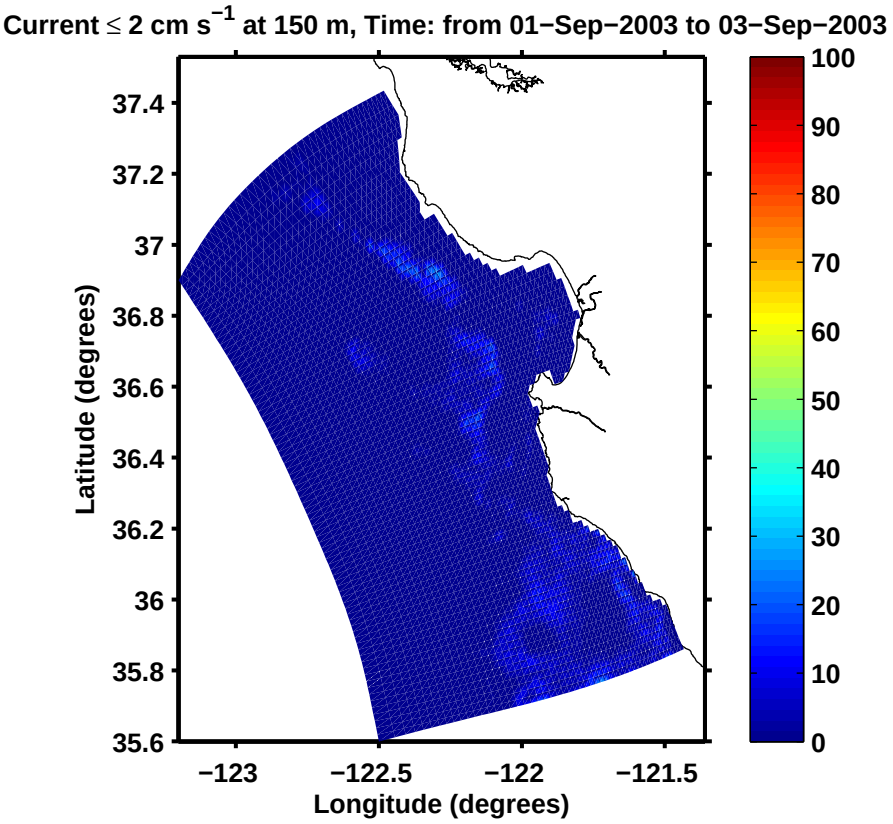

Figure 64. Model current speed threshold of 2 cm/s at 150 m for R2.

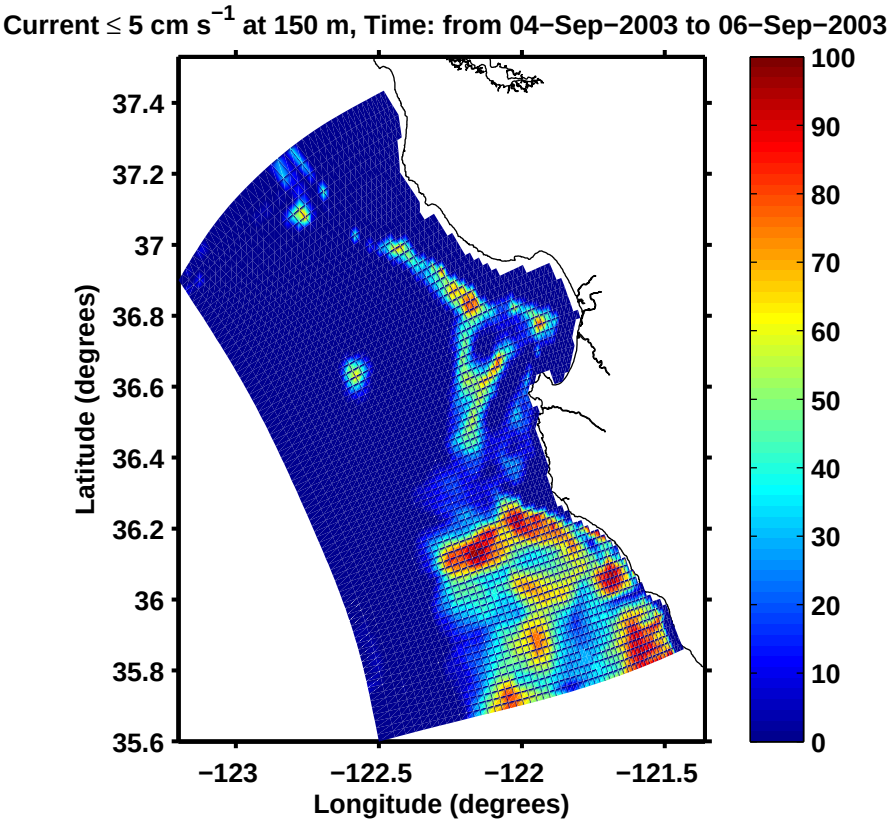

Figure 65. Model current speed threshold of 5 cm/s at 150 m for UW3.

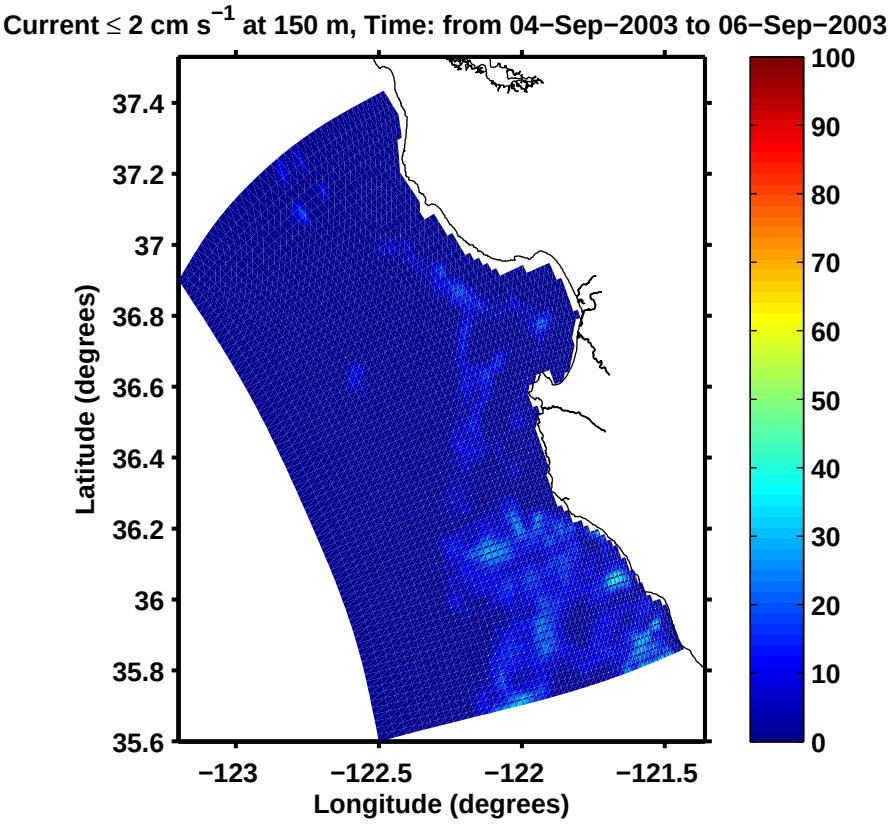

Figure 66. Model current speed threshold of 2 cm/s at 150 m for UW3.

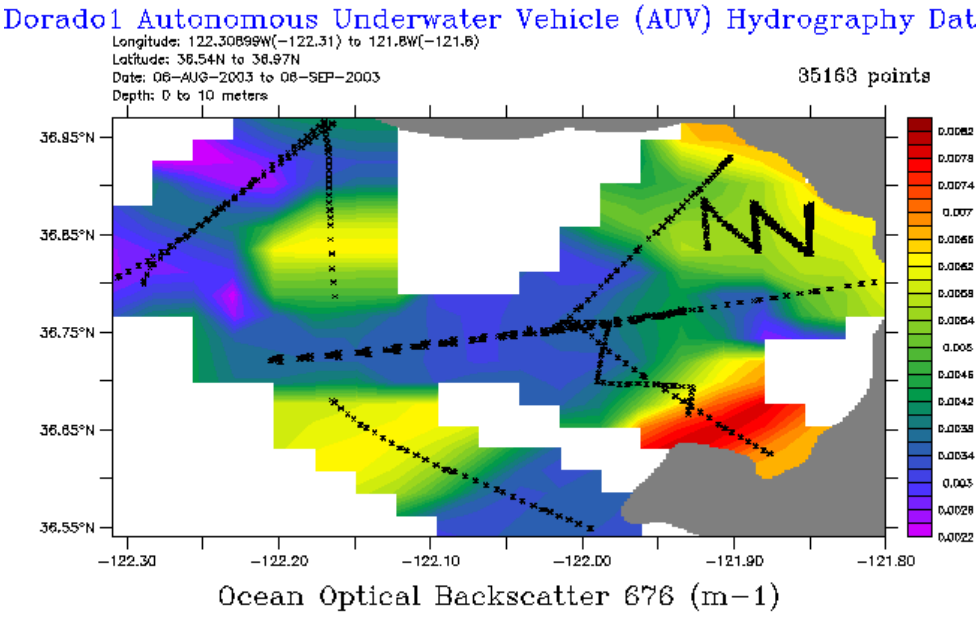

Figure 67. MBARI Dorado AUV ocean optical backscatter data from surface to 10 meters. Black lines denote vehicle survey tracks. Image courtesy http://aosn.mbari.org/lass/servlets/dataset.

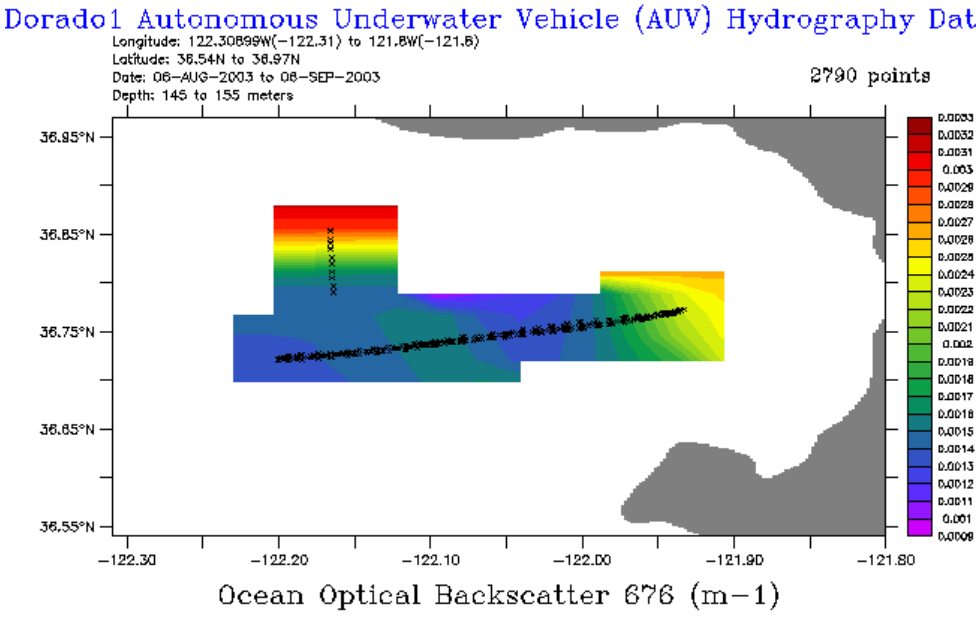

Figure 68. MBARI Dorado AUV ocean optical backscatter data from 145 to 155 m depth. Black lines denote vehicle survey tracks. Image courtesy http://aosn.mbari.org/lass/servlets/dataset.

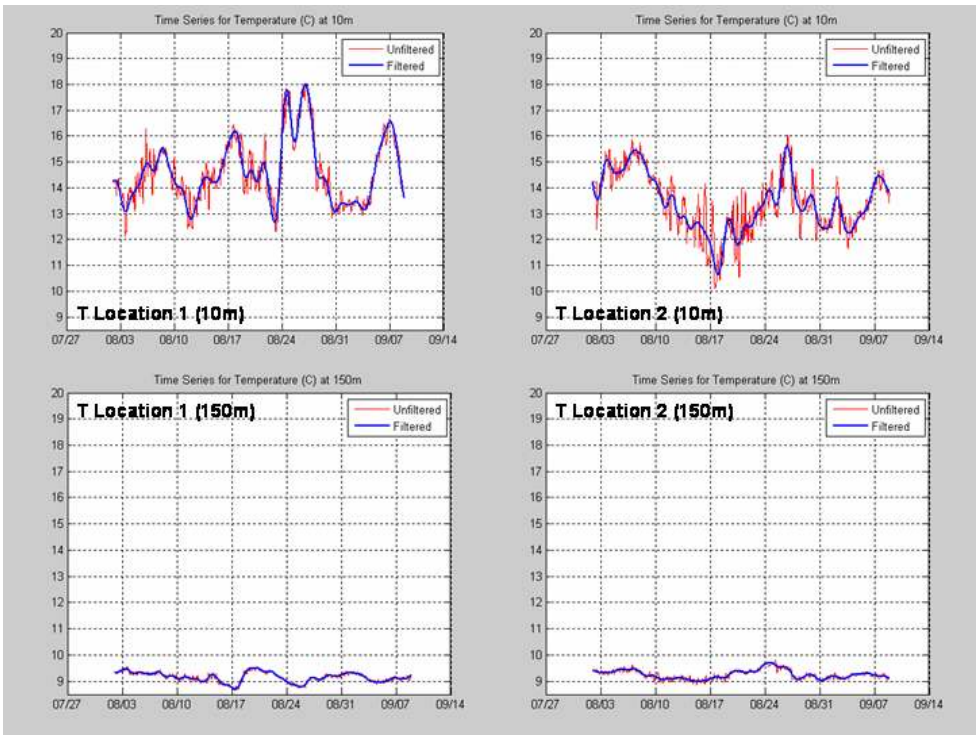

Figure 69. Time series for temperature at Locations 1 and 2 for 10 m and 150 m.

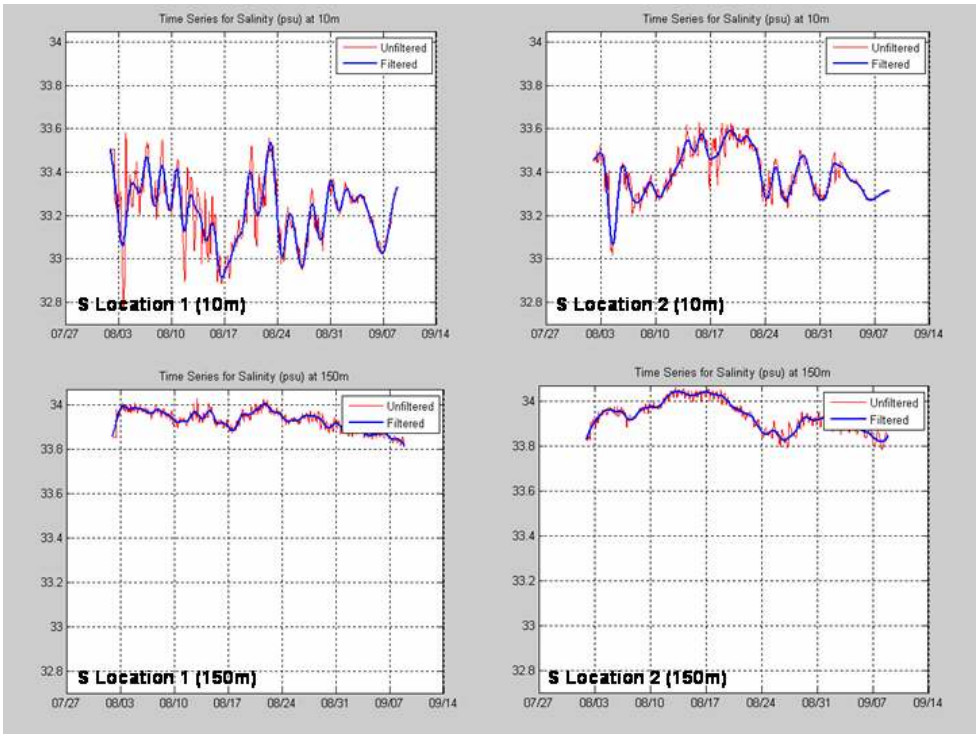

Figure 70. Time series for salinity at Locations 1 and 2 for 10 m and 150 m.

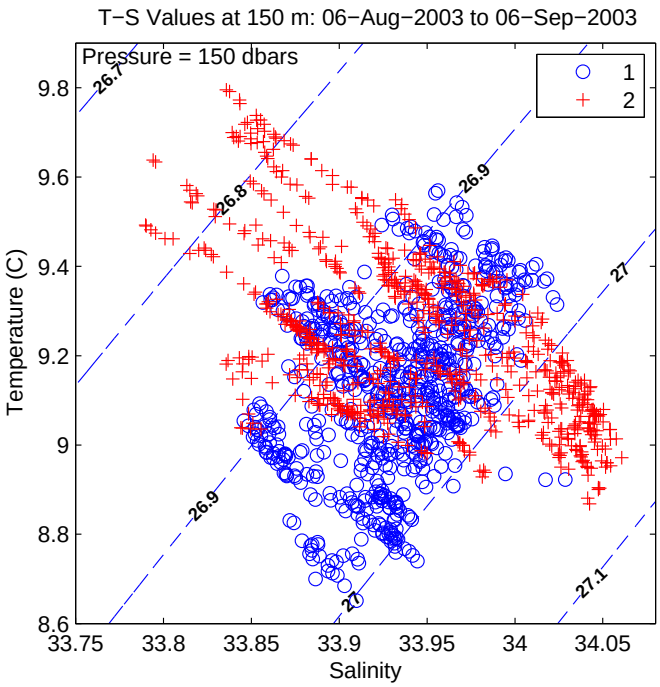

Figure 71. Temperature and salinity for Locations 1 and 2 at 150 m for August 6 - September 6, 2003. Density anomaly (dashed lines) in kg m^{-3}.

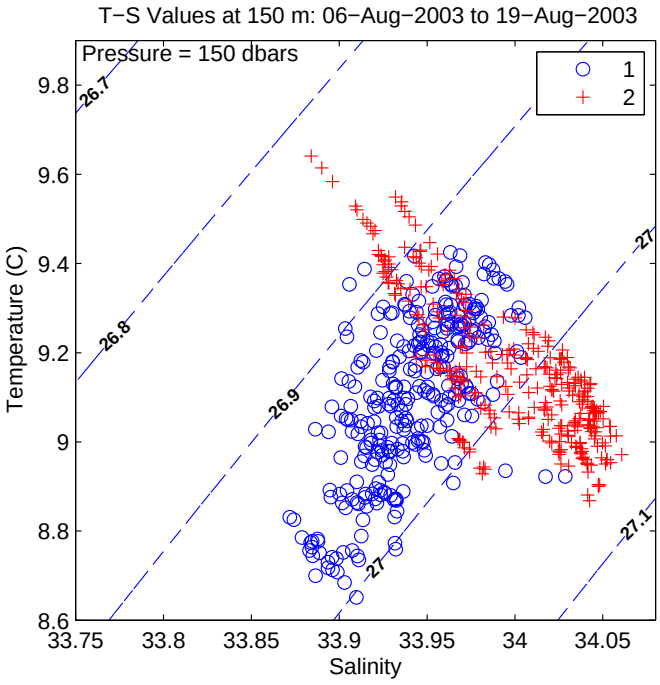

Figure 72. Temperature and salinity for Locations 1 and 2 at 150 m for August 6 – August 19, 2003. Density anomaly (dashed lines) in kg m^{-3}.

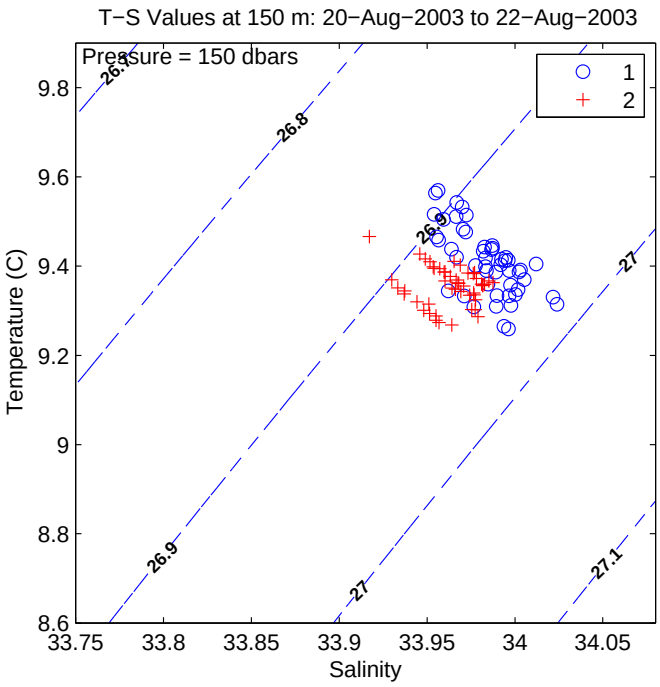

Figure 73. Temperature and salinity for Locations 1 and 2 at 150 m for August 20 – August 22, 2003. Density anomaly (dashed lines) in kg m^{-3}.

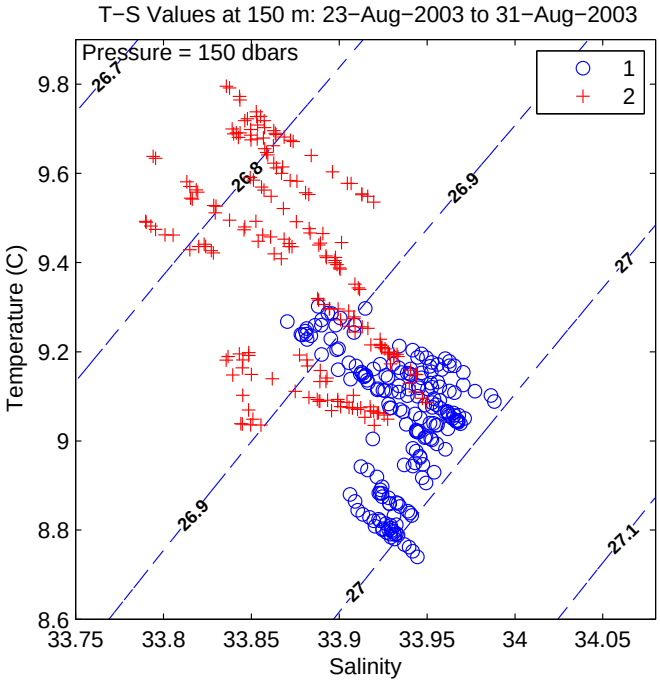

Figure 74. Temperature and salinity for Locations 1 and 2 at 150 m for August 23 – August 31, 2003. Density anomaly (dashed lines) in kg m^{-3}.

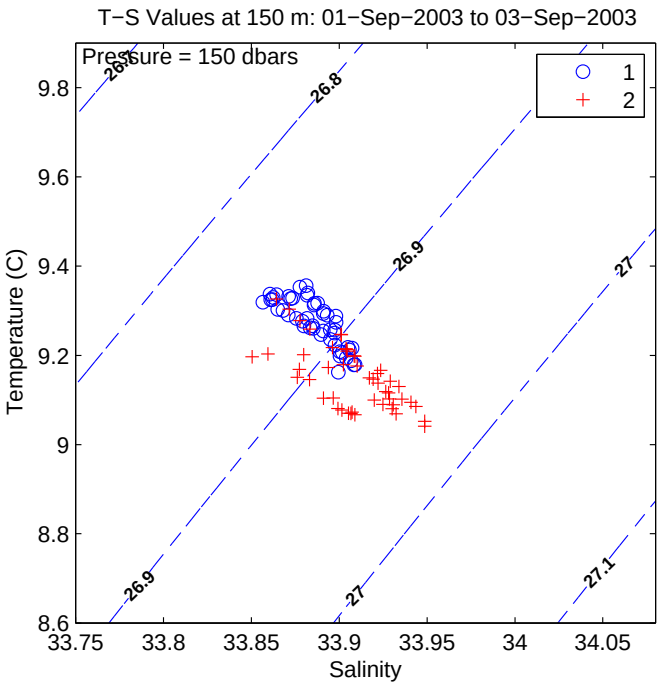

Figure 75. Temperature and salinity for Locations 1 and 2 at 150 m for September 1 - September 3, 2003. Density anomaly (dashed lines) in kg m^{-3}.

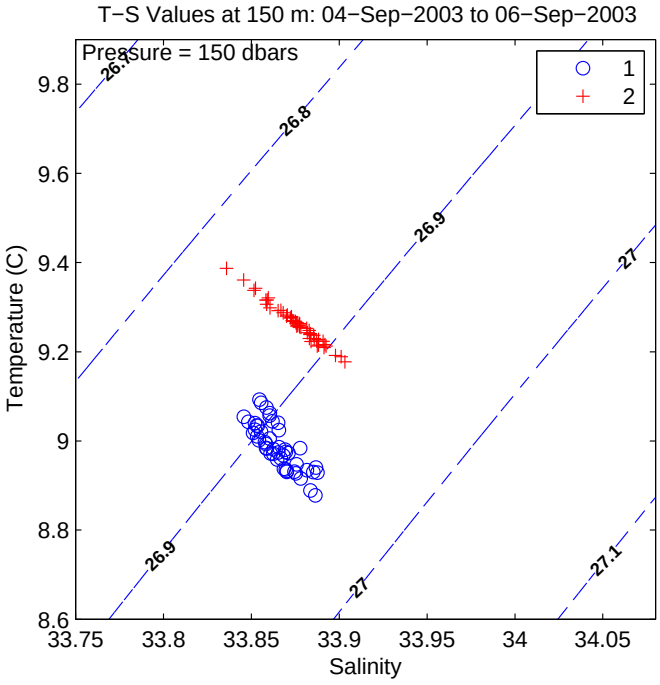

Figure 76. Temperature and salinity for Locations 1 and 2 at 150 m for September 4 - September 6, 2003. Density anomaly (dashed lines) in kg m^{-3}.

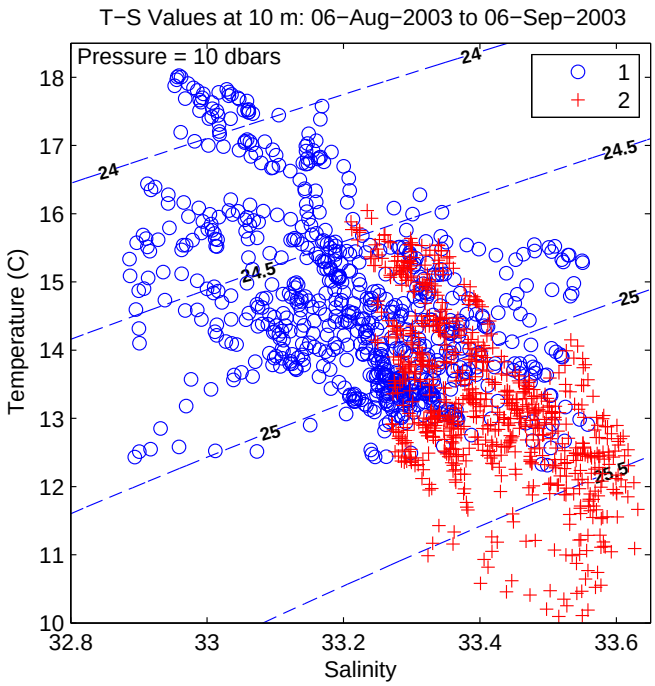

Figure 77. Temperature and salinity for Locations 1 and 2 at 10 m for August 6 - September 6, 2003. Density anomaly (dashed lines) in kg m^{-3}.

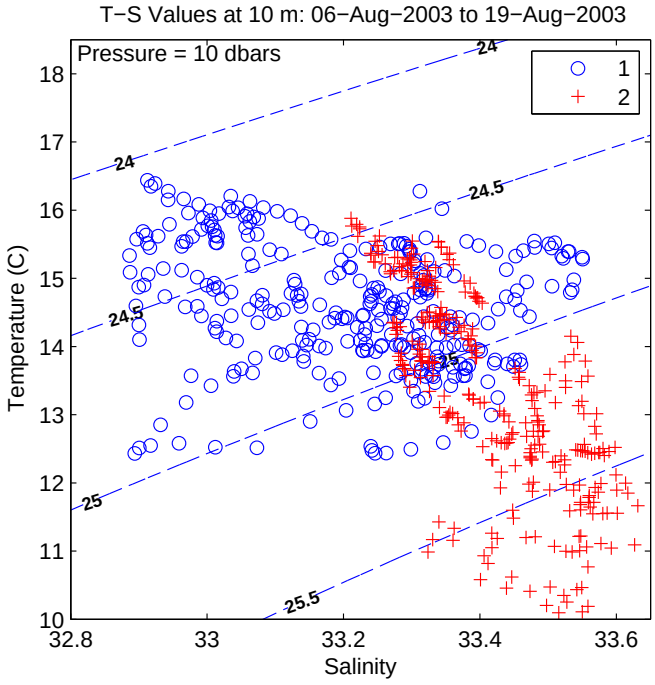

Figure 78. Temperature and salinity for Locations 1 and 2 at 10 m for August 6 – August 19, 2003. Density anomaly (dashed lines) in kg m^{-3}.

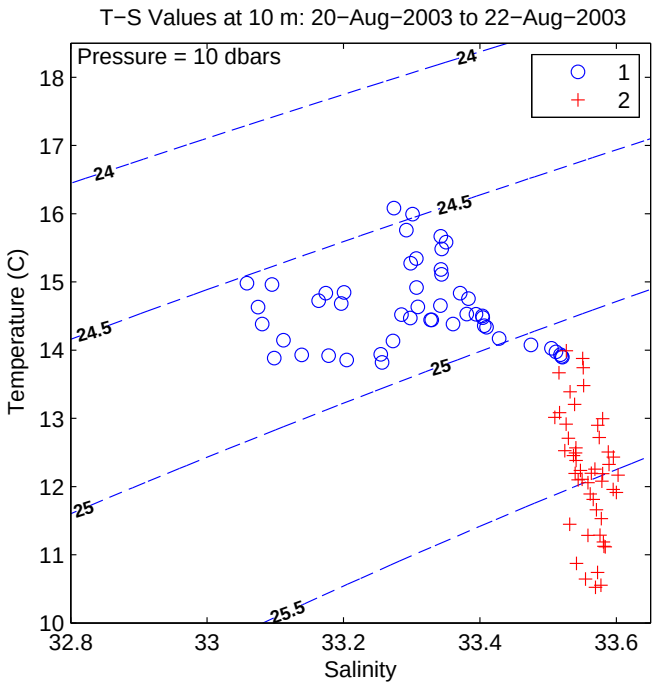

Figure 79. Temperature and salinity for Locations 1 and 2 at 10 m for August 20 – August 22, 2003. Density anomaly (dashed lines) in kg m^{-3}.

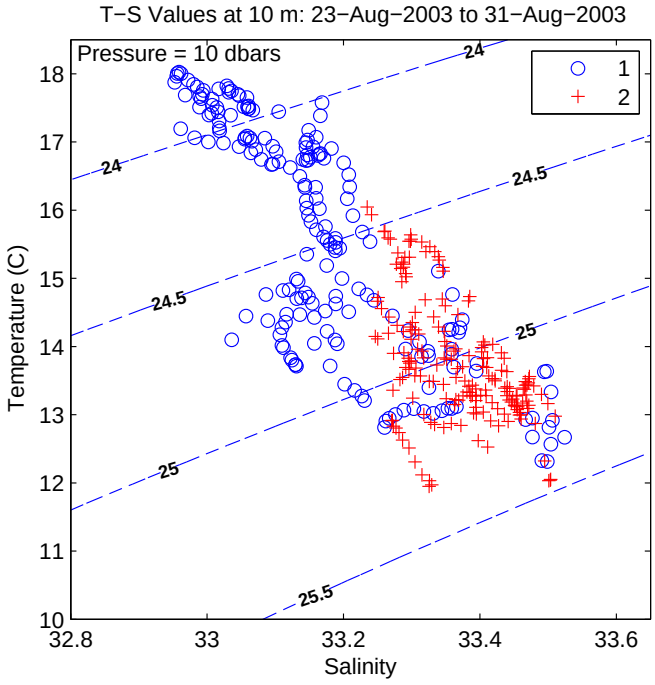

Figure 80. Temperature and salinity for Locations 1 and 2 at 10 m for August 23 – August 31, 2003. Density anomaly (dashed lines) in kg m^{-3}.

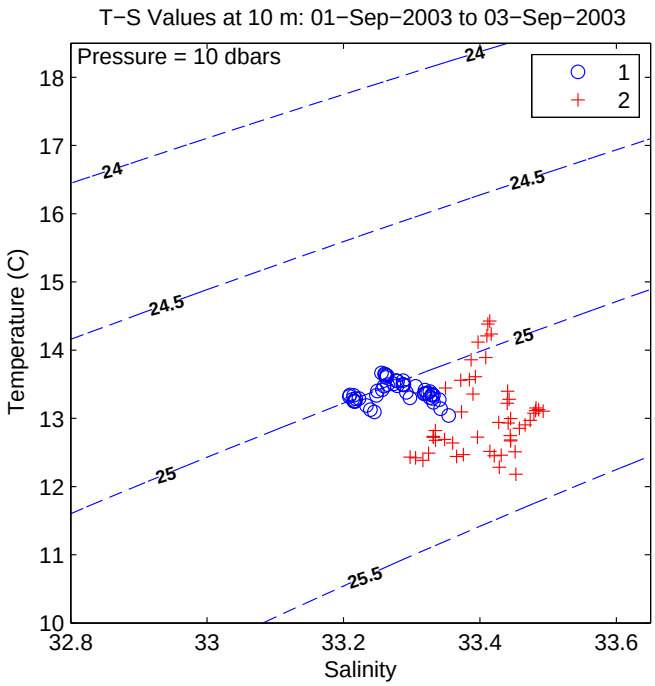

Figure 81. Temperature and salinity for Locations 1 and 2 at 10 m for September 1 - September 3, 2003. Density anomaly (dashed lines) in kg m^{-3}.

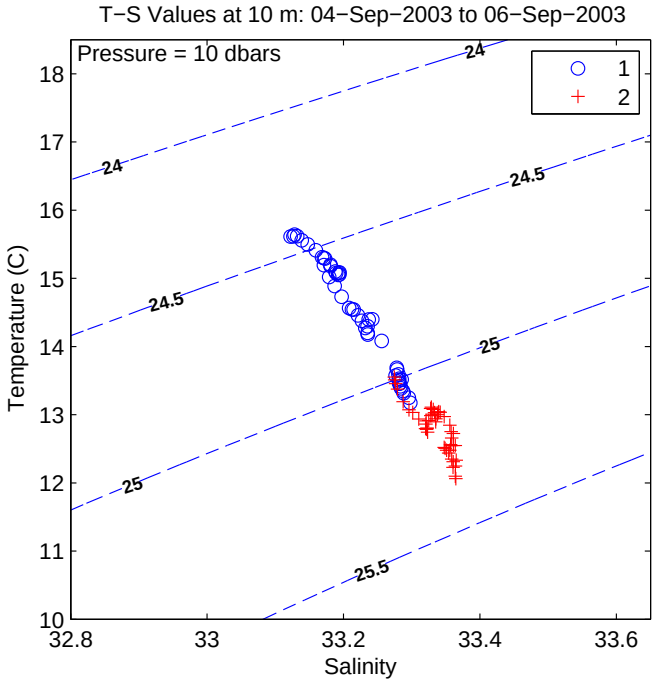

Figure 82. Temperature and salinity for Locations 1 and 2 at 10 m for September 4 - September 6, 2003. Density anomaly (dashed lines) in kg m^{-3}.

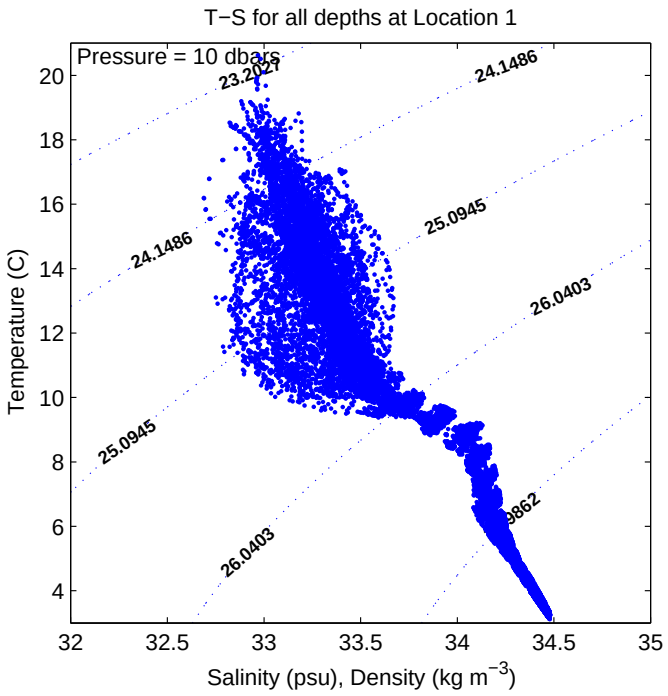

Figure 83. Model T-S data for all depths at Location 1 (outside the bay).

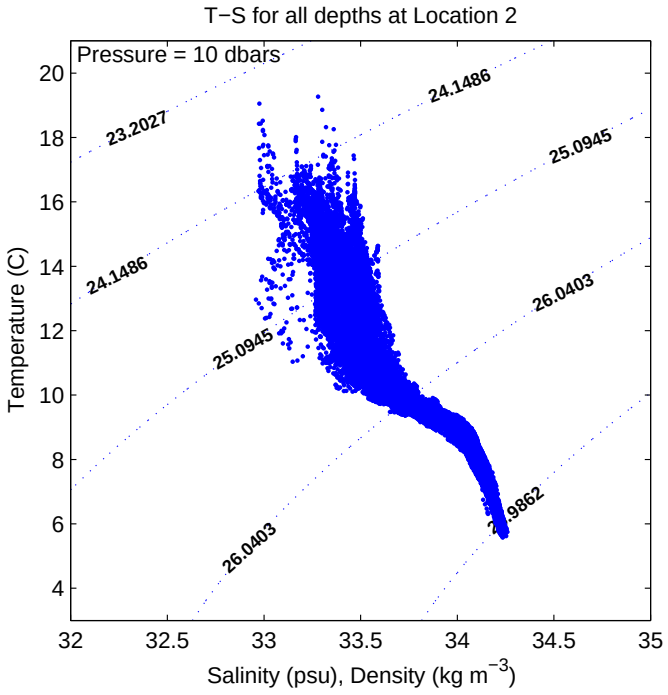

Figure 84. Model T-S data for all depths at Location 2 (inside the bay).

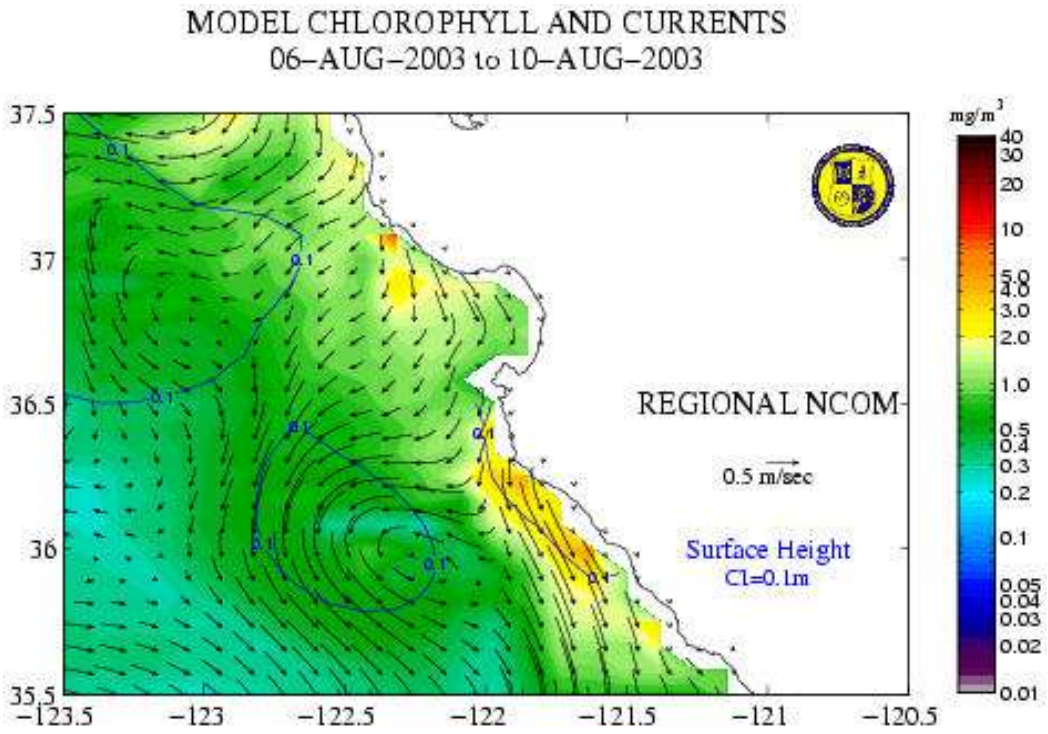

Figure 85. Chlorophyll and currents from Regional NCOM. Image courtesy http://www7320.nrlssc.navy.mil.

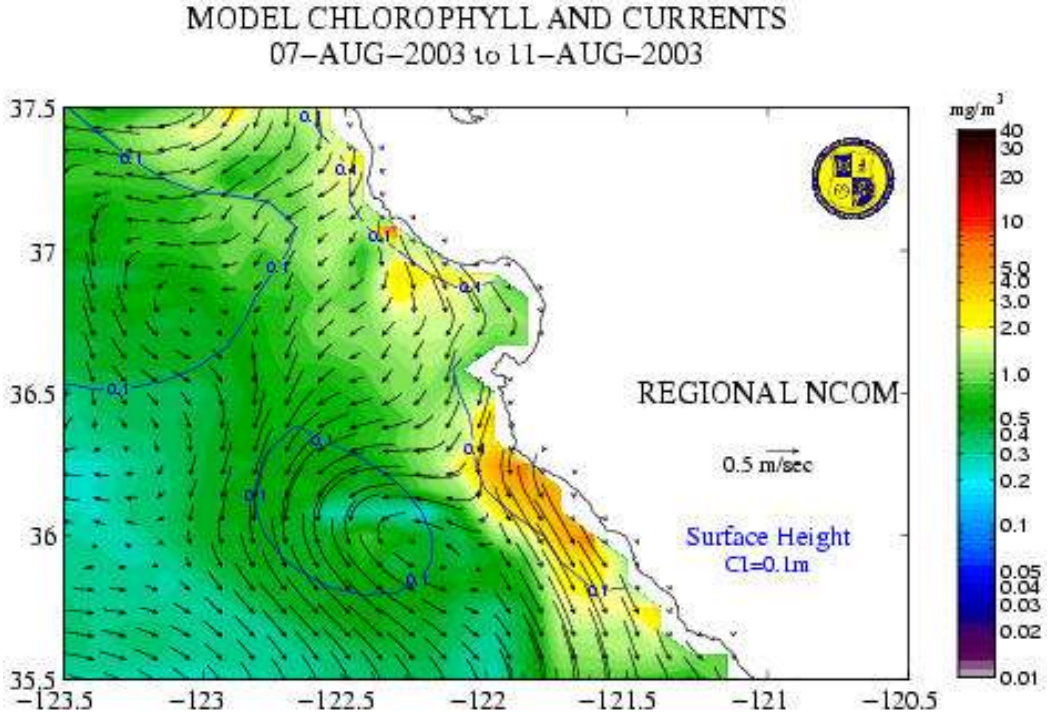

Figure 86. As in Figure 85 to show advection of chlorophyll during UW1.

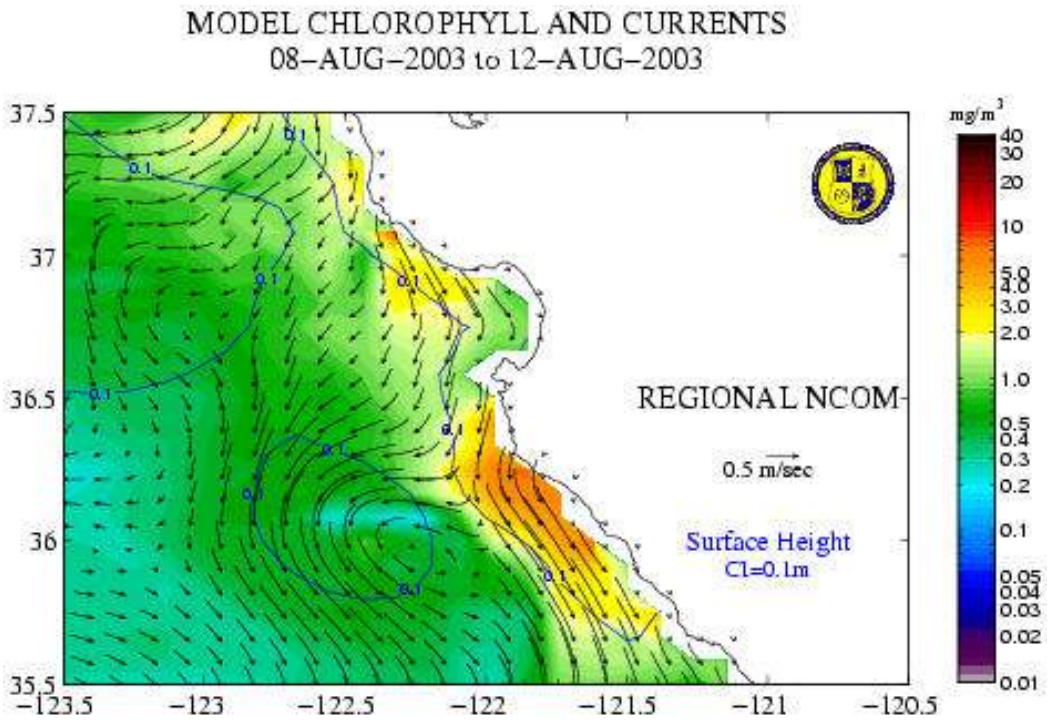

Figure 87. As in Figure 86 to show advection of chlorophyll during UW1.

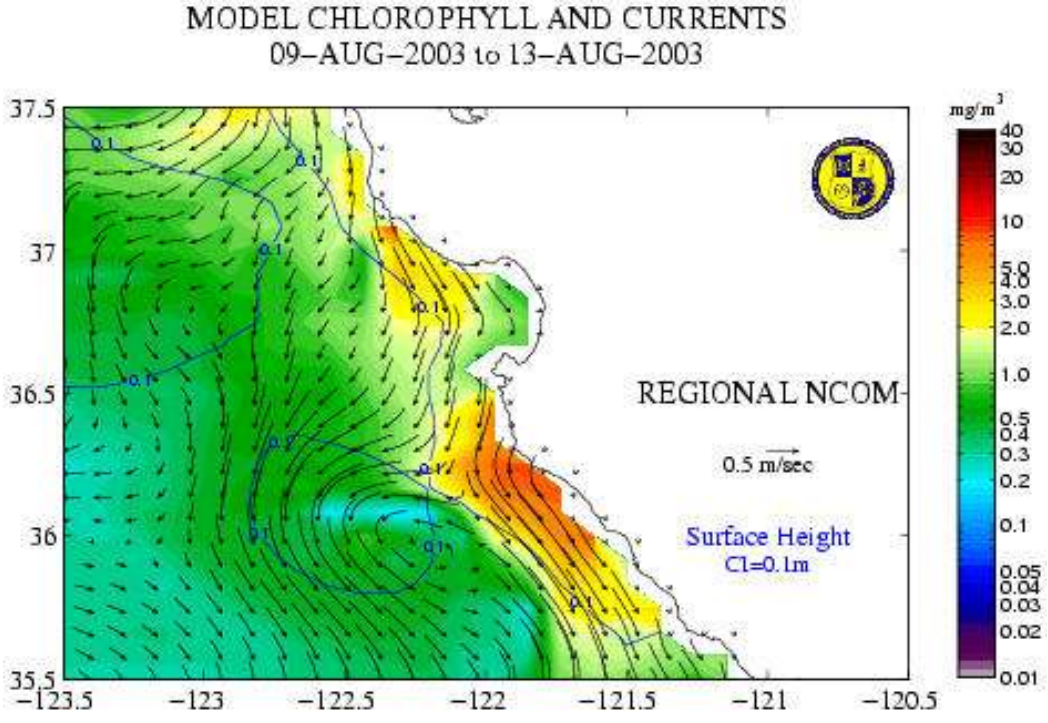

Figure 88. As in Figure 86 to show advection of chlorophyll during UW1.

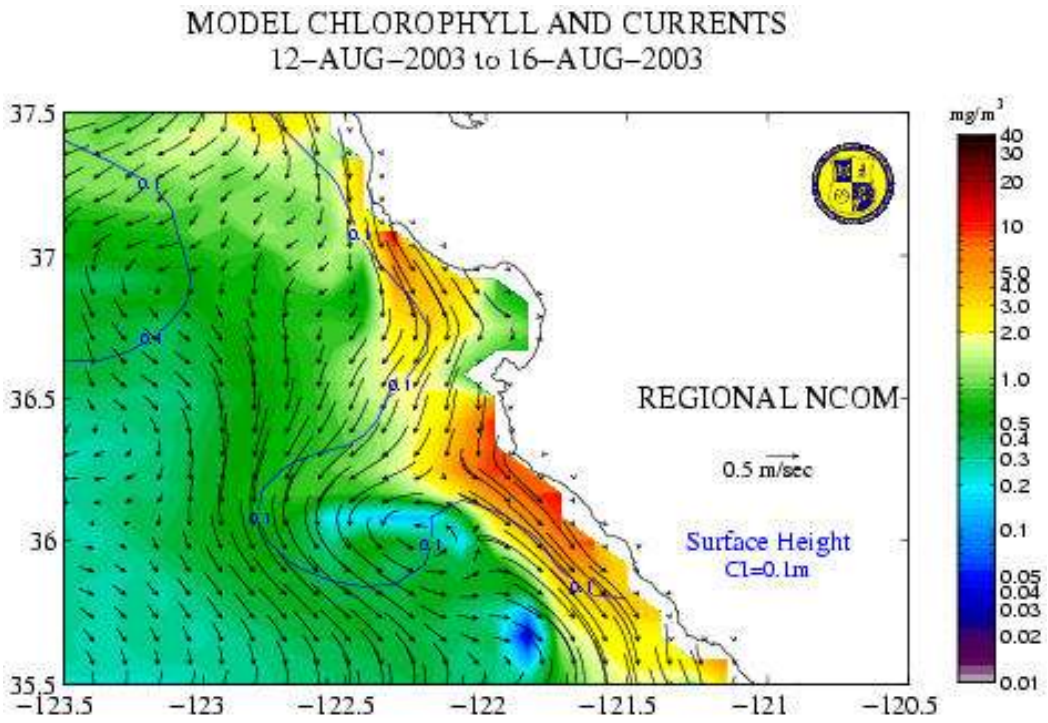

Figure 89. The model predicted chlorophyll concentration to peak around August 12, six days after the onset of upwelling.

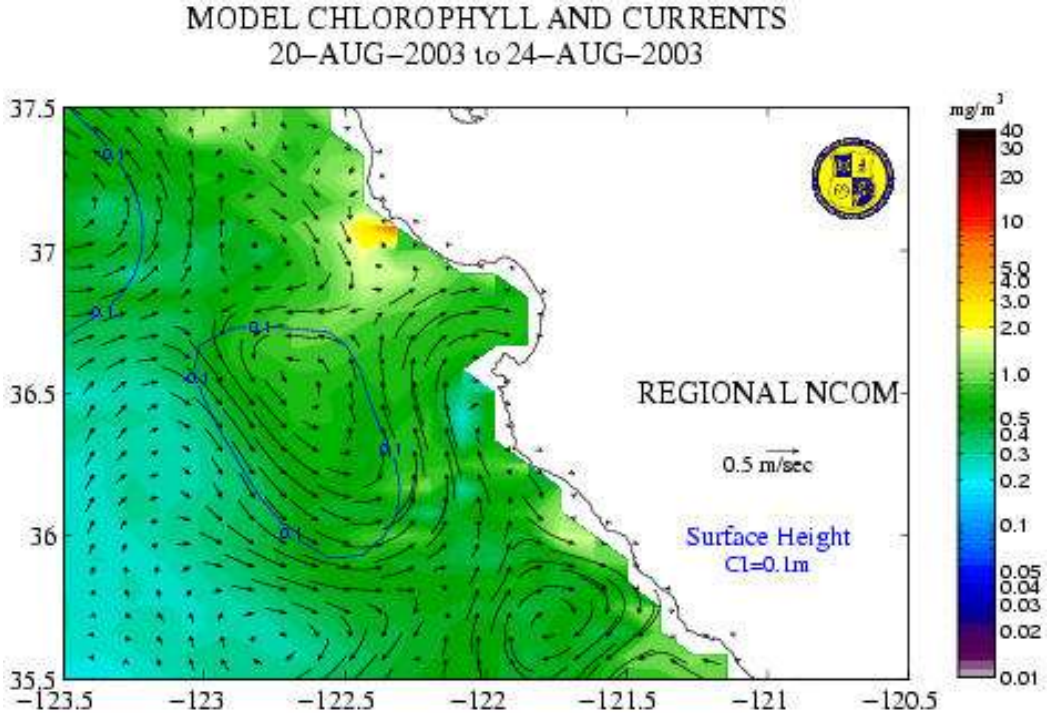

Figure 90. The model predicted the reduction of chlorophyll concentration in the bay during periods of wind relaxation.

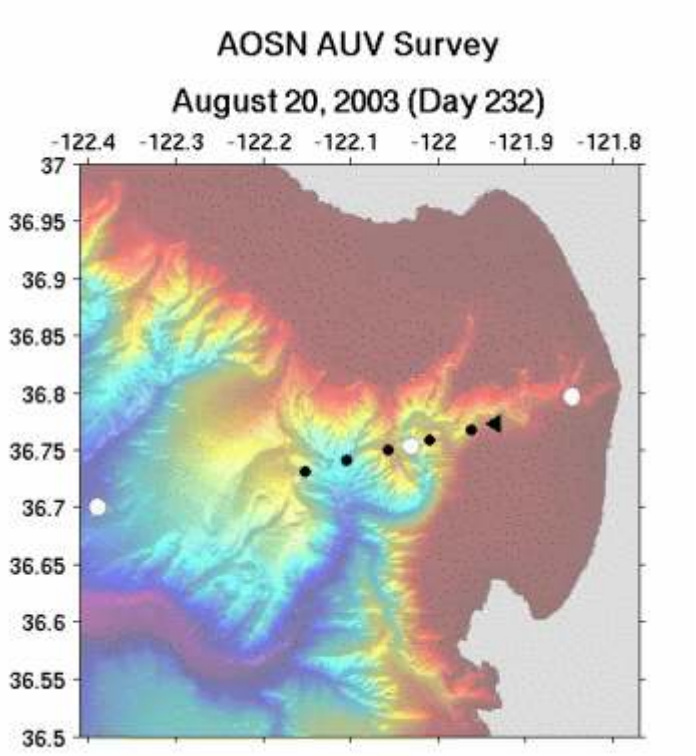

Figure 91. Black dots represent survey track for canyon axis surveys conducted by MBARI Dorado AUV during Summer 2003 AOSN II Experiment. Image courtesy of http://www.mbari.org/aosn/MontereyBay2003/auvctd.htm.

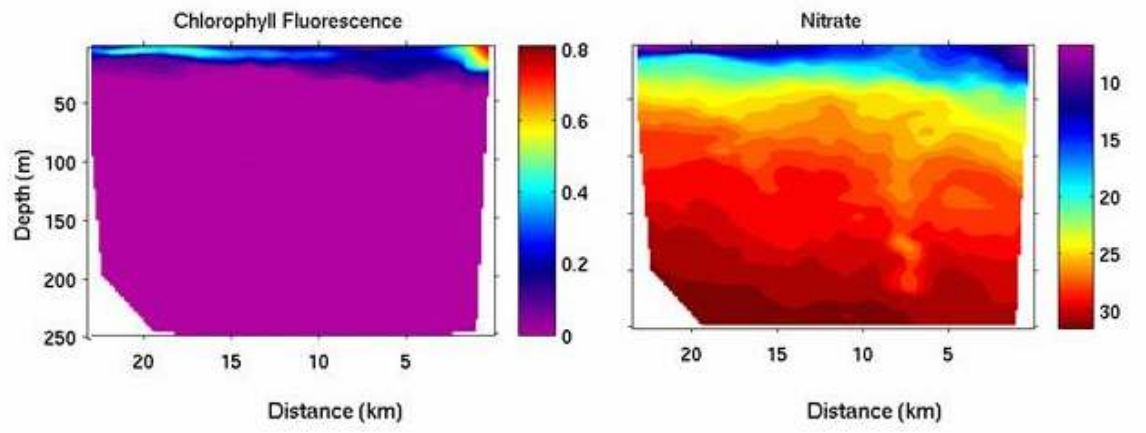

Figure 92. Chlorophyll fluorescence and nitrate data collected by Dorado AUV during canyon axis survey on August 12. The abscissa (x-axis) represents distance in kilometers from the shore. Image courtesy of http://www.mbari.org/aosn/MontereyBay2003/auvctd.htm.

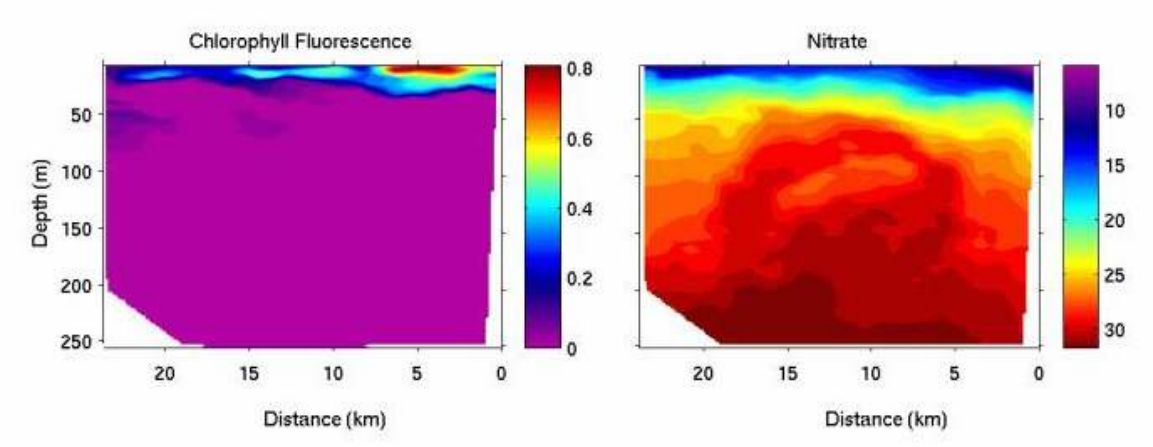

Figure 93. Chlorophyll fluorescence and nitrate data collected by Dorado AUV during canyon axis survey on August 20. The abscissa (x-axis) represents distance in kilometers from the shore. Image courtesy of http://www.mbari.org/aosn/MontereyBay2003/auvctd.htm.

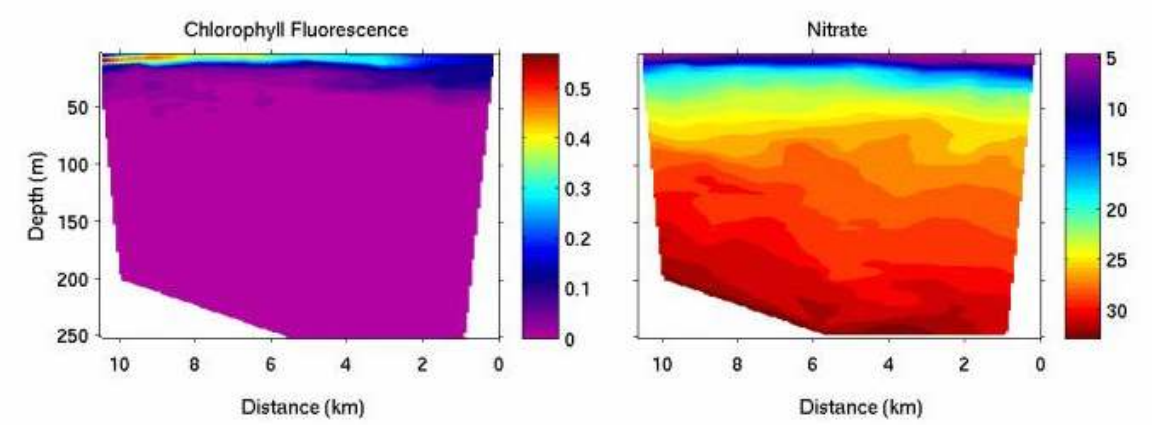

Figure 94. Chlorophyll fluorescence and nitrate data collected by Dorado AUV during canyon axis survey on August 26. The abscissa (x-axis) represents distance in kilometers from the shore. Image courtesy of http://www.mbari.org/aosn/MontereyBay2003/auvctd.htm.

THIS PAGE INTENTIONALLY LEFT BLANK

IV. CONCLUSIONS AND RECOMMENDATIONS

A. CONCLUSIONS

Analysis of the mean current, current variability, temperature, and salinity fields from the high resolution NCOM ICON model suggests that Monterey Bay's oceanographic properties make it conducive to krill accumulation. It has been hypothesized that krill amass where currents are weak and energy is low (Croll et al., 2005; Howard, 2005). The model indicates that Monterey Bay Canyon is an area of weak current flow and of low eddy kinetic energy. For nearly half of the hours between August 6 and September 6, 2003, model mean current speed inside the canyon was less than or equal to 5 cm s^{-1}; flow speed was less than or equal to 2 cm s^{-1} for 20% of the thirty day period. EKE inside the canyon was small (0.002 m^2 s^{-2}) and average diffusivity values were minimal. Ocean optical backscatter data covering the same time period indicated that the amount of particulate matter suspended in the water column was higher toward the canyon head than near the canyon mouth, which is exposed to the stronger circulation of the open ocean. The model predictions combined with the observational data imply that the canyon is an area where floating particles might collect for an extended period of time.

It has also been hypothesized that krill populations thrive in regions of high primary productivity (Croll et al., 2005). Chlorophyll concentration fields (from the Regional NCOM) and mean current fields from NCOM ICON predicted the southward advection of water from the Point Año Nuevo upwelling center into Monterey Bay. Model runs for each day of the thirty day period from August 6 to September 6 showed the timely increase of chlorophyll concentration, an indicator of primary production, in the bay during upwelling, and a decrease in the same during wind relaxation. Contemporary chlorophyll concentration data from the MBARI Dorado AUV also indicated productive surface waters in the bay.

B. LIMITATIONS AND RECOMMENDATIONS

Although the mean current and current variability fields predicted by the Navy Coastal Ocean Model suggest that Monterey Bay is an area of weak current flow and low eddy kinetic energy, each a factor conducive to plankton accumulation, there are limitations to this conclusion. As discussed above, the NCOM ICON model poorly resolves tidal mixing inside Monterey Bay, both at the canyon head and near the shelf break. For this reason, the current and current variability fields predicted by the model may contain inaccuracies.

Once tidal issues within large-scale models (NCOM ICON and others) have been addressed, it would be beneficial to conduct a similar analysis of the other models used during the Summer 2003 AOSN II experiment, the Harvard Ocean Prediction System (HOPS) and the Regional Ocean Modeling System (ROMS). Moreover, subsequent studies should consider a longer time record to capture model-predicted seasonal and interannual changes in circulation. It is also recommended that ecosystem variables (e.g. chlorophyll, nitrate, and phosphate) be included in the high resolution NCOM ICON model to better track the timing and connection between oceanographic circulation and biological observations.

Further studies should also include a wider variety of observational data to substantiate model-predicted circulation features. These data might include CODAR observations of sea surface currents or time series of subsurface ocean structure from moored buoys and AUV surveys in Monterey Bay. Follow on studies might also attempt to correlate concurrent whale sightings and plankton density observations with the models' predictions.

LIST OF REFERENCES

Antal, T.K., Venedictov, T.S., Matorin, D.N., Ostrowska, M., Wozniak, B., & Rubin, A.B. (2001). Measurement of phytoplankton photosynthesis rate using a pump-and-probe fluorometer. *Oceanologia*, **43**, 291-313. Retrieved September 17, 2007 from http://www.iopan.gda.pl/oceanologia/433antal.pdf.

Croll, D.A., Tershy, B.R., Hewitt, R.P., Demer, D.A., Fiedler, P.C., Smith, S.E., et al. (1998). An integrated approach to the foraging ecology of marine birds and mammals. *Deep-Sea Research II*, **45**, 1353-1371.

Croll, D.A., Marinovic, B., Benson, S., Chavez, F.P., Black, N., Ternullo, R., et al. (2005). From wind to whales: trophic links in a coastal upwelling system. *Marine Ecology Progress Series*, **289**, 117-130.

Enriquez, A.G., & Friehe, C.A. (1995). Effects of wind stress and wind stress curl variability on coastal upwelling. *J. Phys. Oceanogr.*, **25**, 1651-1671.

Fiedler, P.C., Reilly, S.B., Hewitt, R.P., Demer, D., Philbrick, V.A., Smith, S., et al. (1998). Blue whale habitat and prey in the California Channel Islands. *Deep Sea Research II*, **45**, 1781-1801.

Garrison, T. (2001). *Essentials of oceanography* (2nd ed.). Pacific Grove, CA: Brooks/Cole.

Giannetti, P. (1993). *The velocity field in the Northeast Atlantic from satellite-tracked drifting buoys*. Unpublished Master's Thesis, Naval Postgraduate School, Monterey, CA.

Howard, D. (2005). Krill in Cordell Bank National Marine Sanctuary. Retrieved October 25, 2006 from http://oceanexplorer.noaa.gov/explorations/02quest/background/krill/krill.html.

Ignatyev, S.M. (1999). Functional-morphological adaptations of the krill to active swimming. Poster on the 2nd International Symposium on Krill, Santa Cruz, California, USA; August 23-27, 1999. Retrieved October 23, 2006 from http://www.ibss.iuf.net/people/ignat/ikrill99.html.

Jaffe, J.S., Ohmann, M.D., & DeRobertis, A. (1999). Sonar estimates of daytime activity levels of *Euphausia pacifica* in Saanich Inlet. *Can. J. Fish. Aquat. Sci.*, **56**, 2000-2010.

Limeburner, R. (Ed.). (1985). Code II: Moored array and large-scale data report. Tech. Rep. **85-35**, 234. Woods Hole, Mass.: Woods Hole Oceanogr. Inst.

Mauchline, J., & Fisher, L.R. (1969). The biology of euphausiids. *Adv. Mar. Biol*., **7**.

Moline, M.A., Blackwell, S.M., Case, J.F., Haddock, S.H.D., Herren, C.M., Orrico, C.M., et al. (unpublished). *Structure and interaction of coastal planktonic communities using bioluminescence*.

Monterey Canyon (2007). Retrieved September 6, 2007, from http://en.wikipedia.org/wiki/Monterey_Canyon.

Pennington, J.T., & Chavez, F.P. (2000). Seasonal fluctuations of temperature, salinity, nitrate, chlorophyll and primary production at station H3/M1 over 1989-1996 in Monterey Bay, CA. *Deep Sea Research II*, **47**, 947-973.

Ramp, S.R., Lermusiaux, P., Davis, R.E., Chao, Y., Fratantoni, D., Leonard, N.E., et al. (2007). The autonomous ocean sensing network (AOSN) predictive skill experiment in the Monterey Bay. *Deep Sea Research*, (submitted).

Rosenfeld, L.K., Shulman, I., Cook, M.S., Paduan, J.D., & Shulman, L. (2007). Development of a tidal model for central California. *Deep Sea Research*, (submitted).

Ryan, J.P., Chavez, F.P., & Bellingham, J.G. (2005). Physical-biological coupling in Monterey Bay, California: topographic influences on phytoplankton ecology. *Marine Ecology Progress Series,* **287**, 23-32.

Service, S.K., Rice, J.A., & Chavez, F.P. (1998). Relationship between physical and biological variables during the upwelling period in Monterey Bay, CA. *Deep-Sea Research II*, **45**, 1669-1685.

Sverdrup, K.A., Duxbury, A.C., & Duxbury, A.B. (2005). *An introduction to the world's oceans* (8th ed.). New York: McGraw Hill.

Talbot, M.M.B., Bate, G.C., & Campbell, E.E. (1990). A review of the ecology of surf-zone diatoms, with special reference to *Anaulus australis*. *Oceanogr. Mar. Biol. Annu. Rev*., **28**, 155-175.

Tizler, M.M. (1973). Diurnal periodicity in the phytoplankton assemblage of a high mountain lake. *Limnology and Oceanography*, **18**, 15-30. Retrieved September 17, 2007 from http://links.jstor.org/sici.

Watkins, J. (2000). Aggregation and Vertical Migration. In Everson, I. (Ed.), *Krill: biology, ecology, and fisheries* (pp. 80-102). London: Blackwell Science.

INITIAL DISTRIBUTION LIST

1. Defense Technical Information Center
   Ft. Belvoir, Virginia

2. Dudley Knox Library
   Naval Postgraduate School
   Monterey, California

3. Department of Oceanography Chair
   Mary L. Batteen
   Naval Postgraduate School
   Monterey, California

4. Jeffrey D. Paduan
   Naval Postgraduate School
   Monterey, California

5. Curtis A. Collins
   Naval Postgraduate School
   Monterey, California

6. Igor Shulman
   Naval Research Laboratory
   Stennis Space Center, Mississippi